Calhoun: The NPS Institutional Archive

Reports and Technical Reports   All Technical Reports Collection

2004

Digital communications over fading channels

Beltz, Nathan E.

Monterey, California. Naval Postgraduate School

http://hdl.handle.net/10945/783

NPS-EC-05-002

NAVAL POSTGRADUATE SCHOOL

MONTEREY, CALIFORNIA

Digital Communications Over Fading Channels

by

R. Clark Robertson
and
Nathan E. Beltz

15 November 2004

Prepared for: Air Force Warfare Information Center

Naval Postgraduate School
Monterey, California 93943-5000

Rear Admiral Patrick W. Dunne, USN   Richard Elster
President   Provost

This report was funded by the Air force Warfare Information Center.

Reproduction of all or part of this report is authorized.

This report was prepared by:

_____   _____
R. CLARK ROBERTSON   NATHAN E. BELTZ
Professor of   Electrical Engineer
Electrical and
Computer Engineering

Reviewed by: Released by:

_____   _____
JOHN P. POWERS   LEONARD A. FERRARI
Chairman,   Dean of Research and Associate
Department of Electrical and   Provost
Computer Engineering

REPORT DOCUMENTATION PAGE		*Form Approved OMB No. 0704-0188*

1. AGENCY USE ONLY (*Leave blank*)	2. REPORT DATE 15 November 2004	3. REPORT TYPE AND DATES COVERED Technical Report 01JAN04 - 31DEC04	

4. TITLE AND SUBTITLE: Title (Mix case letters) Digital Communications Over Fading Channels	5. FUNDING NUMBERS
6. AUTHOR(S) R. Clark Robertson and Nathan E. Beltz	

7. PERFORMING ORGANIZATION NAME(S) AND ADDRESS(ES)
 	
    Naval Postgraduate School
    Monterey, CA 93943-5000
	8. PERFORMING ORGANIZATION REPORT NUMBER
	NPS-EC-05-002

9. SPONSORING / MONITORING AGENCY NAME(S) AND ADDRESS(ES)
    Air Force Information Warfare Center
    102 Hall Blvd., Suite 331
    San Antonio, TX 78243-7020
	10. SPONSORING / MONITORING AGENCY REPORT NUMBER

11. SUPPLEMENTARY NOTES The views expressed in this technical report are those of the author and do not reflect the official policy or position of the Department of Defense or the U.S. Government.

12a. DISTRIBUTION / AVAILABILITY STATEMENT Approved for public release; distribution is unlimited.	12b. DISTRIBUTION CODE

13. ABSTRACT (*maximum 200 words*)

In this report, the probabilities of bit error for the most commonly used digital modulation techniques are analyzed. Analytic solutions are developed for the probability of bit error when the signal is affected by the most commonly encountered impairment to system performance for a wireless channel, the transmission of the signal over a fading channel. In this report, the effect of a slow, flat Ricean fading channel on communications systems performance is examined. Since channel fading significantly degrades the performance of a communication system, the performance of digital communication systems that also use forward error correction channel coding is analyzed for hard decision decoding and, where appropriate, for soft decision decoding. Diversity, another technique to mitigate the effect of fading channels on digital communication systems performance, is also discussed. Also included is a discussion of the effect of narrowband noise interference, both continuous and pulsed, on digital communication systems. We then discuss the analysis of the probability of bit error for the combination of error correction coding and diversity. Following this, we briefly discuss spread spectrum systems. Next, we examine the link budget analysis and various models for channel loss. Finally, we examine in detail the second generation digital wireless standard *Global System for Mobile* (GSM).

14. SUBJECT TERMS	15. NUMBER OF PAGES 103
	16. PRICE CODE

17. SECURITY CLASSIFICATION OF REPORT Unclassified	18. SECURITY CLASSIFICATION OF THIS PAGE Unclassified	19. SECURITY CLASSIFICATION OF ABSTRACT Unclassified	20. LIMITATION OF ABSTRACT UL

THIS PAGE INTENTIONALLY LEFT BLANK

Abstract

    In this report, the probabilities of bit error for the most commonly used digital modulation techniques are analyzed. Analytic solutions are developed for the probability of bit error when the signal is affected by the most commonly encountered impairment to system performance for a wireless channel, the transmission of the signal over a fading channel. In this report, the effect of a slow, flat Ricean fading channel on communications systems performance is examined. Since channel fading significantly degrades the performance of a communication system, the performance of digital communication systems that also use forward error correction channel coding is analyzed for hard decision decoding and, where appropriate, for soft decision decoding. Diversity, another technique to mitigate the effect of fading channels on digital communication systems performance, is also discussed. Also included is a discussion of the effect of narrowband noise interference, both continuous and pulsed, on digital communication systems. We then discuss the analysis of the probability of bit error for the combination of error correction coding and diversity. Following this, we briefly discuss spread spectrum systems. Next, we examine the link budget analysis and various models for channel loss. Finally, we examine in detail the second generation digital wireless standard *Global System for Mobile* (GSM).

THIS PAGE INTENTIONALLY LEFT BLANK

Table of Contents

List of Figures

List of Tables

THIS PAGE INTENTIONALLY LEFT BLANK

1 Introduction

In the last decade, digital communication techniques have begun replacing analog communication techniques, and the trend is accelerating. With analog communications (AM and FM radios for example), the receiver attempts to recover a high fidelity replica of the signal that was originally transmitted. With digital communications, the transmitted signal represents a steam of data bits (ones and zeroes), and the performance of the system is independent of the origin of the bits. Consequently, digital communications systems can easily be used for both voice communications as well as data communications, while the reverse is not true.

Another reason for the move towards digital communications is *signal-to-noise ratio* (SNR), an important figure of merit for any communications system. Unfortunately, all communications systems are affected by various types of noise. If no other noise sources are present, there is always *additive white Gaussian noise* (AWGN) present. Hence, AWGN represents the most benign type of noise that may be present to affect the receiver, and the receiver must be designed to operate reliably in the presence of AWGN. For an FM radio, reliable communications require an input SNR of at least 10 to 15 dB. For a digital communications system, reliable data communications can be obtained with an SNR of around 10 dB, reliable voice communications with an SNR of around 7 dB. For a digital communications system with a type of forward error correction coding known as convolutional coding, a technique not available with analog communications systems, reliable data communications can be obtained with an SNR of around 4 dB, reliable voice communications with an SNR of around 3 dB. For a digital communications system with a type of forward error correction coding referred to as ordinary concatenated coding, reliable data communications can be obtained with an SNR of around 2.4 dB, reliable voice communications with an SNR of around 2.2 dB. For a digital communications system with a type of forward error correction coding referred to as turbo coding, reliable voice and data communications can be obtained with an SNR of less than one dB.

Aside from SNR, another primary figure of merit for communication systems is *bandwidth*. One of the disadvantages of forward error correction coding is that typically bandwidth is increased by between 200% and 300%. We can look at forward error correction coding as a sophisticated way of trading off power requirements (i.e., reducing SNR) in exchange for bandwidth. In digital communications systems, regardless of modulation type, bandwidth is proportional to the bit rate R_b, the number of bits per second that can be reliably transmitted and received. A typical FM voice channel may require 25 to 30 kHz bandwidth. *Pulse-code modulation* (PCM) (digitization

of the analog signal) requires 64 kbits/s for toll quality, while *differential pulse-code modulation* (DPCM) requires 24 to 32 kbits/s. If standard binary digital modulation without error correction coding is used, this implies a required bandwidth of around 128 kHz or 48 to 64 kHz for PCM or DPCM, respectively. Utilizing a *code-excited linear predictive* (CELP) coder for speech encoding, we can reduce the required bit rate to less than 10 kbits/s and the required bandwidth to less than 20 kHz. For example, the second generation (2-G) digital cellular standard IS-95 provides toll quality voice communications and has a maximum data bit rate of 9.6 kbits/s.

In this report, the probabilities of bit error for the most commonly used digital modulation techniques are analyzed. Analytic solutions are developed for the probability of bit error when the signal is affected by the most commonly encountered impairment to system performance for a wireless channel, the transmission of the signal over a fading channel. In this report, the effect of a slow, flat Ricean fading channel on communications systems performance is examined. Since channel fading significantly degrades the performance of a communication system, the performance of digital communication systems that also use forward error correction channel coding is also analyzed for hard decision decoding and, where appropriate, for soft decision decoding. Following this analysis, we examine the link budget analysis and various models for channel loss. Finally, we examine in detail the second generation digital wireless standard *Global System for Mobile* (GSM).

2 Digital Communications over Slow, Flat, Ricean Fading Channels

Many wireless communication channels do not have a line-of-sight (LOS) signal path; for example, modern cellular telephones often have no LOS with their base station. When there is no LOS, the signal is transmitted to the receiver by a phenomenon known as *multipath*; that is, there are multiple signal paths from the transmitter to the receiver as a result of reflection of the original signal off of buildings, terrain features, the ionosphere or troposphere, and so on. On the other hand, the availability of a LOS signal does not preclude a multipath component to the received signal as, for example, when omnidirectional antennas are used for both transmitter and receiver.

As a result of multipath, a signal, say a pulse, will arrive at the receiver multiple times with different amplitudes, phases, and arrival times. Viewed in the frequency domain, this results in different spectral components of the signal being affected differently by the channel; i.e., the frequency response of the channel is not flat over the bandwidth of the signal. This type of distortion is analogous to dispersion in a waveguide.

Since the number of multiple paths and their characteristics such as attenuation and propagation delay will differ from one multipath channel to another in an unpredictable manner, we must model this aspect of the multipath channel as a random process. Motion of either transmitter or receiver results in changes in multipath due to terrain effects and buildings, while atmospheric changes can result in changes in the multipath component of the signal even for stationary transmitters and receivers. Consequently, a multipath channel is a *time-varying* channel. Due to the time-varying nature of the multipath channel, if an identical pulse is transmitted at a later time, in general a different number of pulses with different amplitudes, phases, and arrival times will be received as compared to that received for the first pulse. Since the changes in the received multipath signal components due to either motion or atmospheric changes are effectively random, we must also model the time variations of the multipath channel as a random process. Consequently, each multipath channel must be characterized by *two* parameters, one for the time variations of the channel and another for the frequency variations of the channel.

Channel time variations are characterized by the coherence time $(\Delta t)_c$ of the channel [1]. The coherence time is a measure of the time duration over which the channel attenuation and delay are essentially fixed; that is, the received amplitude and phase are effectively constant over time periods of $(\Delta t)_c$ seconds. If the symbol duration $T_s < (\Delta t)_c$, then the received amplitude and phase are effectively constant for the duration of at least a symbol and the channel is said to be *slowly fading*. On the other hand, if $T_s > (\Delta t)_c$, then the received amplitude and phase fluctuate

over time periods that are short compared to the duration of a symbol, and the channel is said to be *fast fading.*

Channel frequency variations are characterized by the coherence bandwidth $(\Delta f)_c$ of the channel [1]. The frequency components of a signal that are separated in frequency by more than $(\Delta f)_c$ Hz are essentially uncorrelated and are affected differently by the channel. Conversely, frequency components of a signal that are separated in frequency by less than $(\Delta f)_c$ Hz are correlated to at least some minimum defined value and are affected approximately the same by the channel. If the noise equivalent bandwidth of the signal $W > (\Delta f)_c$, then significant distortion of the signal will occur and the channel is said to be *frequency-selective.* On the other hand, if $(\Delta f)_c > W$, then all frequency components of the signal are affected equally by the channel, and the channel is said to be *frequency-nonselective.* This is also referred to as *flat fading.*

Two widely used models for fading channels are the Rayleigh fading channel and the Ricean fading channel, where the Rayleigh fading channel is actually a special case of the Ricean fading channel. The Rayleigh model is used when there is *no* line-of-sight between transmitter and receiver, and all of the received signal power is due to multipath. The Ricean model is used when there *is* a line-of-sight between transmitter and receiver, but a substantial portion of the received signal power is also due to multipath. When there is line-of-sight between transmitter and receiver and virtually none of the received signal power is due to multipath, the non-fading channel model is used.

A general representation of a passband signal is

$$s(t) = \sqrt{2}a_c \cos\left[2\pi f_i(t)t + \theta(t)\right] \tag{1}$$

For Ricean fading channels, a_c is modeled as a Ricean random variable with probability density function (pdf)

$$f_{A_c}(a_c) = \frac{a_c}{\sigma^2} \exp\left[\frac{-(a_c^2 + \alpha^2)}{2\sigma^2}\right] I_0\left(\frac{\alpha a_c}{\sigma^2}\right) u(a_c) \tag{2}$$

where $I_0(\bullet)$ is the zeroth order modified Bessel function of the first kind and $u(\bullet)$ is the unit step function. Note that in this case σ^2 is *not* related to AWGN. This notational inconsistency is unfortunate, but the notation used here is traditional. The average received signal power is obtained from

$$\overline{s^2(t)} = \overline{a_c^2} = \int_0^\infty a_c^2 f_{A_c}(a_c)\, da_c \tag{3}$$

which for Ricean fading can be evaluated to yield

$$\overline{s^2(t)} = \overline{a_c^2} = \alpha^2 + 2\sigma^2 \tag{4}$$

4

For $\alpha \to 0$, (2) simplifies to the Rayleigh pdf

$$f_{A_c}(a_c) = \frac{a_c}{\sigma^2} \exp\left(\frac{-a_c^2}{2\sigma^2}\right) u(a_c) \tag{5}$$

since $I_0(0) = 1$, and the average received power simplifies to

$$\overline{s^2(t)} = \overline{a_c^2} = 2\sigma^2 \tag{6}$$

from which we infer that $2\sigma^2$ represents the non-LOS (diffuse) signal power and α^2 represents the LOS (direct) signal power.

An important parameter for fading channels is the ratio of direct-to-diffuse signal power

$$\zeta = \frac{\alpha^2}{2\sigma^2} \tag{7}$$

Clearly, $\zeta = 0$ corresponds to Rayleigh fading, and for $\zeta \to \infty$ there is no fading.

Since we are interested in the *average* probability of bit error for a particular modulation technique, we obtain the average probability of bit error with fading channels by recognizing that $P_b(a_c)$ is a function of a random variable, and the average probability of bit error is simply the expected value of $P_b(a_c)$. Therefore,

$$P_b = \int_0^\infty P_b(a_c) f_{A_c}(a_c) \, da_c \tag{8}$$

Alternatively, if we define the average energy per symbol-to-noise power spectral density ratio

$$\gamma_s = \frac{E_s}{N_0} = \frac{a_c^2 T_s}{N_0} \tag{9}$$

then

$$P_b = \int_0^\infty P_b(\gamma_s) f_{\Gamma_s}(\gamma_s) \, d\gamma_s \tag{10}$$

Equation (10) is often more convenient to evaluate than (8).

Given the pdf for a_c, we can find the pdf for γ_s from

$$f_{\Gamma_s}(\gamma_s) = \left|\frac{da_c}{d\gamma_s}\right| f_{A_c}\left(a_c = \sqrt{N_0 \gamma_s / T_s}\right) \tag{11}$$

$$f_{\Gamma_s}(\gamma_s) = \frac{N_0}{2a_c T_s} f_{A_c}\left(a_c = \sqrt{N_0 \gamma_s / T_s}\right) \tag{12}$$

5

For Ricean fading channels,

$$f_{\Gamma_s}(\gamma_s) \;\; = \;\; \frac{a_c}{\sigma^2}\frac{N_0}{2a_cT_s}\,\exp\left[\frac{-\left(\frac{\gamma_s N_0}{T_s}+\alpha^2\right)}{2\sigma^2}\right]\,I_0\left(\frac{\alpha\sqrt{\frac{N_0\gamma_s}{T_s}}}{\sigma^2}\right)u(\gamma_s) \tag{13}$$

$$f_{\Gamma_s}(\gamma_s) \;\; = \;\; \frac{\sigma_0^2}{2\sigma^2}\,\exp\left[\frac{-(\gamma_s\sigma_0^2+\alpha^2)}{2\sigma^2}\right]\,I_0\left(\frac{\alpha\sqrt{\gamma_s\sigma_0^2}}{\sigma^2}\right)u(\gamma_s) \tag{14}$$

where $\sigma_0^2 = N_0/T_s$.

Generally, we prefer to express our results in terms of the average energy per bit-to-noise power spectral density ratio γ_b. This is simply related to the average energy per symbol-to-noise power spectral density ratio by

$$\gamma_b = \frac{E_b}{N_0} = \frac{\gamma_s}{q} \tag{15}$$

where $M = 2^q$ and q is a positive integer.

2.1 Coherent Detection (BPSK, QPSK, MPSK, MQAM, GMSK)

In this subsection, the probability of bit error for binary phase-shift keying (BPSK), quadrature phase-shift keying (QPSK), M-ary phase-shift keying (MPSK), M-ary quadrature amplitude keying (MQAM), and Gaussian minimum-shift keying (GMSK) waveforms transmitted over slow, flat fading channels is derived. For each of these signaling techniques, the conditional probability of bit error is of the form

$$P_b(\gamma_s) = \frac{a}{q}\,Q\left(\sqrt{b\gamma_s}\right) \tag{16}$$

where $Q(\bullet)$ is the Q-function and a, b, and q are constants that depend on the modulation type. The constants a, b, and q for BPSK, QPSK, MPSK, MQAM, and GMSK are listed in Table 1. For MQAM with q even, a square constellation is assumed, while for MQAM with q odd, a rectangular constellation is assumed. In the case of BPSK and QPSK, (16) is exact, while for MPSK and MQAM, (16) is an approximation that is obtained by using the lower bound $P_b(P_s) = 1/k$ and an upper bound on P_s, where P_s is the probability of symbol error. Since $P_b = P_b(P_s)P_s$, the use of a lower bound for $P_b(P_s)$ and an upper bound for P_s offset one another to produce a very accurate approximation for P_b. While it is possible to obtain exact expressions for P_b for both MPSK and MQAM, the exact expressions are both significantly more complicated and impossible to obtain for general values of M. In the case of GMSK, (16) is also an approximation where the constant δ in Table 1 is determined by the 3 dB baseband bandwidth-bit duration product BT_b.

Table 1: Modulation dependent constants for equation (16).

Modulation	q	a	b
BPSK	1	1	2
QPSK	2	2	1
MPSK	$\log_2 M$	2	$2\sin^2(\pi/M)$
MQAM	$4, 6, \ldots$	$4\left(1 - 2^{-q/2}\right)$	$3/(2^q - 1)$
MQAM	$3, 5, \ldots$	4	$3/(2^q - 1)$
GMSK	1	1	2δ

For $BT_b = 0.25$, $\delta = 0.68$, while for $BT_b \to \infty$, $\delta = 0.85$ [4]. Consequently, for a very large variation in the 3 dB baseband bandwidth-bit duration product, there is only about one dB variation in the signal-to-noise ratio required to obtain a fixed probability of bit error.

Substituting (14) and (16) into (10), we get

$$P_b = \frac{a}{q} \int_0^\infty Q\left(\sqrt{b\gamma_s}\right) \frac{\sigma_0^2}{2\sigma^2} \exp\left[\frac{-\left(\gamma_s\sigma_0^2 + \alpha^2\right)}{2\sigma^2}\right] I_0\left(\frac{\alpha\sqrt{\gamma_s\sigma_0^2}}{\sigma^2}\right) d\gamma_s \tag{17}$$

Equation (17) cannot be evaluated analytically except for the special case of Rayleigh fading. Before proceeding with an approximate solution of (17) for the general Ricean fading case, we will evaluate (17) for the special case of Rayleigh fading.

2.1.1 Rayleigh Fading

For Rayleigh fading, $\alpha = 0$, and (17) simplifies to

$$P_b = \frac{a}{q} \int_0^\infty Q\left(\sqrt{b\gamma_s}\right) \frac{\sigma_0^2}{2\sigma^2} \exp\left(\frac{-\gamma_s\sigma_0^2}{2\sigma^2}\right) d\gamma_s \tag{18}$$

From (6) and (9), we have

$$\overline{\gamma_s} = \frac{2\sigma^2}{\sigma_0^2} \tag{19}$$

Substituting (19) into (18), we get

$$P_b = \frac{a}{q} \int_0^\infty Q\left(\sqrt{b\gamma_s}\right) \frac{1}{\overline{\gamma_s}} \exp\left(\frac{-\gamma_s}{\overline{\gamma_s}}\right) d\gamma_s \tag{20}$$

The Q-function and the complementary error function are related by

$$Q(x) = \frac{1}{2} \operatorname{erfc}\left(\frac{x}{\sqrt{2}}\right) \tag{21}$$

Substituting (21) into (20), adding $(a/2 - a/2)$ to (20), and using the identity [2]

$$\int_0^\infty e^{-\xi x} \left[1 - \operatorname{erfc}\left(\sqrt{\eta x}\right)\right] dx = \frac{1}{\xi}\sqrt{\frac{\eta}{\xi + \eta}} \tag{22}$$

7

we can evaluate (20) to obtain

$$P_b = \frac{a}{2k} \left(1 - \sqrt{\frac{b\overline{\gamma_s}}{2 + b\overline{\gamma_s}}} \right) \tag{23}$$

Substituting (15) into (23), we get

$$P_b = \frac{a}{2q} \left(1 - \sqrt{\frac{bq\overline{\gamma_b}}{2 + bq\overline{\gamma_b}}} \right) \tag{24}$$

2.1.2   Ricean Fading

In order to evaluate (17) analytically for Ricean fading when $\zeta > 0$, we must approximate the Q-function. We know that the Q-function is upper bounded by

$$Q(z) < \frac{1}{\sqrt{2\pi z^2}} \exp\left(\frac{-z^2}{2} \right) \tag{25}$$

Using (25), we can obtain an upper bound on (16) as

$$P_b(\gamma_s) < \frac{a}{q\sqrt{2\pi b \gamma_s}} \exp\left(\frac{-b\gamma_s}{2} \right) \tag{26}$$

Since (26) is a tight upper bound for $b\gamma_s > 2$ and since the exponential term dominates for $b\gamma_s > 2$, it is reasonable to replace $b\gamma_s$ in the denominator of (26) with $2c$ to obtain the approximation

$$P_b(\gamma_s) \approx \frac{a}{2q\sqrt{\pi c}} \exp\left(\frac{-b\gamma_s}{2} \right) \tag{27}$$

where $c > 1$ and is obtained empirically. Substituting (27) into (17), we get

$$P_b = \frac{a}{2q\sqrt{\pi c}} \int_0^\infty \exp\left(\frac{-b\gamma_s}{2} \right) \frac{\sigma_0^2}{2\sigma^2} \exp\left[\frac{-(\gamma_s \sigma_0^2 + \alpha^2)}{2\sigma^2} \right] I_0 \left(\frac{\alpha\sqrt{\gamma_s \sigma_0^2}}{\sigma^2} \right) d\gamma_s \tag{28}$$

We have the identities [3]

$$\int_0^\infty e^{-\xi x} J_0 \left(2\eta\sqrt{x} \right) dx = \frac{1}{\xi} e^{-\eta^2/\xi} \tag{29}$$

where $J(\bullet)$ is the ordinary Bessel function of the first kind and order zero, and

$$I_n(z) = (-j)^n J_n(jz) \tag{30}$$

where $j = \sqrt{-1}$. Using (29) and (30), we can evaluate (28) to obtain

$$P_b = \frac{a}{2q\sqrt{\pi c}} \frac{2}{2 + b2\sigma^2/\sigma_0^2} \exp\left[\frac{-b\alpha^2}{\sigma_0^2} \left(\frac{1}{2 + b2\sigma^2/\sigma_0^2} \right) \right] \tag{31}$$

From (4) and (9), we have

$$\overline{\gamma_s} = \frac{\overline{a_c^2}}{\sigma_0^2} = \frac{\alpha^2 + 2\sigma^2}{\sigma_0^2} \tag{32}$$

8

Substituting (7) into (32), we get

$$\overline{\gamma_s} = \frac{2\sigma^2}{\sigma_0^2}\,(1+\zeta) \tag{33}$$

and

$$\overline{\gamma_s} = \frac{\alpha^2}{\sigma_0^2}\left(\frac{1+\zeta}{\zeta}\right) \tag{34}$$

Substituting (33) and (34) into (31), we get

$$P_b = \frac{a}{2q\sqrt{\pi c}}\,\frac{2\,(1+\zeta)}{2\,(1+\zeta)+b\overline{\gamma_s}}\,\exp\left[\frac{-b\zeta\overline{\gamma_s}}{2\,(1+\zeta)+b\overline{\gamma_s}}\right] \tag{35}$$

2.2   Summary for Coherent Detection (BPSK, QPSK, MPSK, MQAM, GMSK)

Using the values in Table 1 in (24), we obtain P_b for Rayleigh fading channels.

For BPSK and QPSK and Rayleigh fading,

$$P_b = \frac{1}{2}\left(1 - \sqrt{\frac{\overline{\gamma_b}}{1+\overline{\gamma_b}}}\right) \tag{36}$$

For MPSK and Rayleigh fading,

$$P_b = \frac{1}{q}\left(1 - \sqrt{\frac{q\overline{\gamma_b}\sin^2{(\pi/M)}}{1+q\overline{\gamma_b}\sin^2{(\pi/M)}}}\right) \tag{37}$$

For MQAM with k even and Rayleigh fading,

$$P_b = \frac{2}{q}\left(1 - 2^{-q/2}\right)\left(1 - \sqrt{\frac{3q\overline{\gamma_b}}{2\,(2^q-1)+3q\overline{\gamma_b}}}\right) \tag{38}$$

For MQAM with q odd $(q \geq 3)$ and Rayleigh fading,

$$P_b = \frac{2}{q}\left(1 - \sqrt{\frac{3q\overline{\gamma_b}}{2\,(2^q-1)+3q\overline{\gamma_b}}}\right) \tag{39}$$

For GMSK and Rayleigh fading,

$$P_b = \frac{1}{2}\left(1 - \sqrt{\frac{\delta\overline{\gamma_b}}{1+\delta\overline{\gamma_b}}}\right) \tag{40}$$

For BPSK and QPSK and Ricean fading,

$$P_b \approx \frac{1}{2\sqrt{\pi c}}\left[\frac{\zeta+1}{\overline{\gamma_b}+\zeta+1}\right]\exp\left[\frac{-\zeta\overline{\gamma_b}}{\overline{\gamma_b}+\zeta+1}\right] \tag{41}$$

where $c = 1.0 + 0.1\zeta$ is empirically obtained.

For MPSK and Ricean fading,

$$P_b = \frac{1+\zeta}{q\sqrt{\pi c}\left[1+\zeta+q\sin^2(\pi/M)\overline{\gamma_b}\right]}\,\exp\left[\frac{-q\sin^2(\pi/M)\zeta\overline{\gamma_b}}{1+\zeta+q\sin^2(\pi/M)\overline{\gamma_b}}\right] \tag{42}$$

9

where $c = 1.0 + 0.1\zeta$ is empirically obtained.

For MQAM with k even and Ricean fading,

$$P_b \approx \frac{4\left(1 - 1/2^{q/2}\right)\left(2^q - 1\right)(\zeta + 1)}{q\sqrt{\pi c}\left[3q\overline{\gamma_b} + 2\left(2^q - 1\right)(\zeta + 1)\right]} \exp\left[\frac{-3q\zeta\overline{\gamma_b}}{3q\overline{\gamma_b} + 2\left(2^q - 1\right)(\zeta + 1)}\right] \tag{43}$$

where $c = 1.0 + 0.1\zeta$ is empirically obtained.

For MQAM with k odd and Ricean fading,

$$P_b \approx \frac{4\left(2^q - 1\right)(\zeta + 1)}{q\sqrt{\pi c}\left[3q\overline{\gamma_b} + 2\left(2^q - 1\right)(\zeta + 1)\right]} \exp\left[\frac{-3q\zeta\overline{\gamma_b}}{3q\overline{\gamma_b} + 2\left(2^q - 1\right)(\zeta + 1)}\right] \tag{44}$$

where $c = 1.0 + 0.1\zeta$ is empirically obtained.

For GMSK and Ricean fading,

$$P_b = \frac{1 + \zeta}{2q\sqrt{\pi c}\left(1 + \zeta + q\delta\overline{\gamma_b}\right)} \exp\left(\frac{-q\delta\zeta\overline{\gamma_b}}{1 + \zeta + q\delta\overline{\gamma_b}}\right) \tag{45}$$

where $c = 1.0 + 0.1\zeta$ is empirically obtained.

2.3   Numerical Results for Coherent Detection

The probability of bit error as a function of E_b/N_0 for coherent systems in AWGN is plotted in Figures 1, 2, 3, and 4 for no channel fading, Rayleigh fading, Ricean fading with $\zeta = 4$, and Ricean fading with $\zeta = 10$, respectively. In each figure, MPSK with $M = 8$ and $M = 16$ and MQAM with $M = 16$ and $M = 64$ is plotted.

There are several interesting observations that can be made from an examination of Figures 1–4. First, the performance of 8PSK and 16QAM are almost the same, as are the performance of 16PSK and 64QAM. Second, Rayleigh fading results in significant degradation in performance. For example, at $P_b = 10^{-4}$, BPSK or QPSK requires $E_b/N_0 \approx 8.4$ dB, while for a Rayleigh fading channel $E_b/N_0 \approx 34.0$ dB are required for BPSK or QPSK, a difference of 25.6 dB. For $P_b = 10^{-5}$, with no channel fading, $E_b/N_0 \approx 9.6$ dB is required for BPSK or QPSK, while for Rayleigh fading, $E_b/N_0 \approx 44.0$ dB is required, a difference of 34.4 dB. Third, for Rayleigh fading channels, P_b varies linearly with $(E_b/N_0)^{-1}$ when E_b/N_0 is expressed in dB. Finally, while absolute performance is significantly degraded for Rayleigh fading, the difference between BPSK or QPSK and 64QAM is less for Rayleigh fading than for no channel fading. For example, for $P_b = 10^{-4}$, with no channel fading, the difference in required E_b/N_0 is about 8 dB, while for Rayleigh fading, the difference is about 6 dB.

The results plotted in Figures 3 and 4 do not use the approximate equations developed in this section but are exact. The approximation for BPSK and QPSK is very accurate for $P_b < 0.1$,
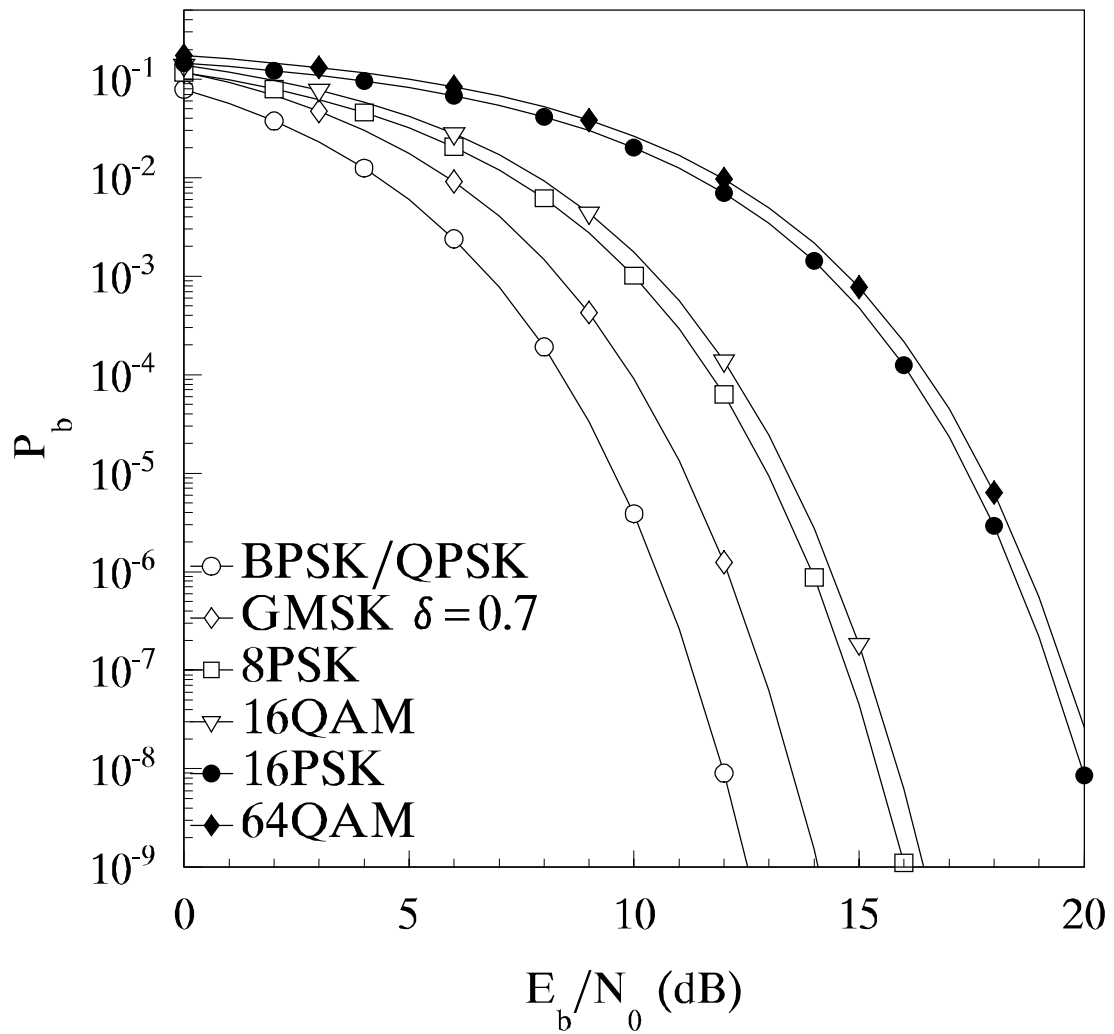
Figure 1: Performance of coherent systems in AWGN with no channel fading.
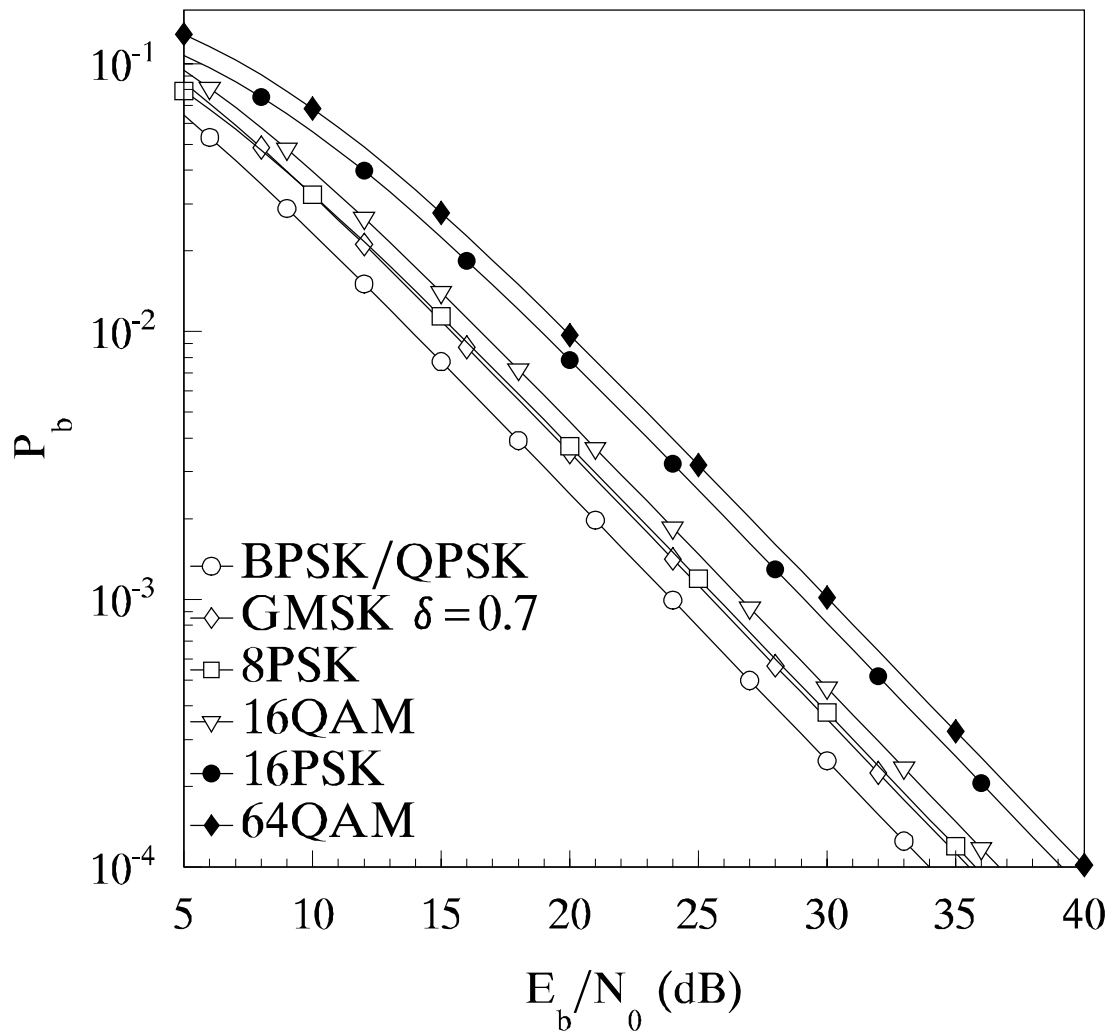
Figure 2: Performance of coherent systems in AWGN over a slow, flat Rayleigh fading channel.
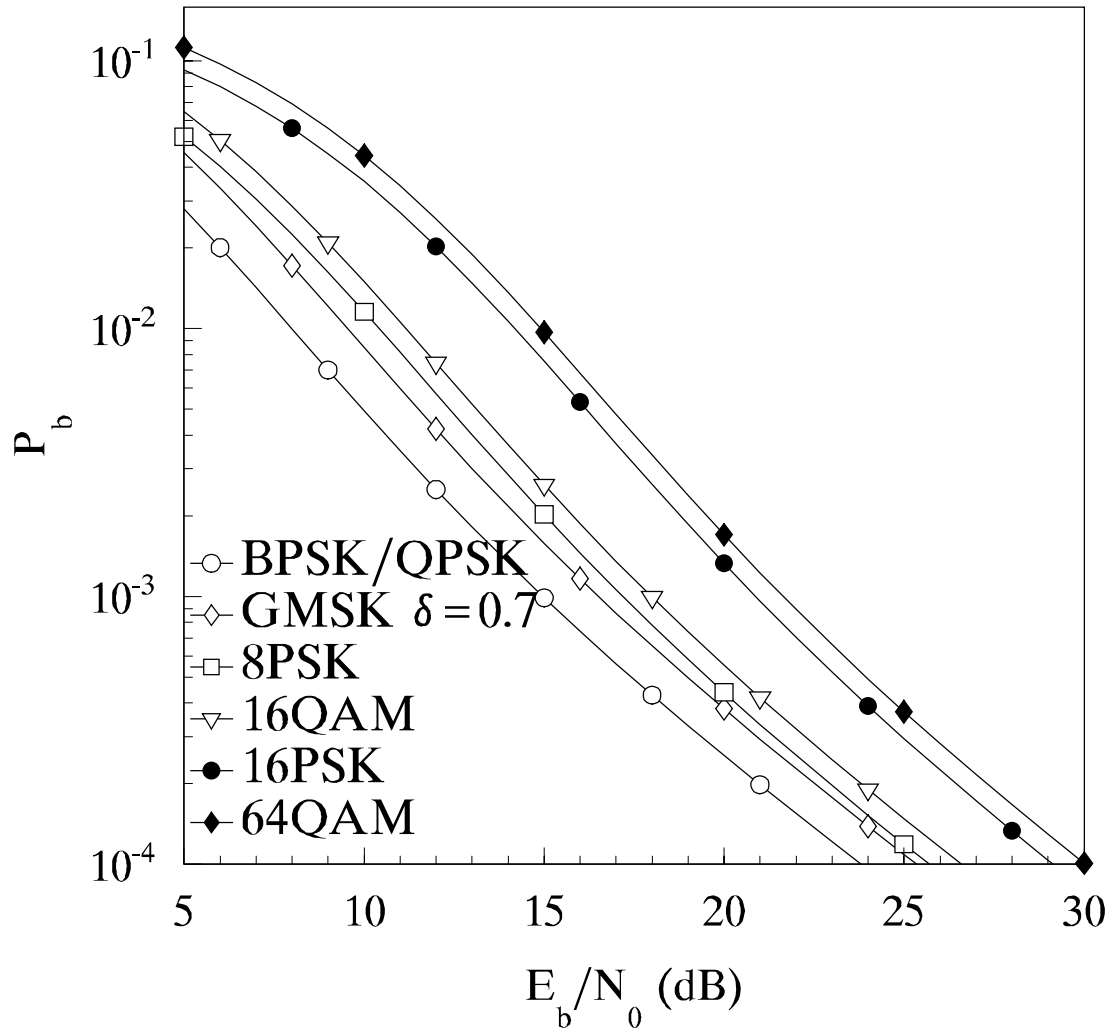
Figure 3: Performance of coherent systems in AWGN over a slow, flat Ricean fading channel with $\zeta = 4$.
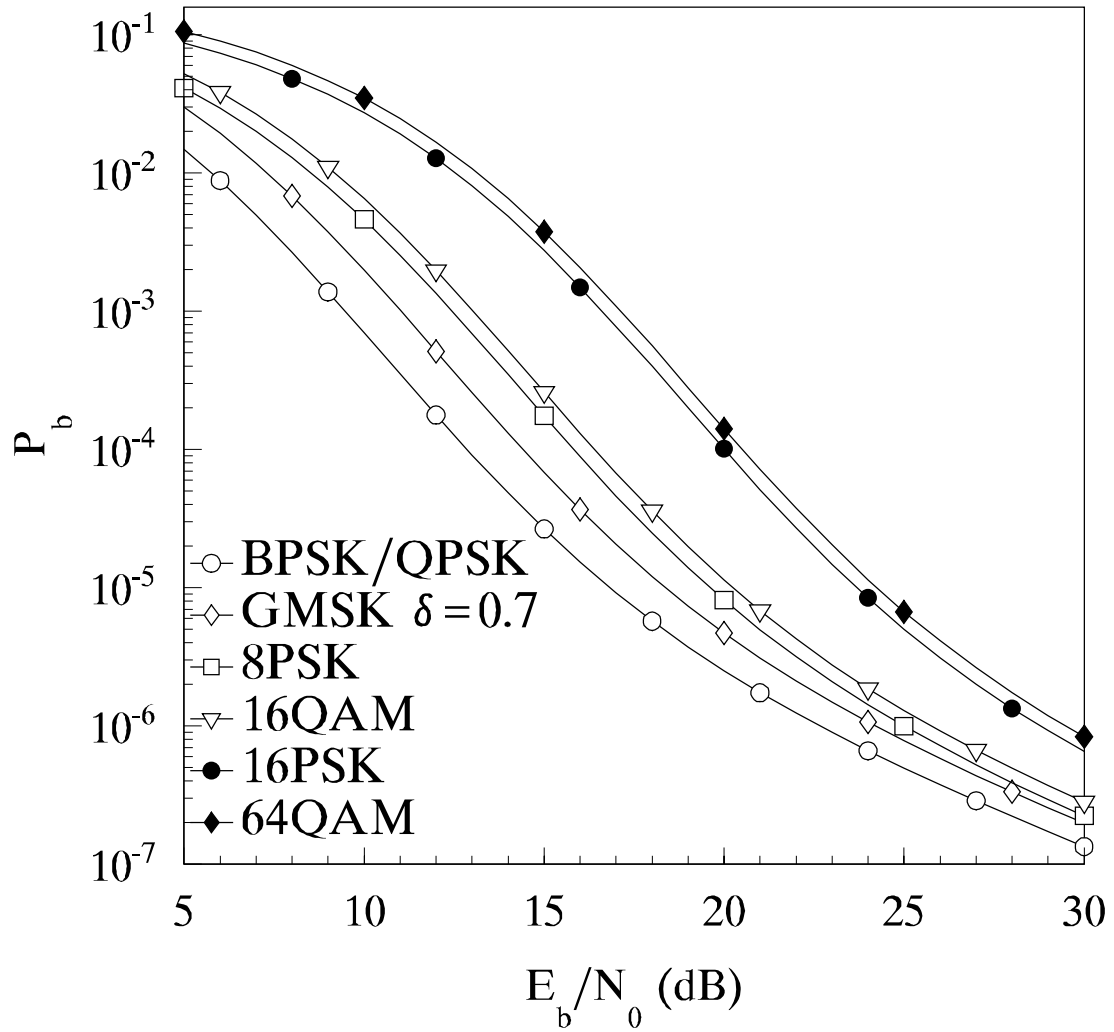
Figure 4: Performance of coherent systems in AWGN over a slow, flat Ricean fading channel with $\zeta = 10$.

while the approximation for 8PSK and 16QAM is very accurate for $P_b < 0.1$ when $\zeta < 5$. The approximation for 16PSK and 64QAM is very accurate for $P_b < 0.05$, while the approximation for 8PSK and 16QAM is very accurate for $P_b < 0.05$ when $\zeta > 5$. A comparison of the exact and approximate probability of bit error for BPSK/QPSK, 16QAM, and 64QAM in AWGN over a slow, flat Ricean fading channel for $\zeta = 4$ and $\zeta = 10$ is shown in Figures 5 and 6, respectively. Comparable results are obtained for 8PSK and 16PSK.

2.4 Noncoherent Detection (DPSK, M-ary Orthogonal Signaling)

The conditional probability of bit error for orthogonal signaling, such as orthogonal MFSK and orthogonal signaling with Walsh functions, with noncoherent detection is given by [1]

$$P_b(\gamma_s) = \frac{M}{2(M-1)} \sum_{n=1}^{M-1} \frac{(-1)^{n+1}}{n+1} \binom{M-1}{n} \exp\left(\frac{-n\gamma_s}{n+1}\right) \tag{46}$$

Substituting (14) and (46) into (10), we obtain

$$
\begin{aligned}
P_b &= \frac{M}{2(M-1)} \int_0^\infty \sum_{n=1}^{M-1} \frac{(-1)^{n+1}}{n+1} \binom{M-1}{n} \exp\left(\frac{-n\gamma_s}{n+1}\right) \\
&\quad \times \frac{\sigma_0^2}{2\sigma^2} \exp\left[\frac{-\left(\gamma_s \sigma_0^2 + \alpha^2\right)}{2\sigma^2}\right] I_0\left(\frac{\alpha\sqrt{\gamma_s \sigma_0^2}}{\sigma^2}\right) d\gamma_s
\end{aligned}
\tag{47}
$$

Interchanging the order of integration and summation in (47), we obtain

$$
\begin{aligned}
P_b &= \frac{M}{2(M-1)} \sum_{n=1}^{M-1} \frac{(-1)^{n+1}}{n+1} \binom{M-1}{n} \frac{\sigma_0^2}{2\sigma^2} \exp\left(\frac{-\alpha^2}{2\sigma^2}\right) \\
&\quad \times \int_0^\infty \exp\left[-\gamma_s\left(\frac{\sigma_0^2}{2\sigma^2} + \frac{n}{n+1}\right)\right] I_0\left(\frac{\alpha\sqrt{\gamma_s \sigma_0^2}}{\sigma^2}\right) d\gamma_s
\end{aligned}
\tag{48}
$$

Using (29) and (30) as well as (7), we can evaluate (48) to obtain

$$
\begin{aligned}
P_b &= \frac{M}{2(M-1)} \sum_{n=1}^{M-1} \frac{(-1)^{n+1}(1+\zeta)}{1+\zeta+n\left(1+\zeta+\overline{\gamma_s}\right)} \binom{M-1}{n} \\
&\quad \times \exp\left[\frac{-n\zeta\overline{\gamma_s}}{1+\zeta+n\left(1+\zeta+\overline{\gamma_s}\right)}\right]
\end{aligned}
\tag{49}
$$

2.5 Summary for Noncoherent Detection (DPSK, M-ary Orthogonal Signaling)

For Ricean fading channels, the probability of bit error for orthogonal signaling, such as orthogonal MFSK and orthogonal signaling with Walsh functions, with noncoherent detection is given
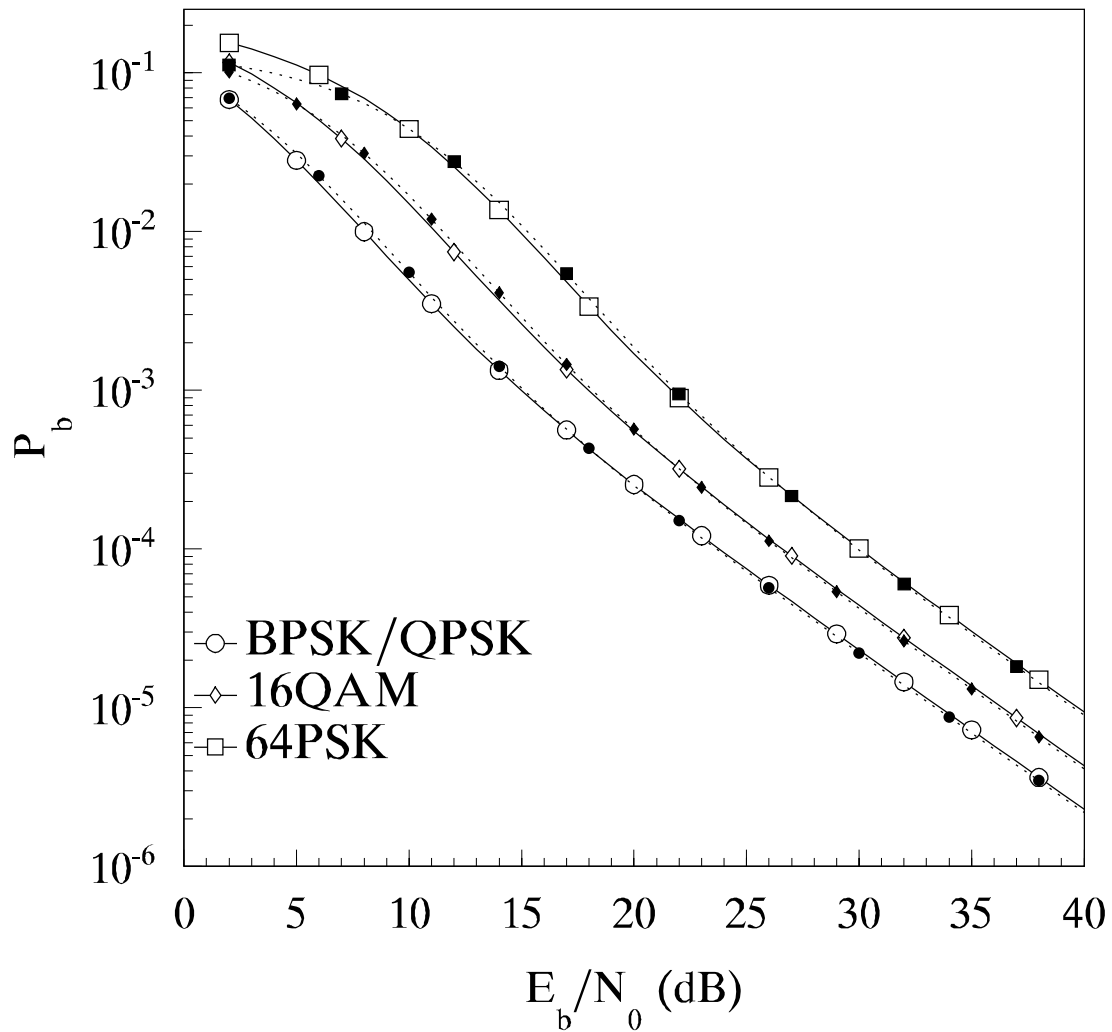
Figure 5: Comparison of exact and approximate performance of BPSK/QPSK, 16QAM, and 64QAM in AWGN over a slow, flat Ricean fading channel with $\zeta = 4$. Approximate results are plotted with a dotted line and indicated by solid symbols; exact results are plotted with a solid line and open symbols.
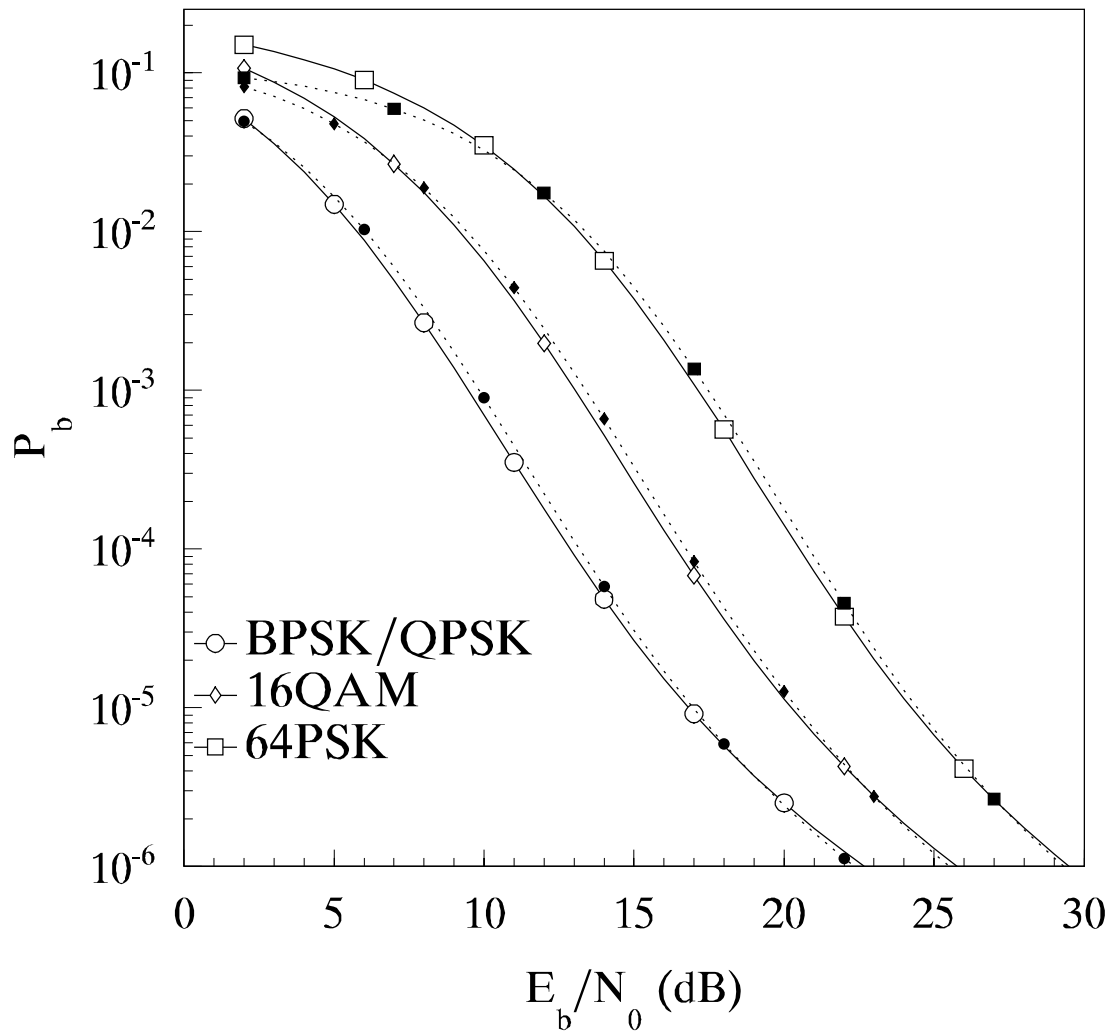
Figure 6: Comparison of exact and approximate performance of BPSK/QPSK, 16QAM, and 64QAM in AWGN over a slow, flat Ricean fading channel with $\zeta = 10$. Approximate results are plotted with a dotted line and indicated by solid symbols; exact results are plotted with a solid line and open symbols.

by

$$P_b = \frac{M}{2(M-1)} \sum_{n=1}^{M-1} \frac{(-1)^{n+1}(1+\zeta)}{1+\zeta+n\left(1+\zeta+\overline{\gamma_s}\right)} \binom{M-1}{n}$$

$$\times \exp\left[\frac{-n\zeta\overline{\gamma_s}}{1+\zeta+n\left(1+\zeta+\overline{\gamma_s}\right)}\right] \tag{50}$$

For BFSK with noncoherent detection, $M = 2$, and

$$P_b = \frac{1+\zeta}{2+2\zeta+\overline{\gamma_b}} \exp\left[\frac{-\zeta\overline{\gamma_b}}{2+2\zeta+\overline{\gamma_b}}\right] \tag{51}$$

The probability of bit error for DPSK is the same as for noncoherent BFSK with twice the signal power, so for DPSK

$$P_b = \frac{1+\zeta}{2(1+\zeta+\overline{\gamma_b})} \exp\left[\frac{-\zeta\overline{\gamma_b}}{1+\zeta+\overline{\gamma_b}}\right] \tag{52}$$

2.6   Numerical Results for Noncoherent Detection

The probability of bit error as a function of E_b/N_0 for noncoherent MFSK in AWGN is plotted in Figures 7, 8, 9, and 10 for no channel fading, Rayleigh fading, Ricean fading with $\zeta = 4$, and Ricean fading with $\zeta = 10$, respectively, for various values of M. The probability of bit error as a function of E_b/N_0 for optimum DPSK can be obtained by shifting the plot for BFSK 3 dB to the left.

Several trends can be seen from an examination of Figures 7, 8, 9, and 10. First, regardless of whether the channel is a fading channel or not, increasing M improves performance in the sense of requiring a smaller E_b/N_0 in order to achieve the same P_b; however, the amount of improvement attained by increasing M is significantly reduced for fading channels. For example, for $P_b = 10^{-5}$ and no channel fading, the required E_b/N_0 is reduced about 6 dB if 32FSK is used instead of BFSK. However, if the channel is a Rayleigh fading channel, the required E_b/N_0 is reduced about 3.6 dB if 32FSK is used instead of BFSK, a difference of over 2 dB. Second, as M increases we rapidly reach a point of diminishing returns. For example, for $P_b = 10^{-5}$ and no channel fading, the required E_b/N_0 is reduced about 4 dB if 8FSK is used instead of BFSK, but changing to 32FSK only reduces the required E_b/N_0 by another 2 dB. Changing from 32FSK to 64FSK results in a further improvement of only about 0.5 dB. For a fading channel, the point of diminishing returns is reached for smaller M and is more pronounced, with less than 1 dB improvement if 32FSK is used

18

instead of 8FSK. Third, from Figure 8 we see that, regardless of the value of M, performance varies linearly with E_b/N_0. Finally, we note that a fading channel significantly degrades performance as compared to a channel with no fading, even when the channel is Ricean with $\zeta = 10$. Intuitively, we might have expected a fading channel with ten times as much power in the line-of-sight component as in the non-line-of-sight component to behave more like a channel with no fading, but such is not the case. For $\zeta > 0$, P_b begins to vary linearly instead of exponentially for large E_b/N_0, just as for a Rayleigh fading channel.
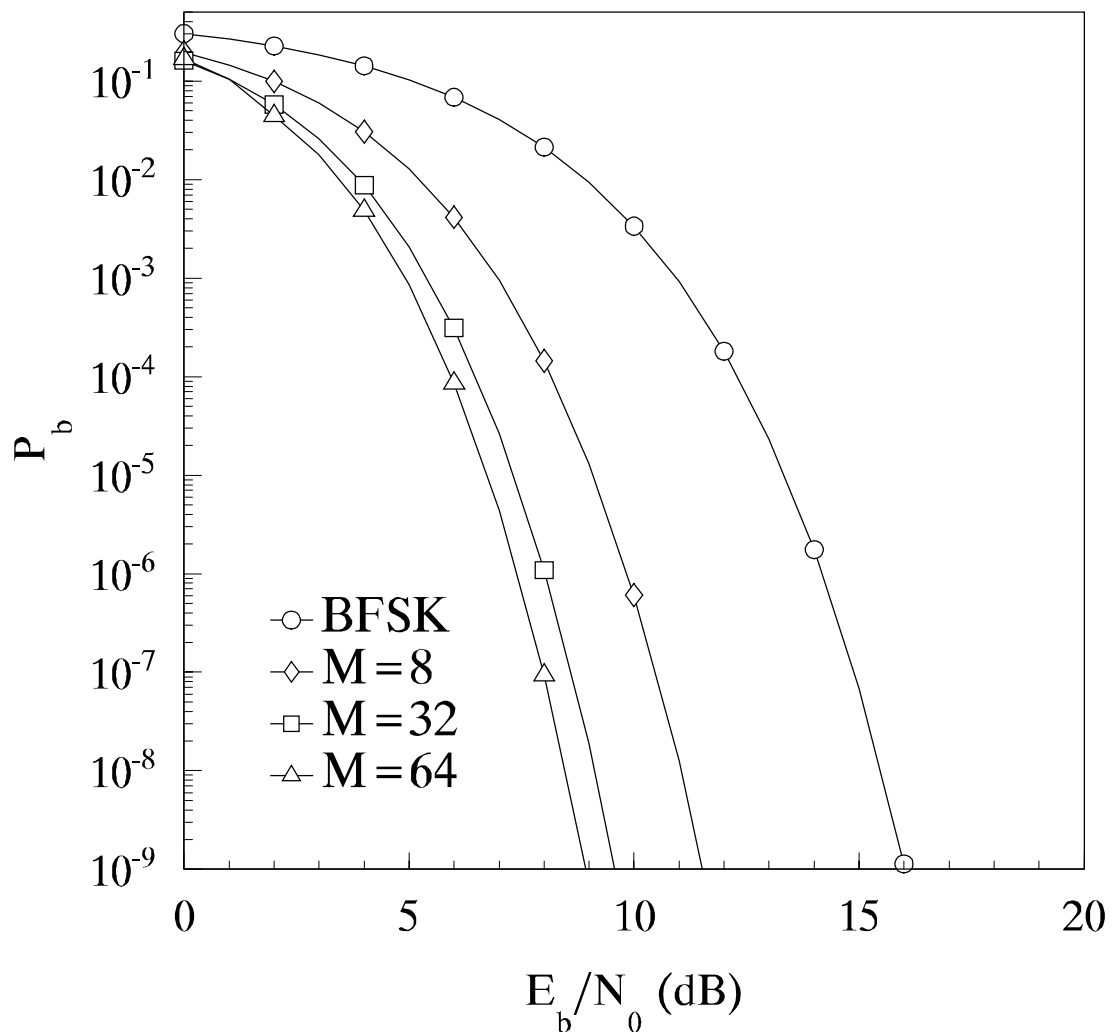
Figure 7: Performance of noncoherent MFSK in AWGN with no channel fading.
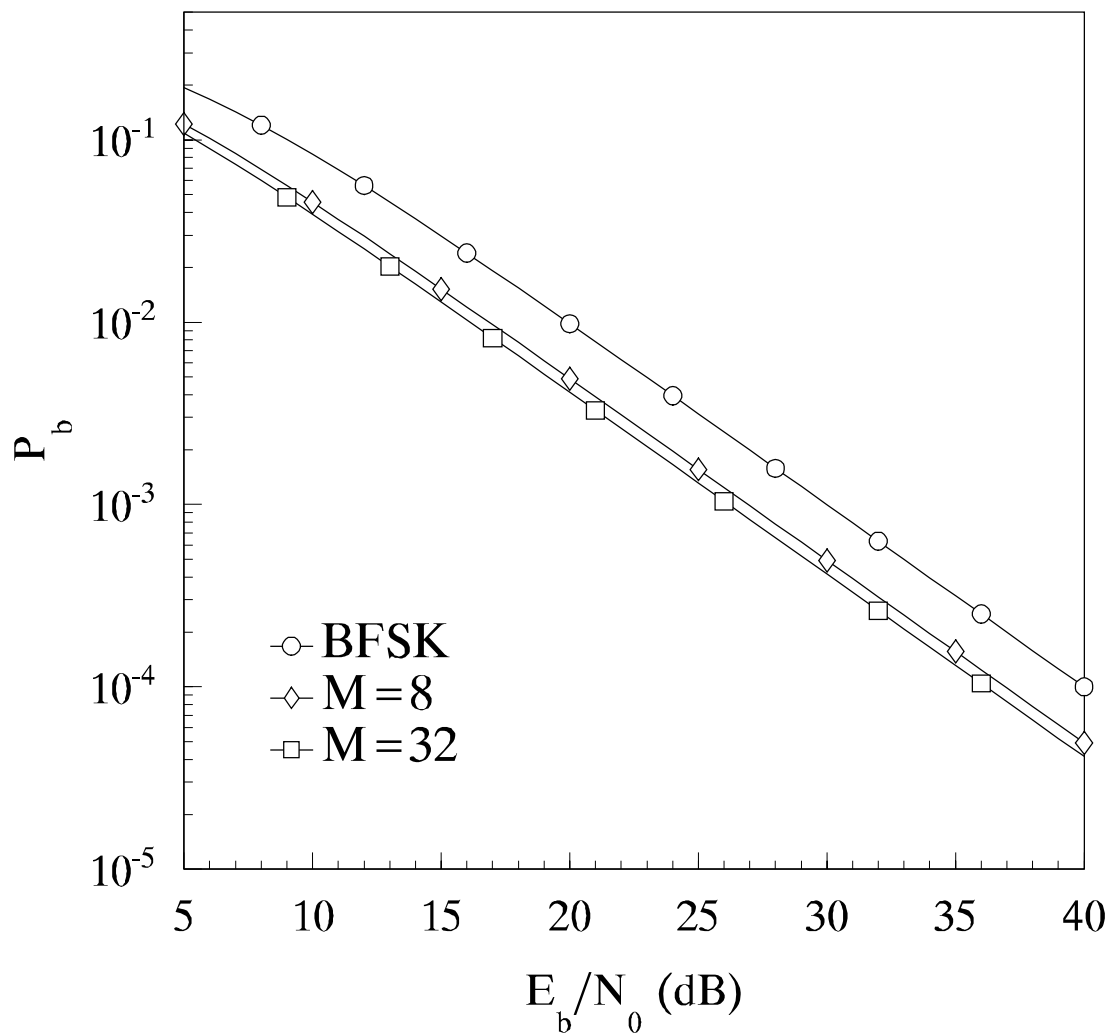
Figure 8: Performance of noncoherent MFSK in AWGN over a slow, flat Rayleigh fading channel.
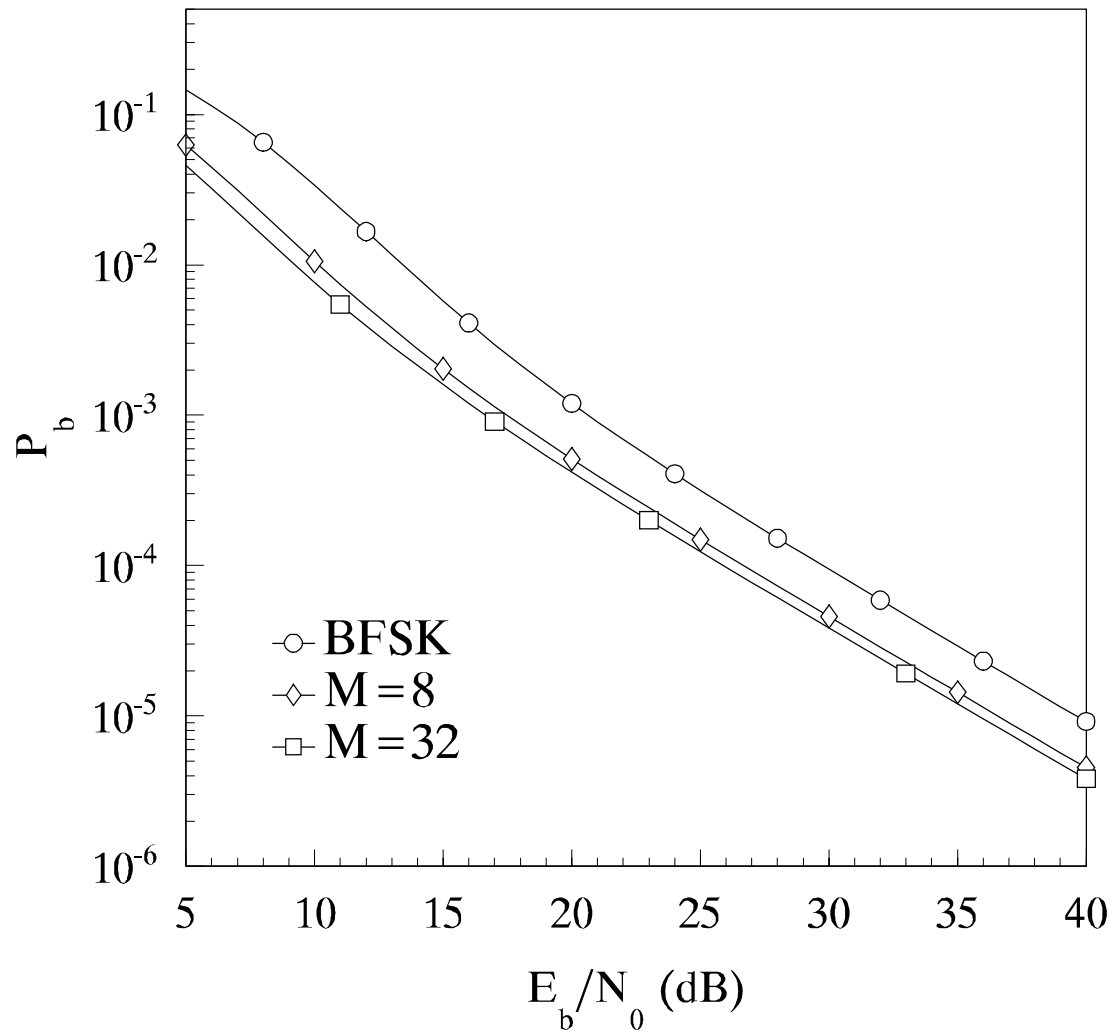
Figure 9: Performance of noncoherent MFSK in AWGN over a slow, flat Ricean fading channel with $\zeta = 4$.
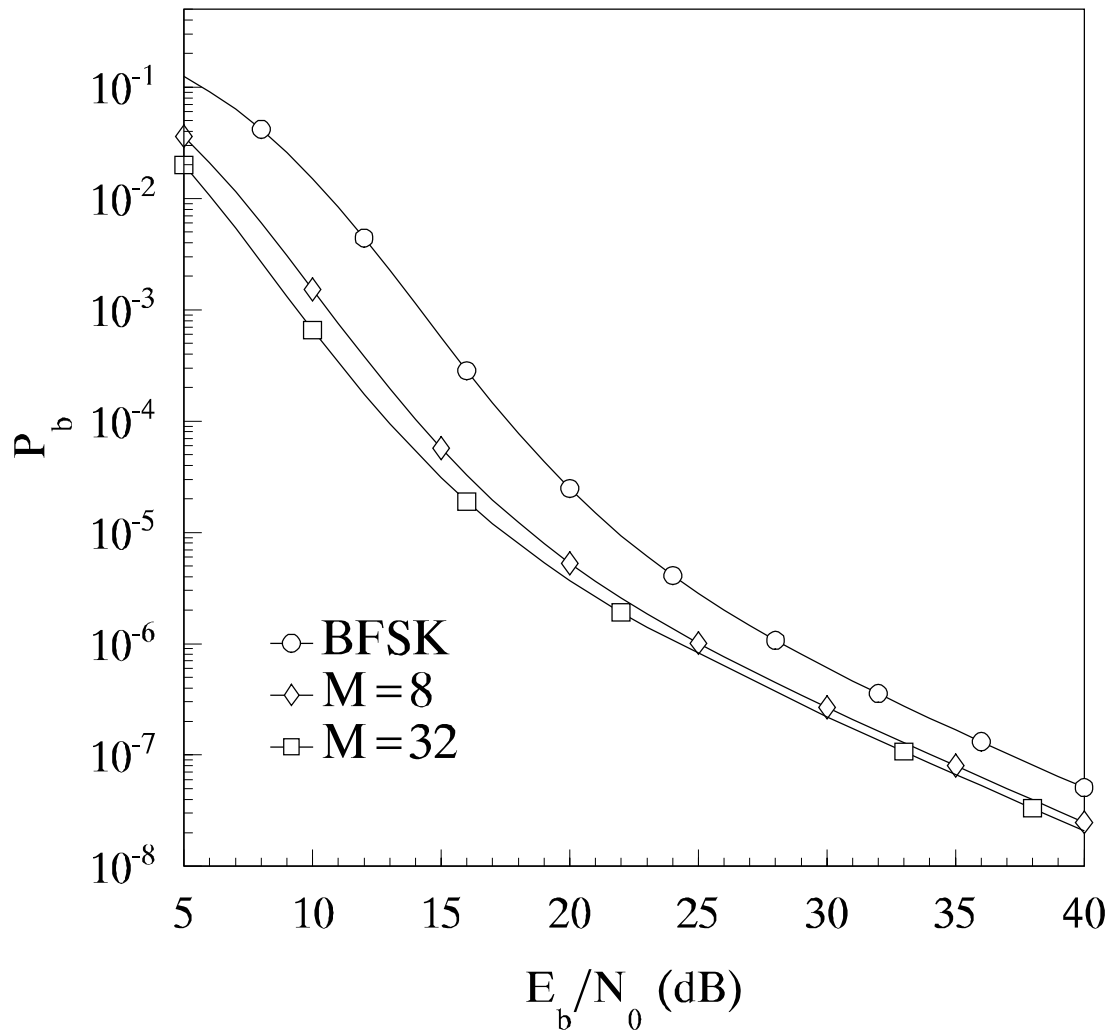
Figure 10: Performance of noncoherent MFSK in AWGN over a slow, flat Ricean fading channel with $\zeta = 10$.

2.7 Waveform Bandwidth

In this subsection, the passband bandwidths of the various modulation techniques that were discussed in this section are presented. There is more than one definition of bandwidth; six different definitions are listed in [11]. Further complicating matters, the bandwidth of a digital communications signal is related to the underlying baseband *pulse-code modulation* (PCM) waveform, or line code, used. In this subsection, the *null-to-null* bandwidth is presented assuming a polar *nonreturn-to-zero* (NRZ) line code. The null-to-null bandwidth is defined as the bandwidth of the main lobe of the signal's power spectral density (PSD) and corresponds to the bandwidth that contains most of the signal power, while the polar NRZ line code is frequently used in digital communications since it gives the smallest bandwidth for a specific bit rate. Unfortunately, not all modulation schemes have well defined main lobes, and of those that do, the percentage of the signal power contained in the main lobe varies from around 90% to over 99%.

The PSDs of the waveform for BPSK, DPSK, QPSK, MPSK, and MQAM all have well defined main lobes that contain 90.3% of the total signal power when polar NRZ signaling is used. The null-to-null bandwidth for these five modulation schemes with polar NRZ signaling is given by

$$B = \frac{2R_b}{q} \tag{53}$$

where R_b is the bit rate and q is the number of bits per symbol ($M = 2^q$).

The PSD of the waveform for M-ary orthogonal signaling with Walsh functions also has a well defined main lobe that contain 90.3% of the total signal power when polar NRZ signaling is used. The null-to-null bandwidth for this modulation scheme with polar NRZ signaling is given by

$$B = \frac{2^{q+1}R_b}{q} \tag{54}$$

where R_b is the bit rate and q is the number of bits per symbol ($M = 2^q$).

The PSD of the waveform for orthogonal MFSK does not have a clearly defined main lobe, and the null-to-null bandwidth is highly dependent on the frequency separation between adjacent signaling frequencies Δf. The null-to-null bandwidth for this modulation scheme with polar NRZ signaling is given by

$$B = (2^q - 1)\,\Delta f + 2R_b/q \tag{55}$$

where R_b is the bit rate and q is the number of bits per symbol ($M = 2^q$). For the most commonly occuring case where $\Delta f = R_b$, (55) simplifies to

$$B = \frac{(2^q + 1)\,R_b}{q} \tag{56}$$

Table 2: Null-to-null bandwidth B and noise equivalent bandwidth B_{eq} as a function of the bit rate R_b and number of bits per symbol q for different modulation types.

Modulation	q	B	B_{eq}
BPSK	1	$2R_b$	R_b
QPSK	2	R_b	$R_b/2$
MPSK	$\log_2 M$	$2R_b/q$	R_b/q
MQAM	$\log_2 M$	$2R_b/q$	R_b/q
Walsh	$\log_2 M$	$2^{q+1}R_b/q$	$2^q R_b/q$
MFSK ($\Delta f = R_b$)	$\log_2 M$	$(2^q + 1) R_b/q$	$2^q R_b/q$

Table 3: GMSK bandwidth as a function of the bit rate R_b for various values of B/R_b [4].

B/R_b	90%	99%	99.9%
0.2	$0.52R_b$	$0.79R_b$	$0.99R_b$
0.25	$0.57R_b$	$0.86R_b$	$1.09R_b$
0.5	$0.69R_b$	$1.04R_b$	$1.33R_b$
$\to \infty$	$0.78R_b$	$1.2R_b$	$2.76R_b$

The null-to-null bandwidth of the modulation techniques discussed in this section, as well as the noise equivalent bandwidth B_{eq}, are listed in Table 2 as a function of bit rate R_b and number of bits per symbol q. The noise equivalent bandwidth is frequently used in communications engineering literature.

The bandwidths containing 90%, 99% and 99.9%of the signal power for GMSK for various values of B/R_b are listed in Table 3.

3 Forward Error Correction Coding

Communication system performance can be improved significantly by implementing *forward error correction coding.* Forward error correction (FEC) coding consists of adding a certain number of redundant bits to the actual data bits in a particular pattern such that recovery of the actual data bits is enhanced. The two primary types of forward error correction codes are *block codes* and *convolutional codes.*

In a system utilizing FEC coding, for every k information data bits, n coded bits are transmitted where $n > k$. Since n coded bits must be transmitted in the time it would otherwise take to transmit k data bits,

$$nT_{b_c} = kT_b \tag{57}$$

where T_{b_c} is the duration of a coded, or channel, bit and T_b is the duration of a data bit. Therefore,

$$T_{b_c} = \frac{k}{n}T_b = rT_b \tag{58}$$

$$R_{b_c} = \frac{R_b}{r} \tag{59}$$

where the coded, or channel, bit rate is $R_{b_c} = 1/T_{b_c}$ and $r = k/n$ is the *code rate.* Since $r < 1$, the coded bit rate is higher than the uncoded bit rate; and for a constant data bit rate, the addition of FEC coding increases the bandwidth by the factor $n/k = 1/r$.

The average transmitted power is the same whether coded or uncoded bits are transmitted:

$$E_{b_c}R_{b_c} = E_b R_b \tag{60}$$

Hence,

$$E_{b_c} = rE_b \tag{61}$$

Since $r < 1$, the average energy per coded bit is less than the average energy per uncoded bit; and for a fixed average energy per data bit, the addition of FEC coding increases the probability of coded bit error.

Coding gain is defined as the difference in the signal-to-noise ratios required by a FEC coded communication system and the same uncoded communication system to achieve a specific probability of bit error:

$$G_{\text{dB}} = \left(\frac{E_b}{N_0}\right)_{uncoded\text{dB}} - \left(\frac{E_b}{N_0}\right)_{coded\text{dB}} \tag{62}$$

Coding gain is a function of both the type of modulation and the type of FEC code. Coding gain can be either positive or negative. We have already seen that FEC increases the probability of

25

coded bit error. For coding gain to be positive, the degradation in coded probability of bit error must be more than compensated for by the enhancement in performance afforded by the code.

3.1 Convolutional Codes with Hard Decision Decoding

When a rate $r = k/n$ convolutional code is employed, the probability of bit error is upper bounded by [5]

$$P_b < \frac{1}{k} \sum_{d=d_{free}}^{\infty} B_d P_d \tag{63}$$

where d_{free} is the free distance of the convolutional code, B_d is the total number of information bit ones on all weight d paths, and P_d is the probability of selecting a weight d output sequence as the transmitted code sequence. The quantities B_d and d_{free} are parameters of the convolutional code chosen, and P_d is determined by the type of modulation, the channel, and whether hard or soft decision decoding is used. For hard decision decoding [5]

$$P_d = \begin{cases} \sum_{i=(d+1)/2}^{d} \binom{d}{i} p^i (1-p)^{d-i} & \text{for } d \text{ odd} \\ \frac{1}{2} \binom{d}{d/2} [p(1-p)]^{d/2} + \sum_{i=1+d/2}^{d} \binom{d}{i} p^i (1-p)^{d-i} & \text{for } d \text{ even} \end{cases} \tag{64}$$

where p is the probability of channel bit error. The probability of channel bit error, or probability of coded bit error, is given by the P_b appropriate to the modulation type with the substitution $\overline{\gamma_b} \to r\overline{\gamma_b}$. For example, if BPSK modulation is used and the channel is a Rayleigh fading channel, then from (36) we get

$$p = \frac{1}{2} \left(1 - \sqrt{\frac{r\overline{\gamma_b}}{1 + r\overline{\gamma_b}}} \right) \tag{65}$$

When evaluating (57), typically only the first five or six terms are used since the series converges rapidly as long as the received signal-to-noise ratio $\overline{\gamma_{b_C}} = r\overline{\gamma_b}$ is greater than the signal-to-noise ratio at cutoff [1]

$$\gamma_{b_0} = \frac{-1}{r} \ln \left(2^{1-r} - 1 \right) \tag{66}$$

For $\overline{\gamma_{b_C}} < \gamma_{b_0}$, (57) rapidly diverges and predicts the absurd result $P_b > 1$.

The free distances and the first eight B_ds of commonly used $r = 1/2$ convolutional codes are listed in Table 4, and the corresponding generator polynomials are listed in Table 5 [6]. The free distances and the first eight B_ds of commonly used $r = 1/3$ convolutional codes are listed in Table 6, and the corresponding generator polynomials are listed in Table 7 [6]. The free distances, the first five B_ds, and the generator polynomials of commonly used $r = 2/3$ and $r = 3/4$ convolutional codes are listed in Tables 8 and 9, respectively [7].

Table 4: Best (maximum free distance) rate 1/2, convolutional code information weight structure.

ν	d_{free}	$B_{d_{free}}$	$B_{d_{free}+1}$	$B_{d_{free}+2}$	$B_{d_{free}+3}$	$B_{d_{free}+4}$	$B_{d_{free}+5}$	$B_{d_{free}+6}$	$B_{d_{free}+7}$
3	5	1	4	12	32	80	192	448	1024
4	6	2	7	18	49	130	333	836	2069
5	7	4	12	20	72	225	500	1324	3680
6	8	2	36	32	62	332	701	2342	5503
7	10	36	0	211	0	1404	0	11633	0
8	10	2	22	60	148	340	1008	2642	6748
9	12	33	0	281	0	2179	0	15035	0

Table 5: Best (maximum free distance) rate 1/2, convolutional code generators (in octal).

ν	Generators	d_{free}	$B_{d_{free}}$	$A_{d_{free}}$
3	7, 5	5	1	1
4	17, 15	6	2	1
5	35, 23	7	4	2
6	75, 53	8	2	1
7	171, 133	10	36	11
8	371, 247	10	2	1
9	753, 561	12	33	11

Table 6: Best (maximum free distance) rate 1/3, convolutional code information weight structure.

ν	d_{free}	$B_{d_{free}}$	$B_{d_{free}+1}$	$B_{d_{free}+2}$	$B_{d_{free}+3}$	$B_{d_{free}+4}$	$B_{d_{free}+5}$	$B_{d_{free}+6}$	$B_{d_{free}+7}$
3	8	3	0	15	0	58	0	201	0
4	10	6	0	6	0	58	0	118	0
5	12	12	0	12	0	56	0	320	0
6	13	1	8	26	20	19	62	86	204
7	15	7	8	22	44	22	-	-	-
7	14	1	0	20	0	53	0	184	0
8	16	1	0	24	0	113	0	287	0

Table 7: Best (maximum free distance) rate 1/3, convolutional code generators (in octal).

ν	Generators	d_{free}	$B_{d_{free}}$	$A_{d_{free}}$
3	7, 7, 5	8	3	2
4	17, 15, 13	10	6	3
5	37, 33, 25	12	12	5
6	75, 53, 47	13	1	1
7	171, 165, 133	15	7	-
7	171, 145, 133	14	1	1
8	367, 331, 225	16	1	1

Table 8: Generator polynomials (in octal) and information weight structure for the best (maximum free distance) rate 2/3, punctured convolutional codes having 2^K states and only two different generator polynomials.

K	Generators	d_{free}	$B_{d_{free}}$	$B_{d_{free}+1}$	$B_{d_{free}+2}$	$B_{d_{free}+3}$	$B_{d_{free}+4}$
2	7,5,7	3	1	10	54	226	853
3	15,13,15	4	8	34	180	738	2989
4	31,33,31	5	25	112	357	1858	8406
5	73,41,73	6	75	0	1571	0	31474
6	163,135,163	6	1	81	402	1487	6793
7	337,251,337	8	395	0	6695	0	235288
8	661,473,661	8	97	0	2863	0	56633

Table 9: Generator polynomials (in octal) and information weight structure for the best (maximum free distance) rate 3/4, punctured convolutional codes having 2^K states and only two different generator polynomials.

K	Generators	d_{free}	$B_{d_{free}}$	$B_{d_{free}+1}$	$B_{d_{free}+2}$	$B_{d_{free}+3}$	$B_{d_{free}+4}$
2	5,7,5,7	3	15	104	540	2520	11048
3	15,17,15,17	4	124	0	4504	0	124337
4	25,37,37,37	4	22	0	1687	0	66964
5	61,53,53,53	5	78	572	3831	24790	152108
6	135,163,163,163	6	919	0	31137	0	1142571
6	121,165,121,165	5	21	252	1903	11995	72115
7	205,307,307,307	6	117	0	8365	0	319782
8	515,737,737,737	6	12	342	1996	12296	78145

3.2 Numerical Results for Hard Decision Decoding

The probability of information bit error as a function of the probability of channel bit error p for systems with convolutional source coding and hard decision decoding is plotted in Figures 11 and 12. Figure 11 is a plot of the performance obtained with a $r = 1/2$ convolutional code with constraint lengths of $\nu = 5$, $\nu = 7$, and $\nu = 9$. Figure 12 is a plot of the performance obtained with a convolutional code implemented with $K = 6$ memory elements with code rates of $r = 1/3$, $r = 1/2$, $r = 2/3$, and $r = 3/4$. For rate $r = 1/n$ codes, $K = 6$ corresponds to $\nu = 7$. The performance plotted in Figures 11 and 12 is independent on the type of noise affecting the signal, modulation type, and whether or not channel fading is a factor. The only restriction on the results plotted in Figures 11 and 12 is the requirement that the channel be memoryless, that is, channel bit errors occur independently.

The probability of bit error as a function of E_b/N_0 for BPSK or QPSK in AWGN with $r = 1/2$ convolutional source coding and hard decision decoding is plotted in Figures 13 and 14 for no channel fading and Rayleigh fading, respectively.

As an example of how to use Figures 11 and 12, suppose we plan to use BPSK over a Rayleigh fading channel and require $P_b = 10^{-5}$. From Figure 11, we see that we require $p = 0.017$ if we use a $r = 1/2$, $\nu = 7$ convolutional code. From Figure 2, we see that for BPSK with Rayleigh fading, for $p = 0.017$ we require a channel signal-to-noise ratio $E_{b_c}/N_0 = 11.5$ dB. From 61, we get $E_b = 2E_{b_c}$ since $r = 1/2$, so $E_b/N_0 = 14.5$ dB is required in order to achieve the target of $P_b = 10^{-5}$. Without error correction coding, $E_b/N_0 = 44$ dB is required, so in this example, the coding gain is 29.5 dB. As a cross-check, for this example we can obtain the same result directly from Figure 14.

3.3 Punctured Convolutional Codes

A *punctured* code is one where one or more parity bits have been systematically deleted [8]. Convolutional codes can be punctured to achieve a higher rate code from the same encoder. Consider the output of a rate 1/2 convolutional code: $v_0^{(1)}v_0^{(2)}, v_1^{(1)}v_1^{(2)}, v_2^{(1)}v_2^{(2)}, v_3^{(1)}v_3^{(2)}, v_4^{(1)}v_4^{(2)}, \ldots$ If this code is punctured by deleting every fourth bit, then the resulting code sequence has three code bits for every two message bits resulting in a rate 2/3 punctured code: $v_0^{(1)}v_0^{(2)}, v_1^{(1)}e, v_2^{(1)}v_2^{(2)}, v_3^{(1)}e, v_4^{(1)}v_4^{(2)}, \ldots$ If the receiver inserts erasures at the location of punctured bits, then the same decoder can be used for either the $r = 1/2$ code or the $r = 2/3$ punctured code. Since the same encoder and decoder can be used, puncturing provides a straightforward method of implementing variable rate error control coding.

Several wireless standards, both for voice and data communications, such as *Large Area Syn-*
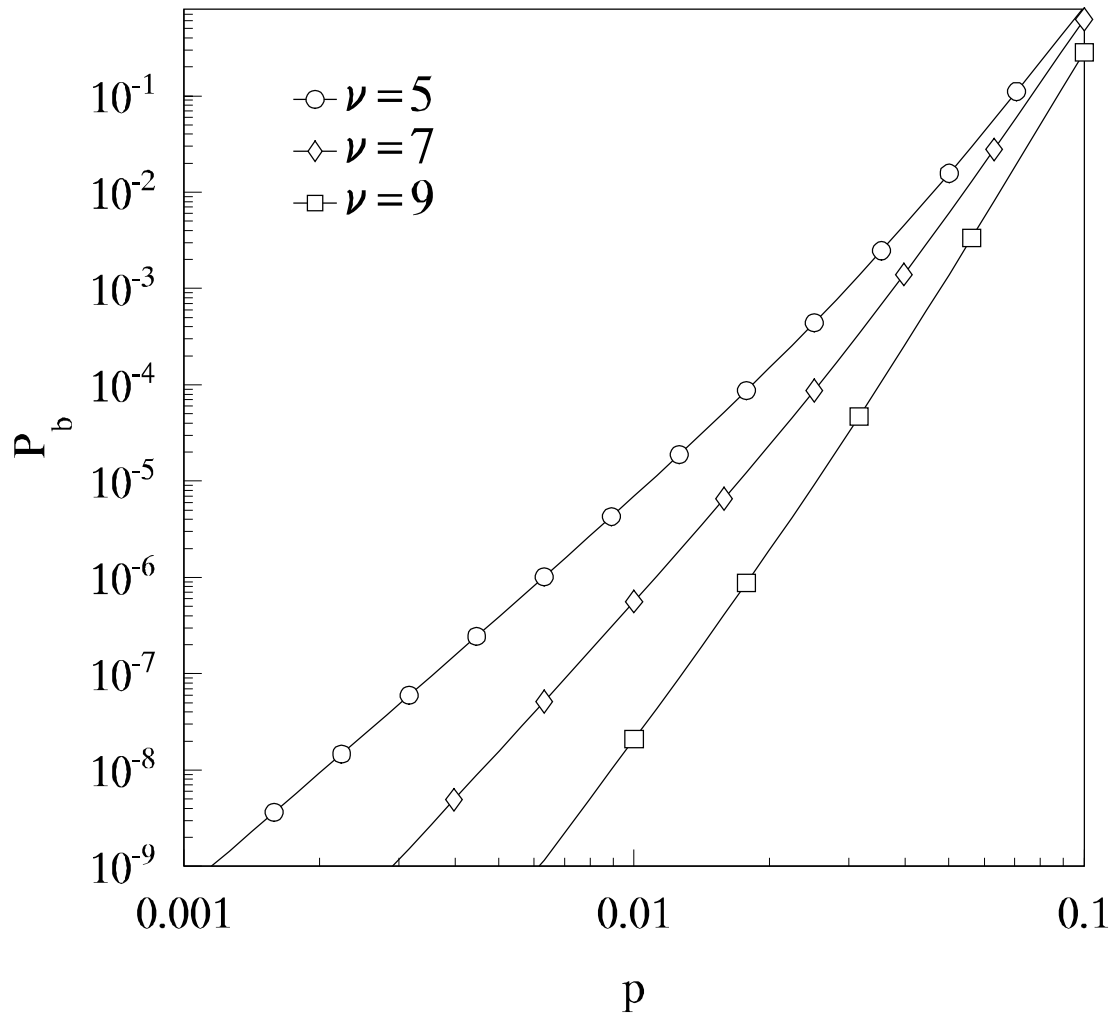
Figure 11: Performance of systems with $r = 1/2$ convolutional source coding and hard decision decoding.
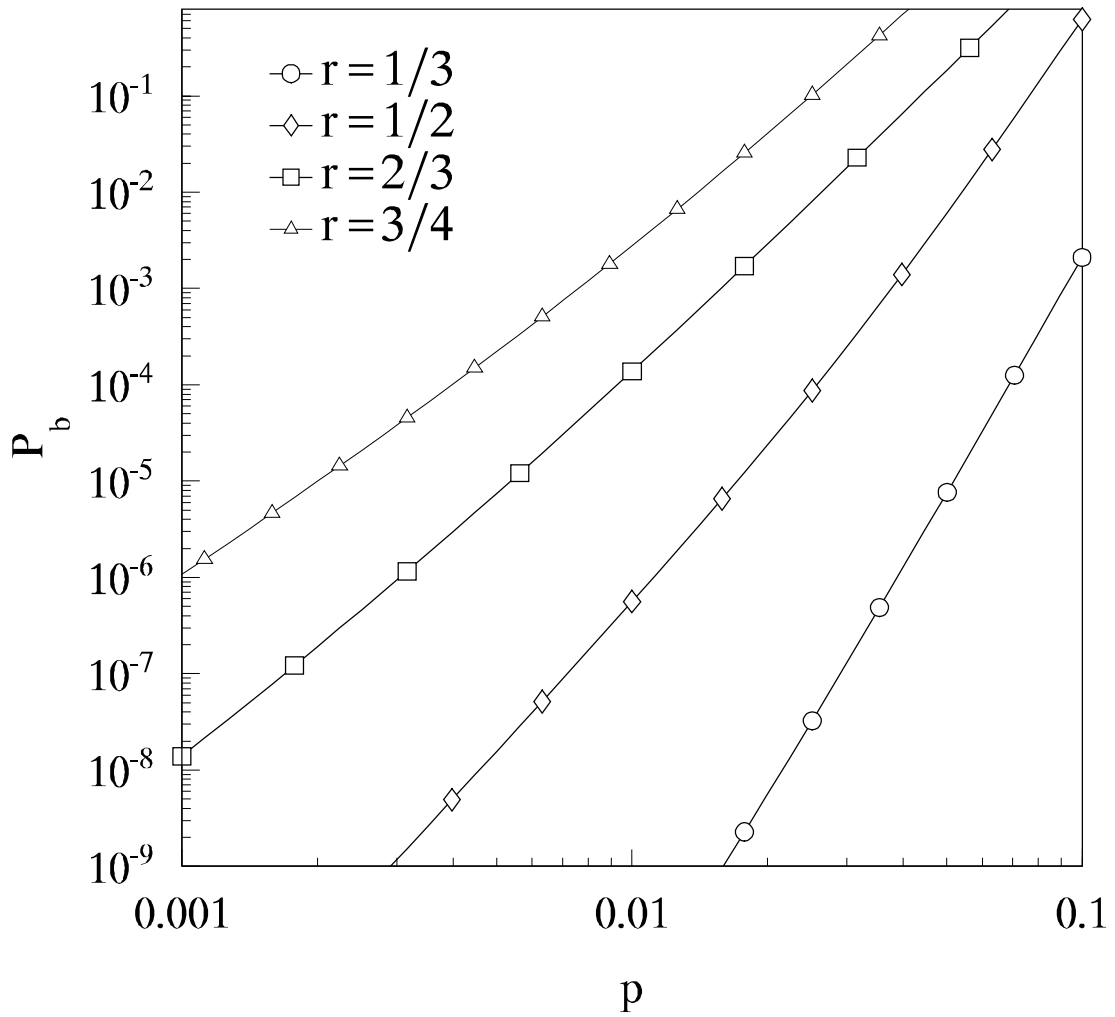
Figure 12: Performance of systems with $K = 6$ convolutional source coding and hard decision decoding.
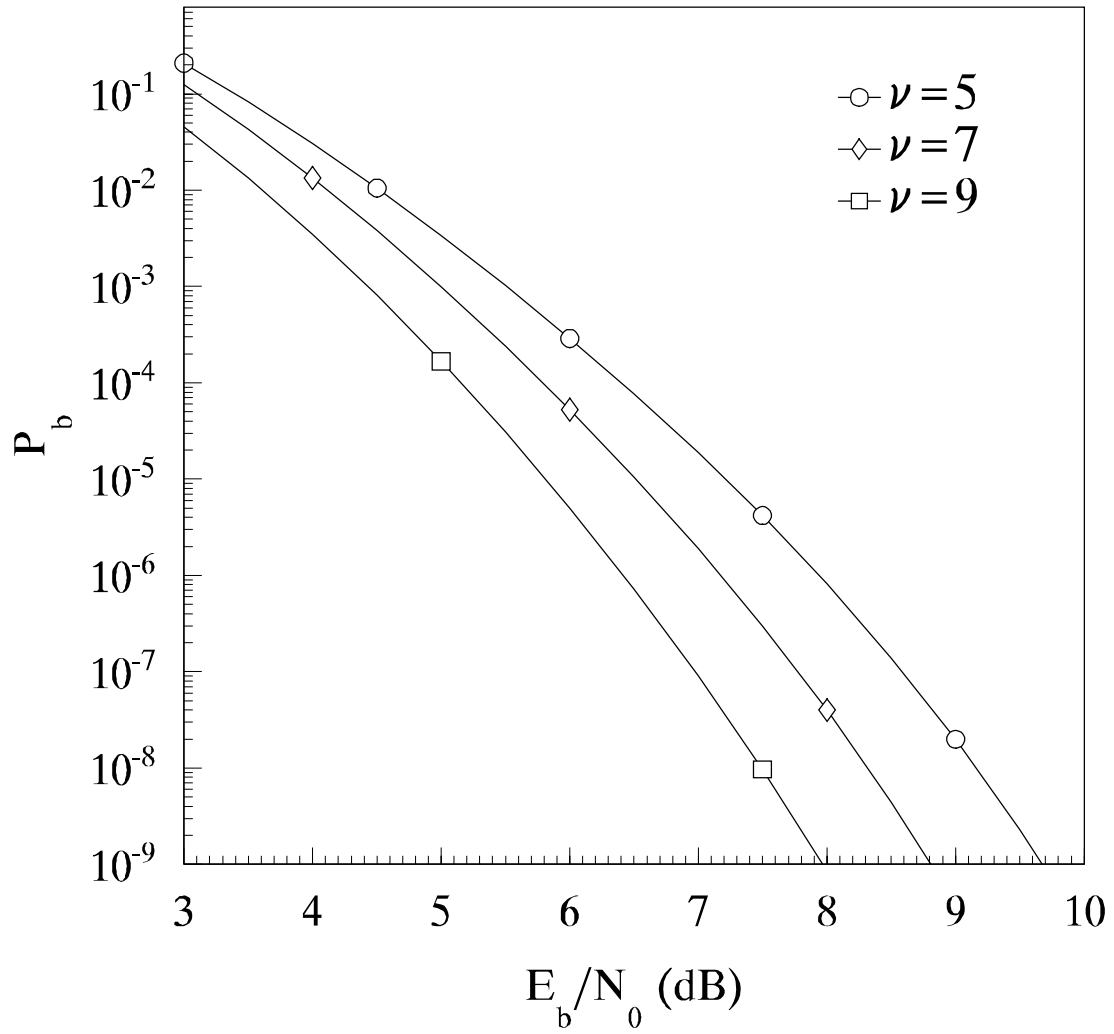
Figure 13: Performance of BPSK/QPSK in AWGN with $r = 1/2$ convolutional source coding and hard decision decoding.
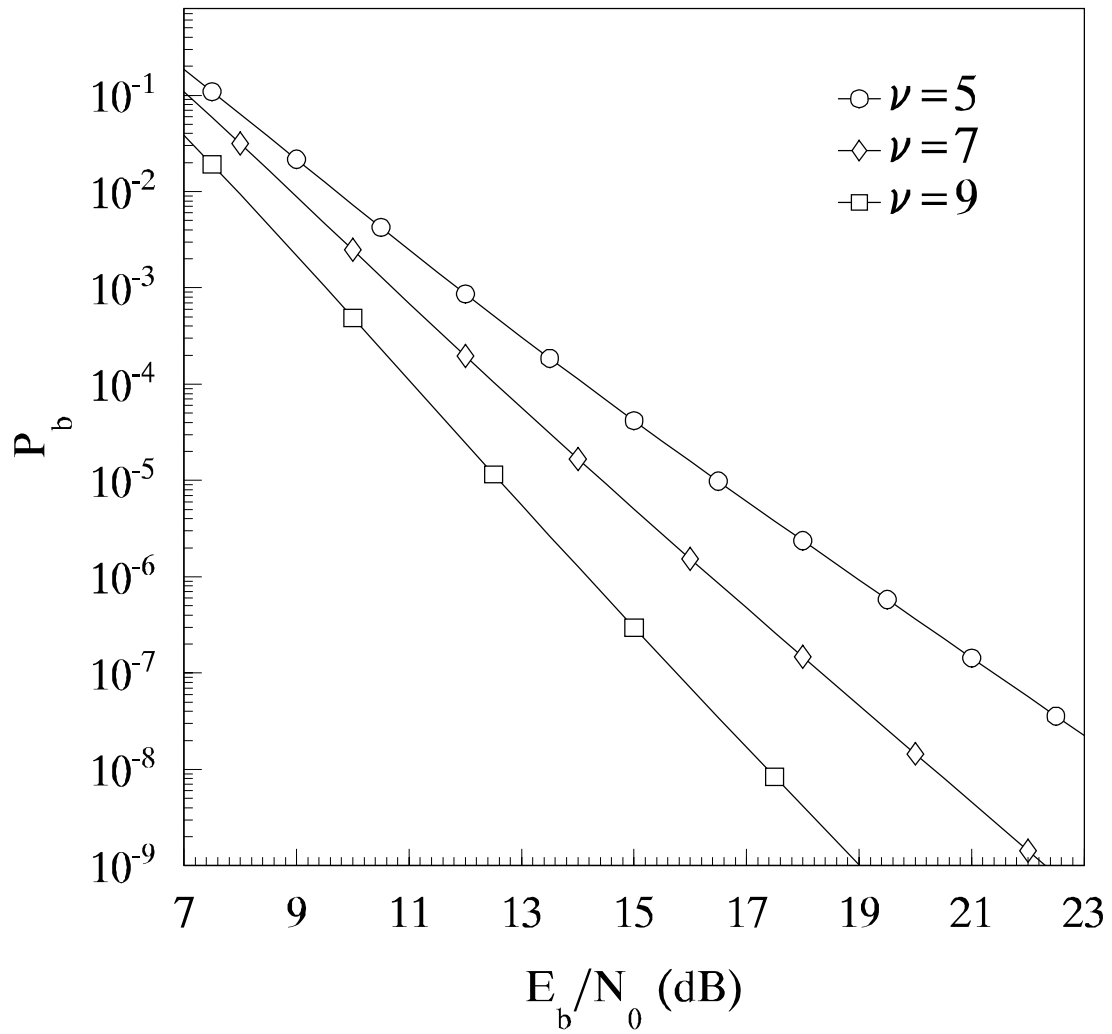
Figure 14: Performance of BPSK/QPSK in AWGN over a slow, flat Rayleigh fading channel with $r = 1/2$ convolutional source coding and hard decision decoding.

Table 10: Allowed combinations of modulation and code rates for the *IEEE 802.11a* WLAN standard.

R_b (Mb/s)	Modulation	Code rate
6	BPSK	1/2
9	BPSK	3/4
12	QPSK	1/2
18	QPSK	3/4
24	16-QAM	1/2
36	16-QAM	3/4
48	64-QAM	2/3
54	64-QAM	3/4

chronized Code-Division Multiple Access (LAS-CDMA), as well as wireless local area networks (WLAN), such as the *IEEE 802.11a* WLAN standard, achieve a variable information bit rate by different combinations of either binary or non-binary modulation and convolutional codes having different code rates. Higher data rates are achieved by combining a higher-order modulation with a high rate convolutional code, while lower data rates are obtained by lowering either the modulation order, the code rate, or both. For example, the *IEEE 802.11a* WLAN standard utilizes BPSK, QPSK, 16-QAM, and 64-QAM in combination with rate 1/2, 2/3, and 3/4 convolutional codes to obtain a variable data bit rate, where the rate 2/3 and rate 3/4 convolutional codes are obtained by puncturing the rate 1/2 convolutional code. The allowed combinations of modulation and code rates for the *IEEE 802.11a* WLAN standard are listed in Table 10.

As might be expected, puncturing reduces the free distance of the convolutional code. In general, there is not a single pair of generator polynomials that simultaneously provides the best $r = 1/2$ code as well as the best $r = 2/3$ and $r = 3/4$ punctured codes. The exception occurs for $K = 2$. If the best rate 1/2 codes are punctured to obtain higher rate codes, the coding gain of the higher rate codes is generally less than that obtained with the best punctured codes. In general, the best higher rate codes generally have better coding gain than the best higher rate punctured codes, which generally have better coding gains than the best higher rate punctured $r = 1/2$ codes, which in general have better coding gains than punctured codes obtained from the best $r = 1/2$ codes. The free distances, $B_{d_{free}}$, and the generator polynomials of the best (maximum free distance) $r = 2/3$ and $r = 3/4$ convolutional codes obtained by puncturing the best rate 1/2 convolutional codes are listed in Tables 11 and 12, respectively.

Table 11: Generator polynomials (in octal) and information weight structure for the best (maximum free distance) rate 2/3 convolutional code obtained by puncturing the best rate 1/2 convolutional codes having 2^K states.

K	Generators	d_{free}	$B_{d_{free}}$	$B_{d_{free}+1}$	$B_{d_{free}+2}$	$B_{d_{free}+3}$	$B_{d_{free}+4}$
2	7,5,7	3	1	10	54	226	853
3	15,17,15	4	10	-	-	-	-
4	23,35,23	4	1	-	-	-	-
5	53,75,75	6	96	-	-	-	-
6	133,171,133	6	3	-	-	-	-
7	247,371,371	7	47	-	-	-	-
8	561,753,561	7	11	-	-	-	-

Table 12: Generator polynomials (in octal) and information weight structure for the best (maximum free distance) rate 3/4 convolutional code obtained by puncturing the best rate 1/2 convolutional codes having 2^K states.

K	Generators	d_{free}	$B_{d_{free}}$	$B_{d_{free}+1}$	$B_{d_{free}+2}$	$B_{d_{free}+3}$	$B_{d_{free}+4}$
2	5,7,5,7	3	15	104	540	2520	11048
3	15,17,15,17	4	124	0	4504	0	124337
4	23,35,35,23	3	1	-	-	-	-
5	53,75,75,75	4	3	-	-	-	-
6	133,171,133,171	5	42	-	-	-	-
7	247,371,371,371	6	239	-	-	-	-
8	561,753,561,561	6	52	-	-	-	-

3.4 Convolutional Codes with Soft Decision Decoding

For soft decision decoding, the probability of bit error is upper bounded by (63), but P_d is no longer given by (64). In general, P_d is different for different modulation schemes and types of receiver.

3.4.1 Effective Weight d Path Signal-to-Noise Ratio

The probability of selecting a sequence that is a Hamming distance d from the actual transmitted code sequence P_d can often be expressed as a function of the *effective weight d path signal-to-noise ratio*

$$\gamma_d = \sum_{i=1}^{d} \gamma_{b_i} \tag{67}$$

where γ_{b_i} is the received average energy per information bit-to-noise power spectral density ratio of the signal representing the ith incorrect channel bit on the selected sequence. When there is no channel fading, $\gamma_{b_i} = \gamma_b$ is simply a parameter, and

$$\gamma_d = d\gamma_b \tag{68}$$

For fading channels, γ_{b_i}, $i = 1, 2, \ldots, d$, are modeled as independent random variables, and γ_d is the sum of d independent random variables.

The Laplace transform of a function $f(x)$ is defined

$$F_X(s) = \mathcal{L}\{f_X(x)\} = \int_0^\infty f_X(x)e^{-sx}\,dx \tag{69}$$

and the inverse Laplace transform is defined

$$f_X(x) = \mathcal{L}^{-1}\{F_X(s)\} \tag{70}$$

Since for fading channels γ_d is the sum of d independent random variables, the Laplace transform of the probability density function of γ_d is given by

$$F_{\Gamma_d}(s) = \mathcal{L}\{f_{\Gamma_d}(\gamma_d)\} = F_{\Gamma_{b_i}}^d(s) \tag{71}$$

where

$$F_{\Gamma_{b_i}}(s) = \mathcal{L}\left\{f_{\Gamma_{b_i}}(\gamma_{b_i})\right\} \tag{72}$$

is the Laplace transform of the probability density function of γ_{b_i}. For Ricean fading channels,

$$f_{\Gamma_{b_i}}(\gamma_{b_i}) = \frac{\sigma_0^2}{2\sigma^2}\exp\left[\frac{-(\gamma_{b_i}\sigma_0^2 + \alpha^2)}{2\sigma^2}\right] I_0\left(\frac{\alpha\sqrt{\gamma_{b_i}\sigma_0^2}}{\sigma^2}\right) u(\gamma_{b_i}) \tag{73}$$

where $\sigma_0^2 = N_0/T_b$. Substituting (73) into (69), we get

$$F_{\Gamma_{b_i}}(s) = \int_0^\infty \frac{\sigma_0^2}{2\sigma^2} \exp\left[\frac{-(\gamma_{b_i}\sigma_0^2 + \alpha^2)}{2\sigma^2}\right] I_0\left(\frac{\alpha\sqrt{\gamma_{b_i}\sigma_0^2}}{\sigma^2}\right) \exp\left(-s\gamma_{b_i}\right) d\gamma_{b_i} \tag{74}$$

Using (29) and (30), we can evaluate (74) to obtain

$$F_{\Gamma_{b_i}}(s) = \frac{\sigma_0^2}{2\sigma^2}\left(\frac{1}{s + \sigma_0^2/2\sigma^2}\right) \exp\left[\frac{-\alpha^2}{2\sigma^2}\left(\frac{s}{s + \sigma_0^2/2\sigma^2}\right)\right] \tag{75}$$

We have the identities [9]

$$\mathcal{L}\left\{e^{-az}f(z)\right\} = F_Z(s + a) \tag{76}$$

and

$$\mathcal{L}\left\{a^{-\nu/2}z^{\nu/2}I_\nu\left(2\sqrt{az}\right)\right\} = \frac{1}{s^{\nu+1}}\exp(a/s), \ \nu > -1 \tag{77}$$

Substituting (75) into (71) and using (76) and (77), we obtain

$$f_{\Gamma_d}(\gamma_d) = \frac{\gamma_d^{(d-1)/2}}{(d\alpha^2/\sigma_0^2)^{(d-1)/2}\, 2\sigma^2/\sigma_0^2} \exp\left[\frac{-(\gamma_d + d\alpha^2/\sigma_0^2)}{2\sigma^2/\sigma_0^2}\right] I_{d-1}\left(\frac{\alpha\sigma_0\sqrt{d\gamma_d}}{\sigma^2}\right) u\left(\gamma_d\right) \tag{78}$$

For Rayleigh fading, this reduces to

$$f_{\Gamma_d}(\gamma_d) = \frac{\gamma_d^{d-1}}{\overline{\gamma_b}^d(d-1)!}\, e^{-\gamma_d/\overline{\gamma_b}}\, u\left(\gamma_d\right) \tag{79}$$

where $\overline{\gamma_b} = 2\sigma^2/\sigma_0^2$.

3.4.2   Soft Decision Detection with BPSK and GMSK

For soft decision detection with BPSK or GMSK, we assume that the receiver is a *maximal ratio combiner* [1], in which case

$$P_d\left(\gamma_d\right) = Q\left(\sqrt{br\gamma_d}\right) \tag{80}$$

where b is given in Table 1, and

$$P_d = \int_0^\infty P_d(\gamma_d) f_{\Gamma_d}(\gamma_d)\, d\gamma_d \tag{81}$$

Substituting (79) and (80) into (81), we obtain for the special case of Rayleigh fading

$$P_d = \left(\frac{1-\mu}{2}\right)^d \sum_{m=0}^{d-1}\left(\begin{array}{c} d-1+m \\ m \end{array}\right)\left(\frac{1+\mu}{2}\right)^m \tag{82}$$

where

$$\mu = \sqrt{\frac{br\overline{\gamma_b}}{2 + br\overline{\gamma_b}}} \tag{83}$$

37

We have the identity [3]

$$\int_0^\infty x^{m+n/2} e^{-\alpha x} J_n \left(2\beta\sqrt{x}\right) dx = \frac{m! \beta^n}{\alpha^{m+n+1}} e^{-\beta^2/\alpha} \mathcal{L}_m^n \left(\beta^2/\alpha\right) \tag{84}$$

where $\mathcal{L}_m^n(\bullet)$ is a Laguerre polynomial and is defined

$$\mathcal{L}_m^n \left(\beta^2/\alpha\right) = \sum_{p=0}^m \frac{(-1)^p}{p!} \left(\begin{array}{c} m+n \\ m-p \end{array}\right) \left(\frac{\beta^2}{\alpha}\right)^p \tag{85}$$

Note that

$$\mathcal{L}_0^n(x) = 1 \tag{86}$$

$$\mathcal{L}_1^n(x) = n+1-x \tag{87}$$

Approximating the Q-function in the same manner as in Section 2.1.2, we get

$$P_d(\gamma_d) \approx \frac{1}{2\sqrt{\pi rc}} \exp\left(\frac{-br\gamma_d}{2}\right) \tag{88}$$

where $c = 1.0 + 0.1\zeta$ and is obtained empirically. Substituting (78) and (88) into (81), we get

$$P_d = \frac{\exp\left(\frac{-d\alpha^2}{2\sigma^2}\right)}{4\sqrt{\pi rc}} \int_0^\infty \frac{\gamma_d^{(d-1)/2}}{(d\alpha^2/\sigma_0^2)^{(d-1)/2} \sigma^2/\sigma_0^2} \exp\left[-\gamma_d \left(\frac{rb}{2} + \frac{\sigma_0^2}{2\sigma^2}\right)\right] I_{d-1}\left(\frac{\alpha\sigma_0\sqrt{d\gamma_d}}{\sigma^2}\right) d\gamma_d \tag{89}$$

Using (30), (84), and (86), we can evaluate (89) to obtain

$$P_d = \frac{1}{2\sqrt{\pi rc}} \left(\frac{2}{2 + br2\sigma^2/\sigma_0^2}\right)^d \exp\left[\frac{-brd\alpha^2}{\sigma_0^2} \left(\frac{1}{2 + br2\sigma^2/\sigma_0^2}\right)\right] \tag{90}$$

From (33) and (34), we get

$$\overline{\gamma_b} = \frac{2\sigma^2}{\sigma_0^2} (1+\zeta) \tag{91}$$

and

$$\overline{\gamma_b} = \frac{\alpha^2}{\sigma_0^2} \left(\frac{1+\zeta}{\zeta}\right) \tag{92}$$

Substituting (91) and (92) into (90), we get

$$P_d = \frac{1}{2\sqrt{\pi rc}} \left[\frac{2(1+\zeta)}{2(1+\zeta) + br\overline{\gamma_b}}\right]^d \exp\left[\frac{-brd\zeta\overline{\gamma_b}}{2(1+\zeta) + br\overline{\gamma_b}}\right] \tag{93}$$

38

3.5 Numerical Results for Soft Decision Decoding

The probability of bit error as a function of E_b/N_0 for BPSK or QPSK in AWGN with rate $r = 1/2$ convolutional source coding and soft decision decoding for several different constraint lengths is plotted in Figures 15 and 16 for no channel fading and Rayleigh fading, respectively, while the probability of bit error as a function of E_b/N_0 for BPSK or QPSK in AWGN with $K = 6$ convolutional source coding and soft decision decoding for several different code rates is plotted in Figures 17, 18, 19, and 20 for no channel fading, Rayleigh fading, Ricean fading with $\zeta = 4$, and Ricean fading with $\zeta = 10$, respectively.

A comparison of the exact and approximate probability of bit error for BPSK/QPSK in AWGN with rate $r = 1/2$ convolutional source coding and soft decision decoding for several different constraint lengths over a slow, flat Ricean fading channel for $\zeta = 4$ is shown in Figure 21. As can be seen, the approximate probability of bit error is accurate to within a few tenths of a dB for $10^{-3} > P_b > 10^{-6}$. Comparable results are obtained for other code rates and number of memory elements K and for other values of ζ.

Continuing the example from Section 3.2, we see from Figure 16 that for BPSK with Rayleigh fading, for $P_b = 10^{-5}$ we require $E_b/N_0 = 7.5$ dB. This represents a further 7 dB coding gain over that obtained with hard decision decoding for an overall coding gain of 36.5 dB when soft decision decoding is used.

3.6 Binary Block Codes with Hard Decision Decoding

When an (n, k) binary block code that can correct t channel bit errors in each block of n bits is employed, the probability of bit error is accurately approximated by [5]

$$P_b \approx \frac{1}{n} \sum_{i=t+1}^{n} i \binom{n}{i} p^i (1-p)^{n-i} \tag{94}$$

where p is the probability of channel bit error. As with convolutional codes, the probability of channel bit error, or probability of coded bit error, is given by the P_b appropriate to the modulation type with the substitution $\overline{\gamma_b} \to r\overline{\gamma_b}$. When n is large, the series in (60) is dominated by the first two or three terms. In computing (60), when n is large, numerical difficulties are sometimes encountered in computing the binomial coefficient for i small relative to n. In that case, we can use the upper bound

$$\frac{m^n}{n!} > \binom{m}{n} \tag{95}$$

which is very tight when $m >> n$.
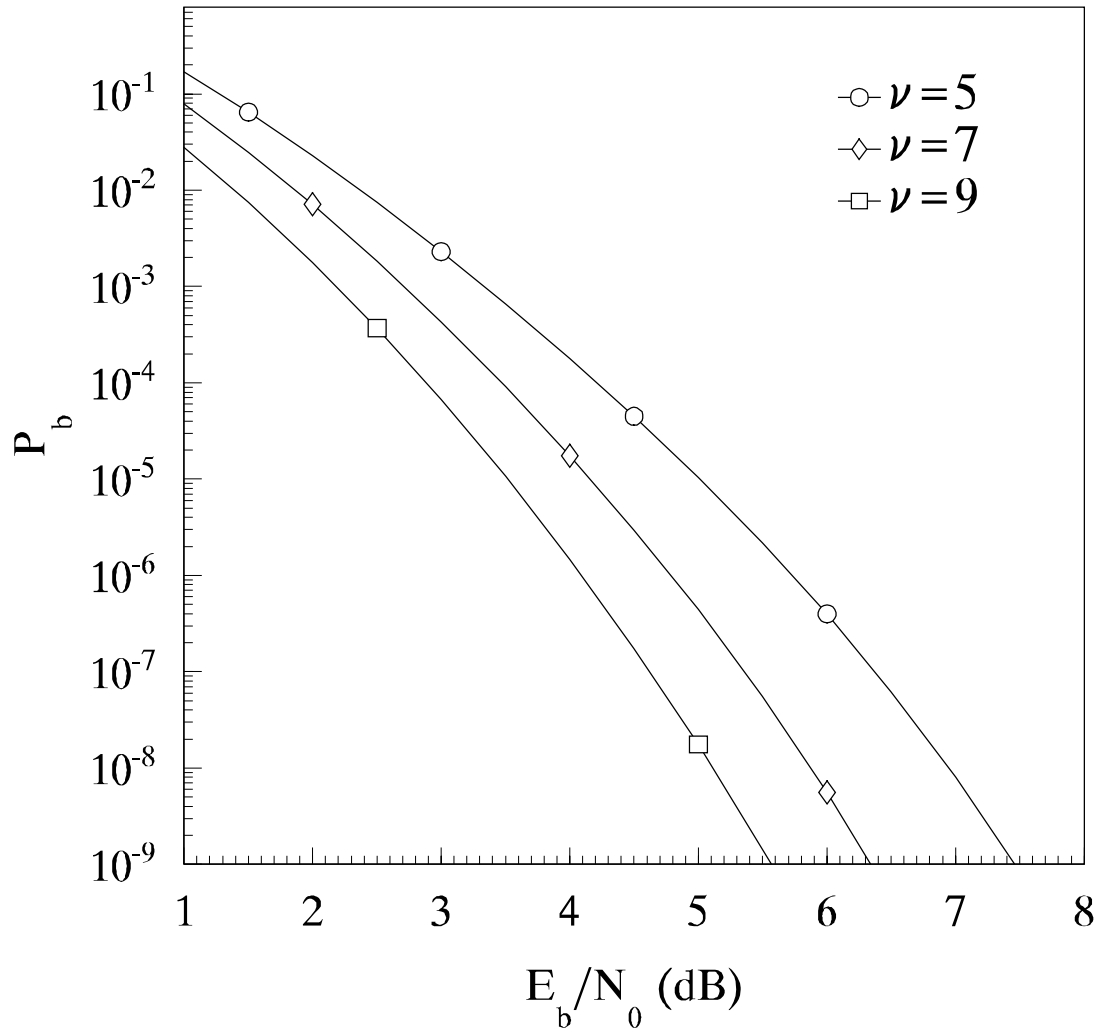
Figure 15: Performance of BPSK/QPSK in AWGN with $r = 1/2$ convolutional source coding and soft decision decoding.
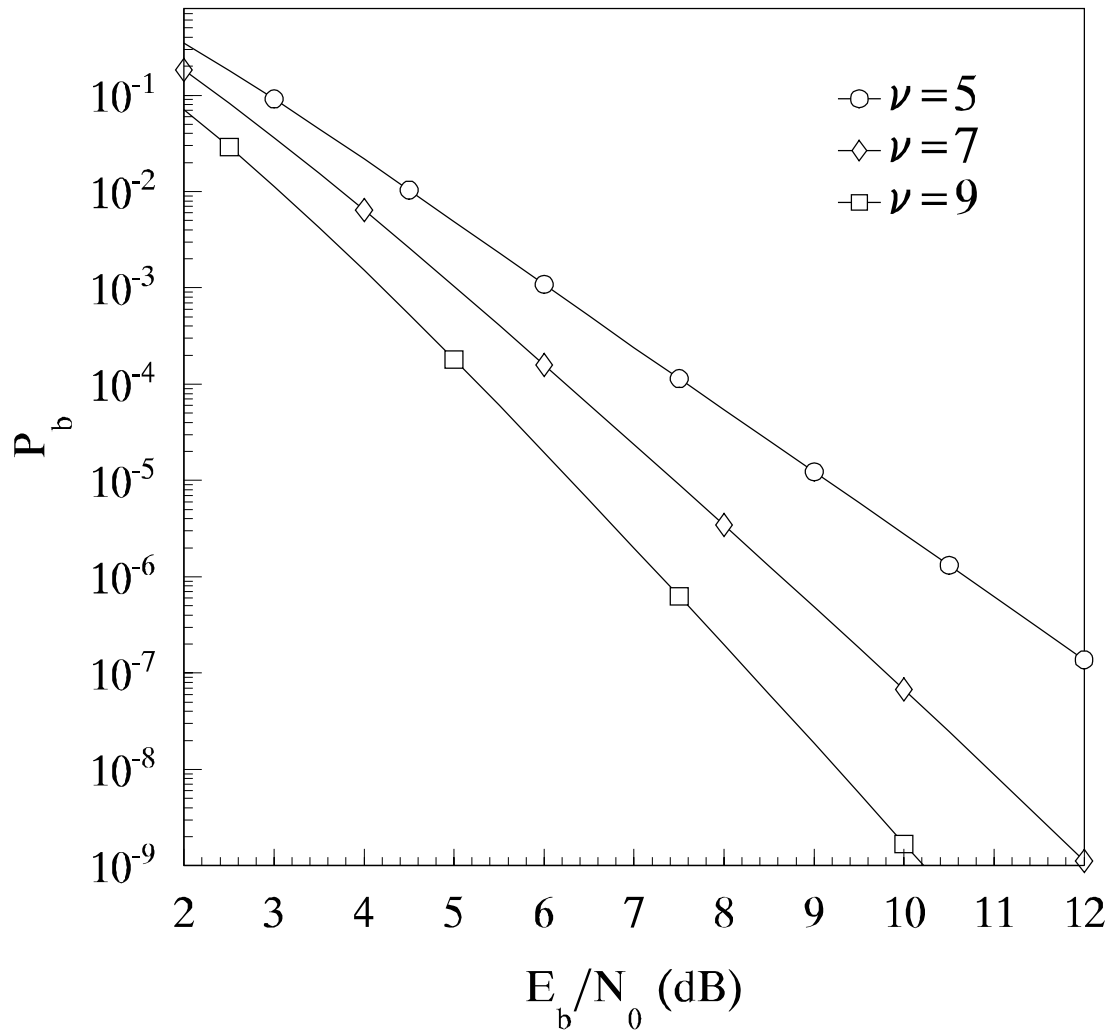
Figure 16: Performance of BPSK/QPSK in AWGN over a slow, flat Rayleigh fading channel with $r = 1/2$ convolutional source coding and soft decision decoding.
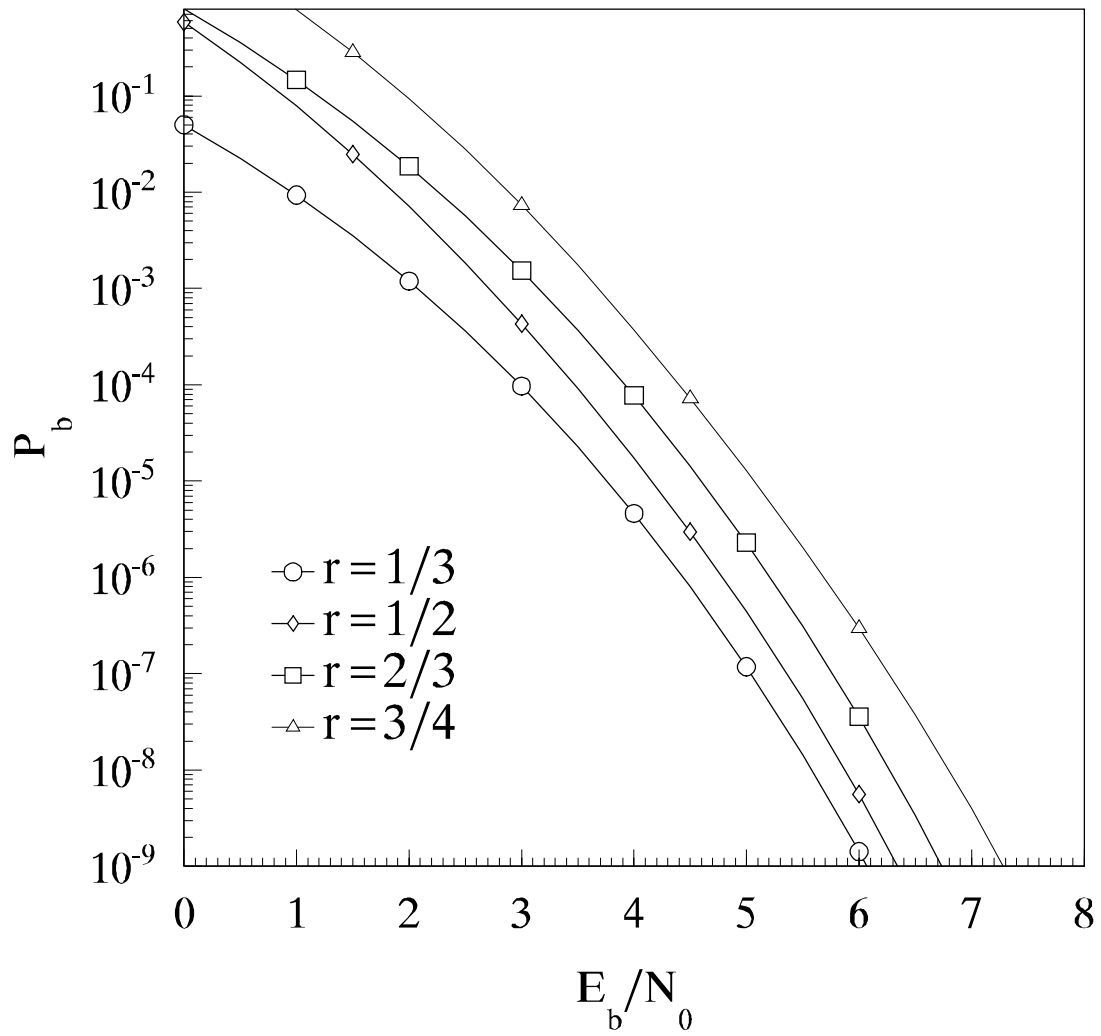
Figure 17: Performance of BPSK/QPSK in AWGN with $K = 6$ convolutional source coding and soft decision decoding.
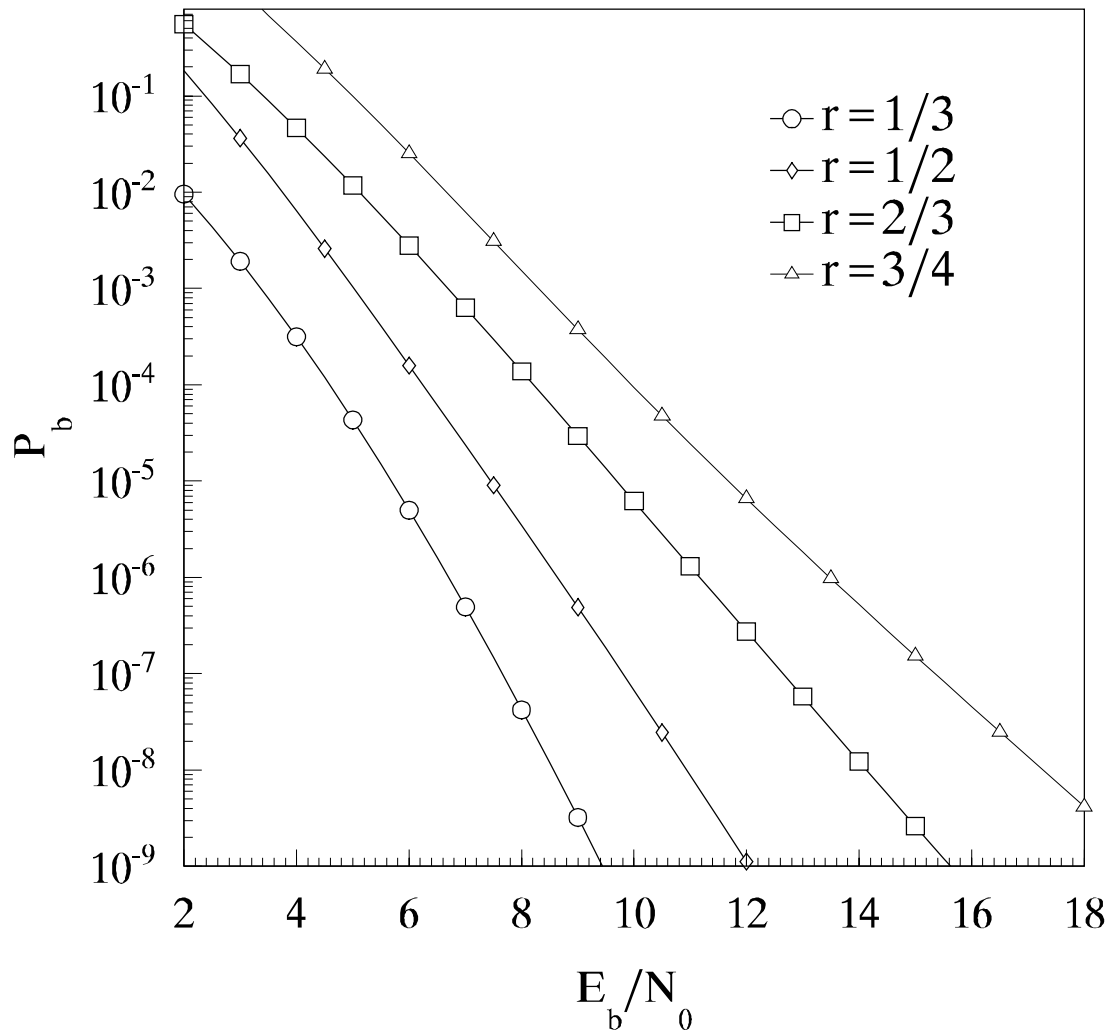
Figure 18: Performance of BPSK/QPSK in AWGN over a slow, flat Rayleigh fading channel with $K = 6$ convolutional source coding and soft decision decoding.
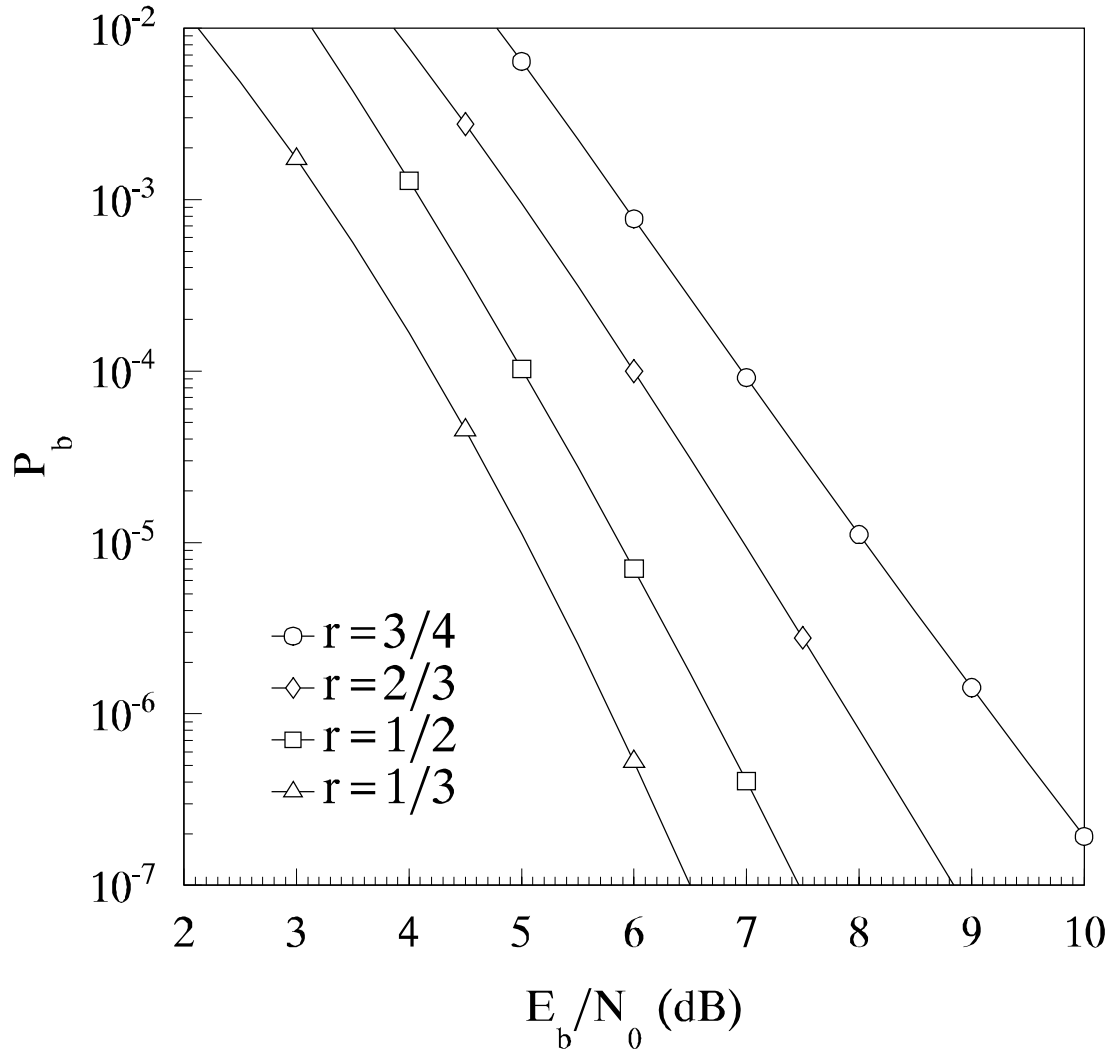
Figure 19: Performance of BPSK/QPSK in AWGN with $K = 6$ convolutional source coding and soft decision decoding over a slow, flat Ricean fading channel with $\zeta = 4$.
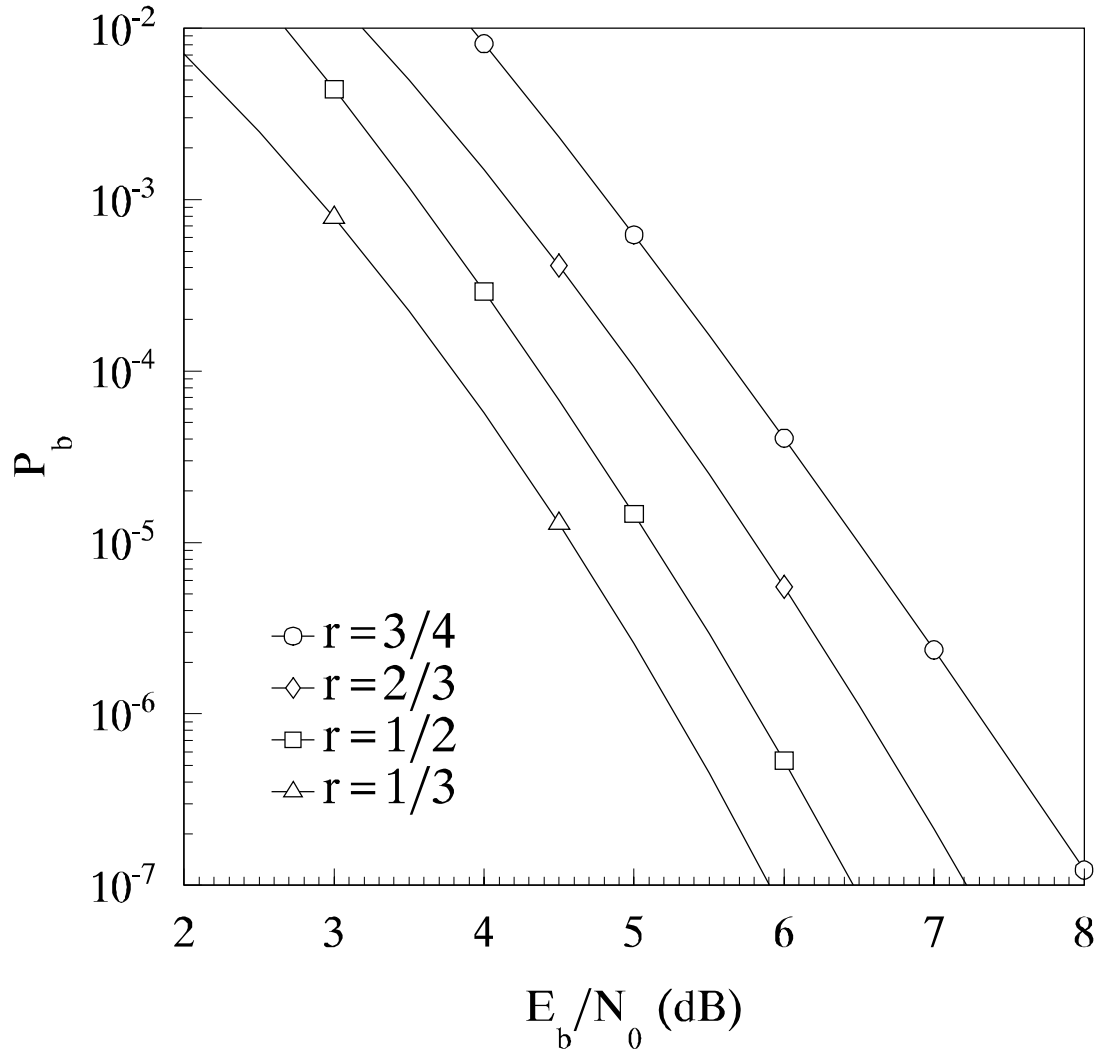
Figure 20: Performance of BPSK/QPSK in AWGN with $K = 6$ convolutional source coding and soft decision decoding over a slow, flat Ricean fading channel with $\zeta = 10$.
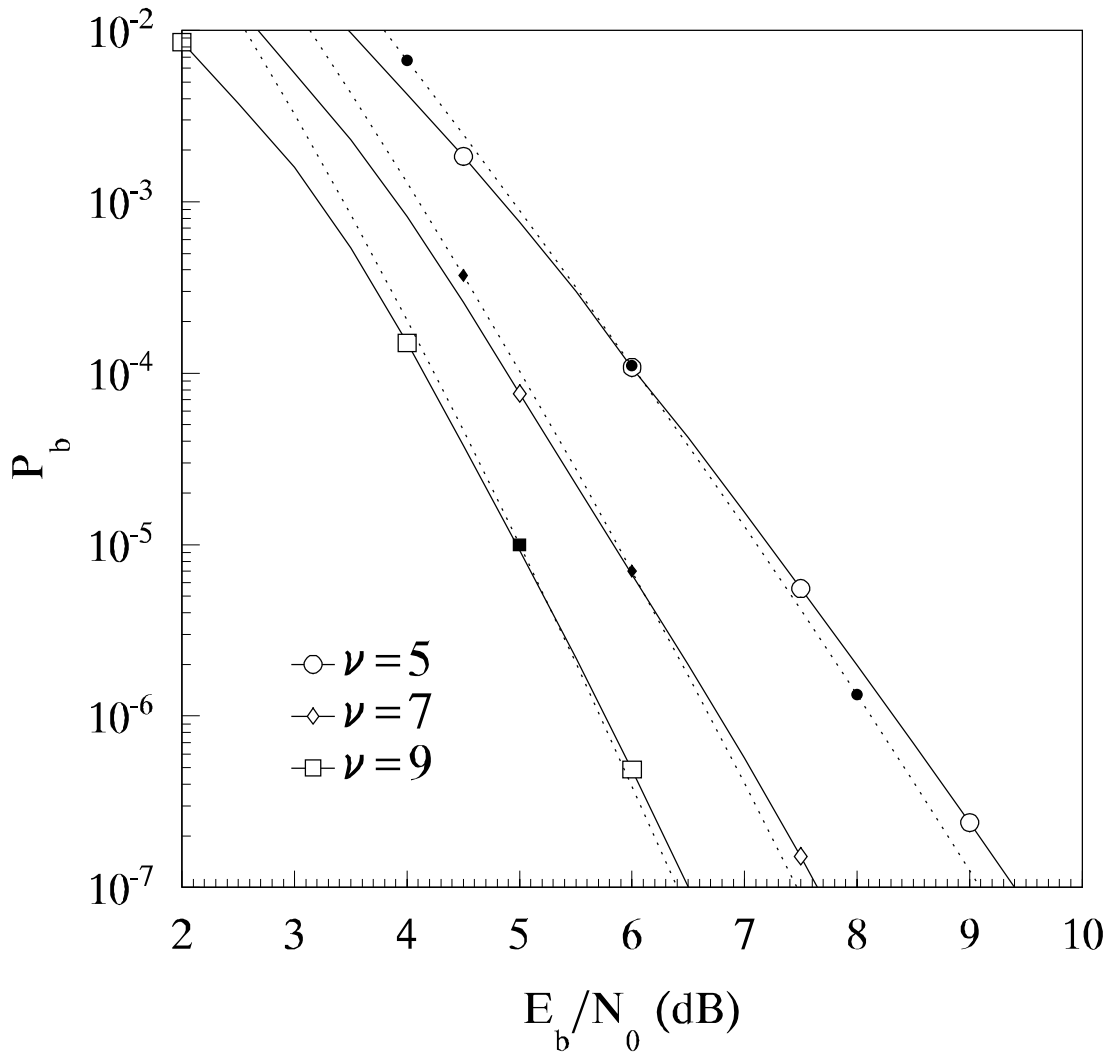
Figure 21: Comparison of exact and approximate performance of BPSK/QPSK in AWGN with $r = 1/2$ convolutional source coding and soft decision decoding over a slow, flat Ricean fading channel with $\zeta = 4$. Approximate results are plotted with a dotted line and indicated by solid symbols; exact results are plotted with a solid line and open symbols.

3.7 Reed-Solomon Codes with Binary Modulation and Hard Decision Decoding

When an (n, k) Reed-Solomon code that can correct t channel symbol errors in each block of n symbols is used with binary modulation, the probability of symbol error is accurately approximated by [5]

$$P_s \approx \frac{1}{n} \sum_{i=t+1}^{n} i \begin{pmatrix} n \\ i \end{pmatrix} p_s^i (1 - p_s)^{n-i} \tag{96}$$

where for m bits per Reed-Solomon symbol

$$p_s = 1 - (1 - p)^m \tag{97}$$

and p is the probability of channel bit error. As with convolutional codes and binary block codes, the probability of channel bit error, or probability of coded bit error, is given by the P_b appropriate to the modulation type with the substitution $\overline{\gamma_b} \to r\overline{\gamma_b}$.

In the case of binary modulation and a non-binary error correcting code such as we have here, we cannot obtain an exact analytic expression for the probability of bit error but must rely on upper and lower bounds, which are given by

$$P_s \geq P_b \geq \frac{P_s}{m} \tag{98}$$

3.8 Reed-Solomon Codes with M-ary Modulation and Hard Decision Decoding

When an (n, k) Reed-Solomon code that can correct t channel symbol errors in each block of n symbols is used with orthogonal M-ary modulation such as MFSK and $M = 2^m$, the probability of bit error is accurately approximated by

$$P_b \approx \frac{n+1}{2n^2} \sum_{i=t+1}^{n} i \begin{pmatrix} n \\ i \end{pmatrix} p_s^i (1 - p_s)^{n-i} \tag{99}$$

where p_s is the probability of *coded symbol* error for the M-ary modulation used. When $M \neq 2^m$ or when non-orthogonal modulation, such as MPSK or MQAM, is used, then the probability of symbol error is given by (96), and the probability of bit error can only be upper and lower bounded using (98). For MPSK or MQAM, p_s in (96) is the probability of *coded symbol* error for the M-ary modulation used, just as in (99). For orthogonal M-ary modulation when $M \neq 2^m$, the appropriate p_s must be determined as was done for the case of binary modulation in the last subsection.

THIS PAGE INTENTIONALLY LEFT BLANK

4 Narrowband Noise Interference

In this section, the effect of narrowband noise interference on various digital communications signals is investigated. Narrowband noise is defined as any noise other than AWGN regardless of the actual bandwidth of the narrowband noise relative to the bandwidth of the communication signal. The narrowband noise may be due to either an intentional source, such as jamming noise, or an unintentional source, such as another communications system operating nearby in the same bandwidth as the desired signal. Although there are many different types of narrowband noise, in this report only narrowband noise with a flat PSD over the bandwidth of the noise, where the noise bandwidth is at least as large as the receiver bandwidth, is considered. This type of noise is equivalent to bandlimited AWGN.

4.1 Continuous Narrowband Noise Interference

For continuous narrowband noise interference with a flat PSD over the bandwidth of the noise and the noise bandwidth is at least as large as the receiver bandwidth, the noise interference affects the receiver as if it were AWGN. Since the noise interference and the AWGN can be modeled as independent random processes, the overall noise PSD is the sum of the PSD of the AWGN and the PSD of the noise interference. If we designate the one-sided noise PSD *at the receiver's matched filter input* by N_I, then the total noise PSD at the matched filter input is

$$N_T = N_0 + N_I \tag{100}$$

Now all of the expressions for probability of bit error P_b in Section 2, the probability of channel bit error p in Sections 3.1, 3.6, and 3.7, the expression for P_d in Section 3.4.2, and the probability of channel symbol error p_s in Section 3.8 can be modified to take continuous narrowband noise interference into account by replacing $\overline{\gamma_b}$ defined by (15) with

$$\overline{\gamma_b} = \frac{E_b}{N_0 + N_I} \tag{101}$$

Rearranging (101), we get

$$\overline{\gamma_b} = \left[\left(\frac{E_b}{N_0} \right)^{-1} + \left(\frac{E_b}{N_I} \right)^{-1} \right]^{-1} \tag{102}$$

When narrowband noise interference is present, an important figure of merit is the ratio of interference power-to-signal power J/S. Since the average received signal power is $S = E_b/T_b$ and the average received noise interference power at the input to the matched filter is $J = N_I/T_b$, (102) can be expressed in terms of J/S:

$$\overline{\gamma_b} = \left[\left(\frac{E_b}{N_0} \right)^{-1} + \frac{J}{S} \right]^{-1} \tag{103}$$

When $J/S >> (E_b/N_0)^{-1}$, (103) simplifies to

$$\overline{\gamma_b} \approx \left(\frac{J}{S}\right)^{-1} = \frac{S}{J} \qquad (104)$$

4.2 Continuous Narrowband Noise Interference Bandwidth and Received Power

The total narrowband noise interference power at the receiver input J_T is related to the noise PSD by

$$N_I = \frac{J_T}{B_I} \qquad (105)$$

where B_I is the bandwidth of the narrowband noise. It is assumed that $B_I \geq B_{eq}$, where B_{eq} is the receiver noise equivalent bandwidth, and that the bandwidth of the narrowband noise completely overlaps the bandwidth of the receiver. Of course, the relationship between the total narrowband noise interference power at the receiver input and the transmitted narrowband noise interference power has to be determined by a link budget analysis for the interference waveform. Link budgets are discussed in Section 8. The noise interference power coupled into the receiver is $J = N_I B_{eq}$, so the relationship between the interference noise power at the receiver input and that at the matched filter input is

$$J = J_T \frac{B_{eq}}{B_I} \qquad (106)$$

from which we see that the effect of the narrowband noise interference is maximized when $B_I = B_{eq}$.

4.3 Pulsed Narrowband Noise Interference

In some instances, digital communications systems may encounter narrowband noise interference that is not constant. In this section, the effect of pulsed-noise interference on digital communications systems is considered. The narrowband noise interference is assumed to have a PSD identical to the one assumed in Section 4.1, but in addition the narrowband noise is also assumed to turn on and off.

In order to make a fair comparison between the effect of continuous narrowband noise interference and that of pulsed-noise interference, we assume that the average received narrowband noise power is the same in each case. As a result, if we designate ρ as the fraction of time that the pulsed-noise interference is on, then the PSD of the pulsed-noise interference when it is present is given by

$$N_I' = \frac{N_I}{\rho} \qquad (107)$$

Clearly, when the narrowband noise is off, there is no effect on the receiver, and the performance is the same as when only AWGN is present. When the narrowband noise is on, the effect on the receiver is the same as for continuous narrowband noise interference where

$$\overline{\gamma_b} = \left[\left(\frac{E_b}{N_0}\right)^{-1} + \frac{J}{\rho S}\right]^{-1} \tag{108}$$

Since $1 \geq \rho > 0$, the effect of pulsed-noise interference is to increase the effect of the interference signal on the receiver when the pulsed-noise interference is present.

If we define T_R to be the time between the beginning of one pulse and the beginning of the next (i.e., $1/T_R$ is the repetition rate of the pulsed-noise interference), then for $\rho T_R >> T_s$, we can obtain the probability of bit error for the different modulation types discussed in Section 2 when pulsed-noise interference is present from

$$P_b = (1 - \rho) P_b \left(\overline{\gamma_b} = \frac{E_b}{N_0}\right) + \rho P_b \left\{\overline{\gamma_b} = \left[\left(\frac{E_b}{N_0}\right)^{-1} + \frac{J}{\rho S}\right]^{-1}\right\} \tag{109}$$

since ρ is the probability that a particular symbol is affected by the pulsed-noise interference and $(1 - \rho)$ is the probability that a particular symbol is affected by AWGN only.

When $J/S >> (E_b/N_0)^{-1}$ and $E_b/N_0 >> 1$, (109) is approximated by

$$P_b \approx \rho P_b \left[\overline{\gamma_b} = \left(\frac{J}{\rho S}\right)^{-1}\right] \tag{110}$$

Similarly, the probability of channel bit error used to obtain the probability of bit error with forward error correction coding and hard decision decoding discussed in Sections 3.1, 3.6, and 3.7 when pulsed-noise interference is present is given by

$$p = (1 - \rho) p \left(\overline{\gamma_b} = \frac{E_b}{N_0}\right) + \rho p \left\{\overline{\gamma_b} = \left[\left(\frac{E_b}{N_0}\right)^{-1} + \frac{J}{\rho S}\right]^{-1}\right\} \tag{111}$$

and when $J/S >> (E_b/N_0)^{-1}$ and $E_b/N_0 >> 1$, (111) is approximated by

$$p \approx \rho p \left[\overline{\gamma_b} = \left(\frac{J}{\rho S}\right)^{-1}\right] \tag{112}$$

Finally, the probability of channel symbol error used to obtain the probability of bit error with forward error correction coding and hard decision decoding discussed in Section 3.8 when pulsed-noise interference is present is given by

$$p_s = (1 - \rho) p_s \left(\overline{\gamma_b} = \frac{E_b}{N_0}\right) + \rho p_s \left\{\overline{\gamma_b} = \left[\left(\frac{E_b}{N_0}\right)^{-1} + \frac{J}{\rho S}\right]^{-1}\right\} \tag{113}$$

and when $J/S >> (E_b/N_0)^{-1}$ and $E_b/N_0 >> 1$, (113) is approximated by

$$p_s \approx \rho p_s \left[\overline{\gamma_b} = \left(\frac{J}{\rho S}\right)^{-1}\right] \tag{114}$$

4.4 BPSK with Narrowband Noise Interference

As an example, the performance of BPSK with AWGN and narrowband noise interference will be presented in this section for both no channel fading and Rayleigh fading. For no channel fading, from (16) and Table 1, we obtain

$$P_b = Q\left(\sqrt{2\gamma_b}\right) \tag{115}$$

since $\gamma_b = \overline{\gamma_b}$ when there is no channel fading, and for Rayleigh fading, from (24) and Table 1, we obtain

$$P_b = \frac{1}{2}\left(1 - \sqrt{\frac{1}{1 + (\overline{\gamma_b})^{-1}}}\right) \tag{116}$$

4.4.1 BPSK with Continuous Narrowband Noise Interference

Substituting (103) into (115) and (116), we get for no channel fading and for Rayleigh fading, respectively,

$$P_b = Q\left(\sqrt{2\left[\left(\frac{E_b}{N_0}\right)^{-1} + \frac{J}{S}\right]^{-1}}\right) \tag{117}$$

and

$$P_b = \frac{1}{2}\left(1 - \sqrt{\frac{1}{1 + \left(\frac{E_b}{N_0}\right)^{-1} + \frac{J}{S}}}\right) \tag{118}$$

When $J/S >> (E_b/N_0)^{-1}$, we get for no channel fading and for Rayleigh fading, respectively,

$$P_b \approx Q\left(\sqrt{2\left(\frac{J}{S}\right)^{-1}}\right) \tag{119}$$

and

$$P_b \approx \frac{1}{2}\left(1 - \sqrt{\frac{1}{1 + \frac{J}{S}}}\right) \tag{120}$$

The exact and approximate performance of BPSK with continuous narrowband noise interference and no channel fading, (117) and (119), respectively, as a function of J/S for $E_b/N_0 = 12.0$ dB is illustrated in Figure 22. When $E_b/N_0 = 12.0$ dB and there is no other noise or other impairment such as channel fading, then for BPSK, $P_b = 10^{-8}$, which can be seen is the asymptotic limit for small J/S in Figure 22. From Figure 22, we can see that for $J/S > -2$ dB that the exact and approximate results are essentially identical. Since $(E_b/N_0)^{-1} = -12.0$ dB, we can conclude that in order to use the approximate expression for P_b when there is no channel fading that J/S must be

Figure 22: Exact and approximate performance of BPSK with continuous narrowband noise interference and no channel fading for $E_b/N_0 = 12.0$ dB.

at least 10 dB greater than $(E_b/N_0)^{-1}$. We can also see that using the approximate expression for P_b leads to completely misleading results when J/S is not at least 10 dB greater than $(E_b/N_0)^{-1}$.

The exact and approximate performance of BPSK with continuous narrowband noise interference and Rayleigh fading, (118) and (120), respectively, as a function of J/S for $E_b/N_0 = 44.0$ dB is illustrated in Figure 23. When $E_b/N_0 = 44.0$ dB and there is no other noise or other impairment besides channel fading, then for BPSK, $P_b = 10^{-5}$, which can be seen is the asymptotic limit for small J/S in Figure 23. From Figure 22, we can see that for $J/S > -34$ dB that the exact and approximate results are essentially identical. Since $(E_b/N_0)^{-1} = -44.0$ dB, we can conclude that in order to use the approximate expression for P_b when there is Rayleigh fading that J/S must be at least 10 dB greater than $(E_b/N_0)^{-1}$, just as in the case of no channel fading. We can also see that using the approximate expression for P_b leads to misleading results when J/S is not at least 10 dB greater than $(E_b/N_0)^{-1}$, again just as in the case of no channel fading.

Since the approximate expression for P_b is accurate for the two extremes of no channel fading and Rayleigh fading when J/S is at least 10 dB greater than $(E_b/N_0)^{-1}$, we can conclude that this requirement applies for Ricean fading in general, regardless of the ratio of direct-to-diffuse signal power ζ.

4.4.2 BPSK with Pulsed Narrowband Noise Interference

Substituting (115) and (116) into (109), we get for no channel fading and for Rayleigh fading, respectively,

$$P_b = (1 - \rho) Q \left(\sqrt{\frac{2E_b}{N_0}} \right) + \rho Q \left\{ \sqrt{2 \left[\left(\frac{E_b}{N_0} \right)^{-1} + \frac{J}{\rho S} \right]^{-1}} \right\} \tag{121}$$

and

$$P_b = \frac{1}{2} - \frac{(1 - \rho)}{2} \sqrt{\frac{1}{1 + \left(\frac{E_b}{N_0} \right)^{-1}}} - \frac{\rho}{2} \sqrt{\frac{1}{1 + \left(\frac{E_b}{N_0} \right)^{-1} + \frac{J}{\rho S}}} \tag{122}$$

When $J/S >> (E_b/N_0)^{-1}$ and $E_b/N_0 >> 1$, we get for no channel fading and for Rayleigh fading, respectively,

$$P_b \approx \rho Q \left[\sqrt{2 \left(\frac{J}{\rho S} \right)^{-1}} \right] \tag{123}$$

and

$$P_b \approx \frac{(1 - \rho)}{4} \left(\frac{E_b}{N_0} \right)^{-1} + \frac{\rho}{2} \left(1 - \sqrt{\frac{1}{1 + \frac{J}{\rho S}}} \right) \tag{124}$$

The performance of BPSK with pulsed narrowband noise interference and no channel fading, given by (121), as a function of J/S for $\rho = 0.1$ and $E_b/N_0 = 12.0$ dB is illustrated in Figure 24.
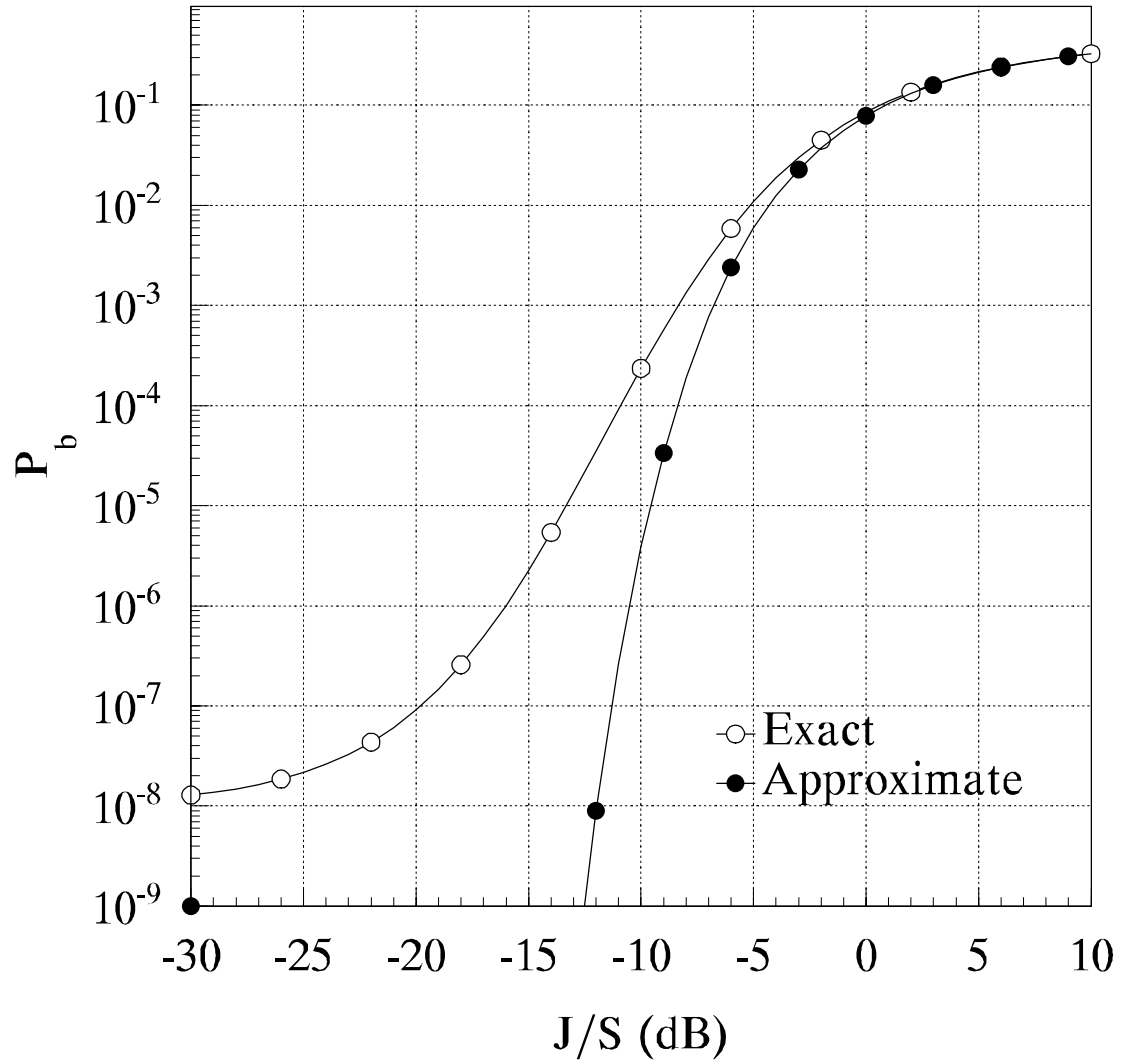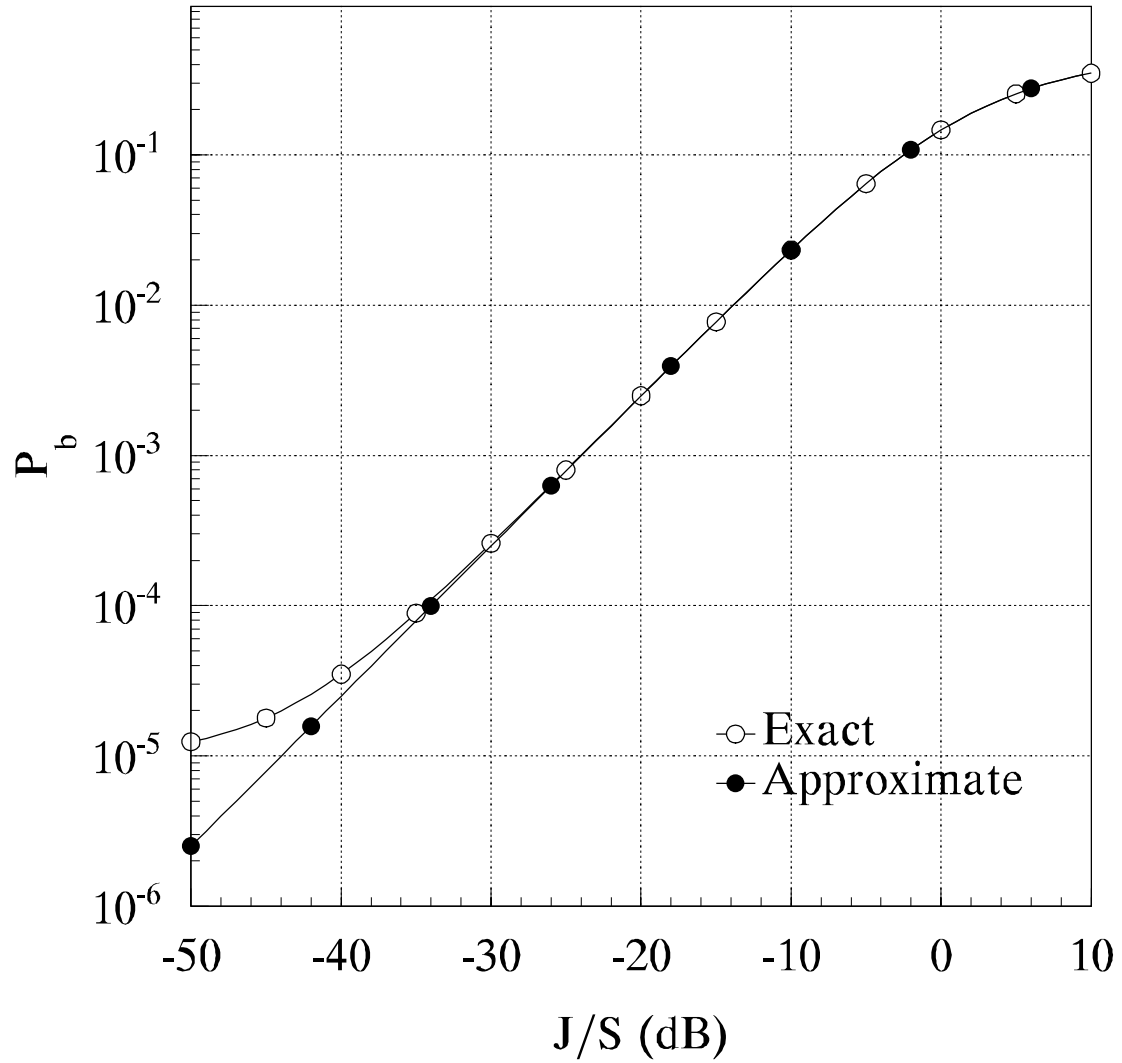
Figure 23: Exact and approximate performance of BPSK with continuous narrowband noise interference and Rayleigh fading for $E_b/N_0 = 44.0$ dB.

Also plotted for comparison purposes is the performance of BPSK with continuous narrowband noise interference ($\rho = 1.0$) and no channel fading. As can be seen from Figure 24, when J/S is large, continuous noise interference degrades performance more than pulsed-noise interference, but for smaller J/S, the opposite is true. For example, pulsed-noise interference with a J/S that is 7 dB less than the J/S for continuous noise interference is required to obtain $P_b = 10^{-3}$. As expected, the performance for both continuous and pulsed-noise interference asymptotically approach the same value for very small J/S.
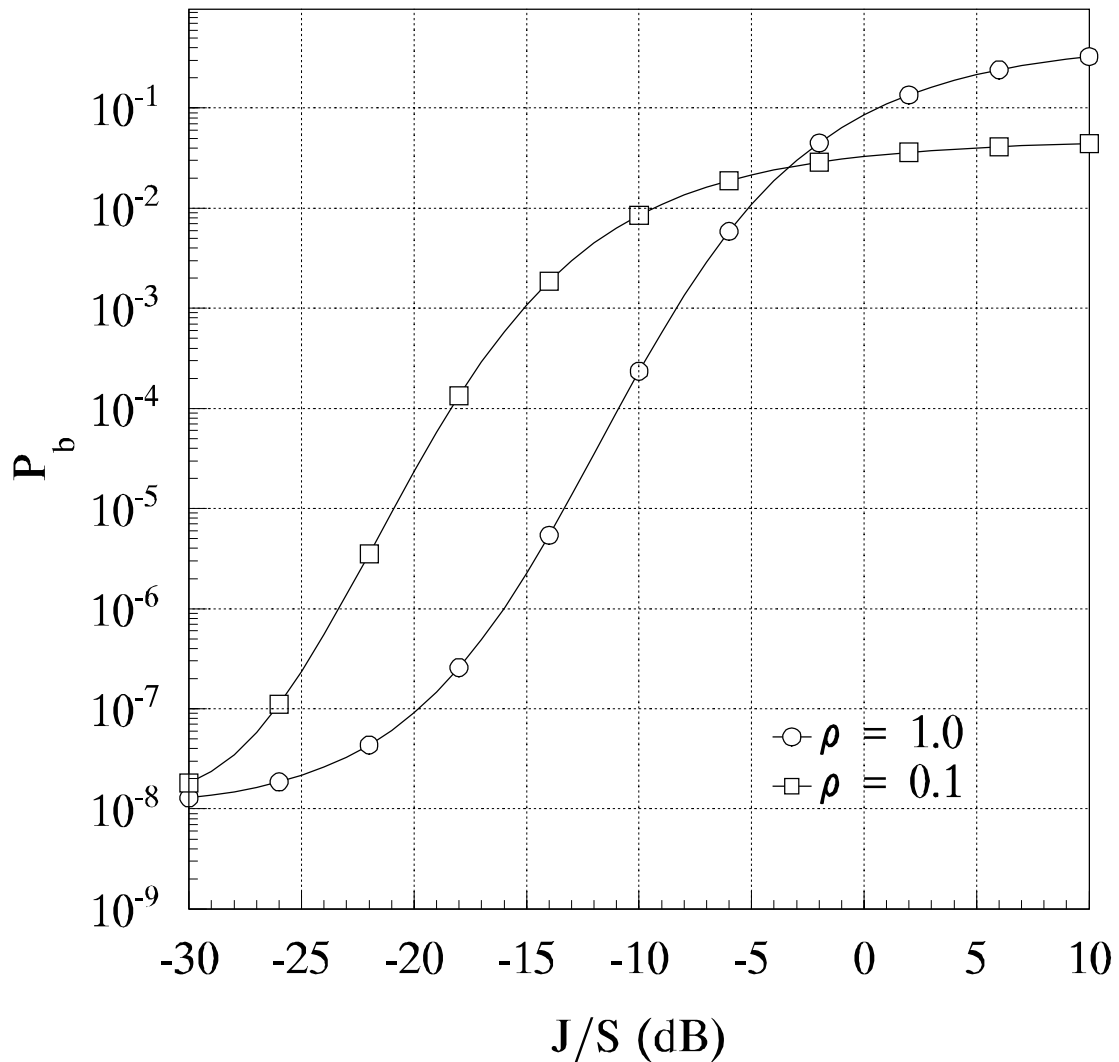
Figure 24: Performance of BPSK with no channel fading and pulsed-noise interference for $E_b/N_0 = 12.0$ dB.

The performance of BPSK with pulsed narrowband noise interference and Rayleigh fading, given by (122), as a function of J/S for $\rho = 0.1$ and $E_b/N_0 = 44.0$ dB is illustrated in Figure 25. Also plotted for comparison purposes is the performance of BPSK with continuous narrowband noise interference ($\rho = 1.0$) and Rayleigh fading. As can be seen from Figure 25, when J/S is large, continuous noise interference degrades performance more than pulsed-noise interference, just as in the case of no channel fading, but for smaller J/S, there is virtually no difference in performance whether the noise interference is pulsed or continuous.
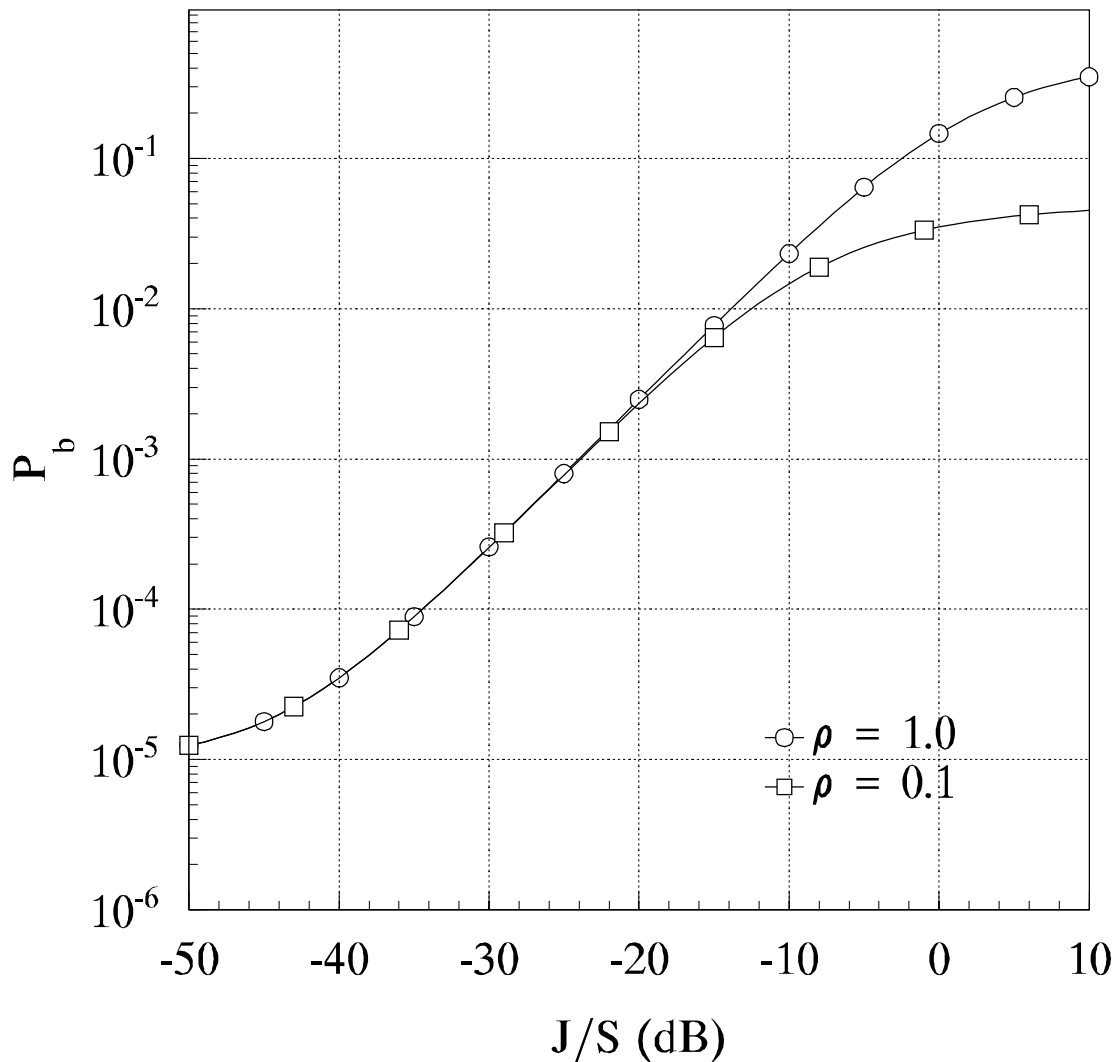
Figure 25: Performance of BPSK with Rayleigh fading and pulsed-noise interference for $E_b/N_0 = 44.0$ dB.

Finally, analogous to the case of continuous noise interference discussed in the last section, it is reasonable to assume that the approximate expressions given by (123) and (124) will be accurate when $J/\rho S \geq 10 \, (E_b/N_0)^{-1}$. Furthermore, we can conclude that this requirement applies for Ricean fading in general, regardless of the ratio of direct-to-diffuse signal power ζ.

5 Diversity

Diversity is a procedure that consists of transmitting and/or receiving the same symbol multiple times in order to provide redundancy at the receiver. The basic idea of diversity is that some of the received redundant symbols will be more reliable than others, and the demodulation decision will be made using the more reliable symbols. In order for diversity to be useful, each redundant symbol must be received independently. Diversity is analogous to a repetition code.

Diversity can be implemented in a number of ways. *Space diversity* consists of using multiple antennas at the receiver in order to receive the transmitted symbol multiple times. Generally, in order for the signal to be received independently, each of the antennas must be at least 10 wavelengths apart. *Time diversity* consists of transmitting the same symbol multiple times. In order for the signal to be received independently over a fading channel, each of the diversity transmissions must be separated in time by a time greater than the coherence time $(\Delta t)_c$ of the channel. *Frequency diversity* consists of transmitting the same symbol on multiple carrier frequencies at the same time. In order for the signal to be received independently over a fading channel, each of the diversity transmissions must be separated in frequency by a frequency greater than the coherence bandwidth $(\Delta f)_c$ of the channel. It is not uncommon for systems to utilize more than one kind of diversity. For example, fast frequency-hopped (FFH) spread spectrum with diversity is essentially a hybrid utilizing both frequency and time diversity.

Frequency diversity and space diversity are examples of *parallel* diversity since the redundant symbols are received simultaneously; although, these two different ways of implementing diversity have a decidedly different effect on signal bandwidth. Time diversity and FFH systems with diversity are examples of *sequential* diversity since the redundant symbols are received one at a time. For parallel diversity systems, if the information bit rate is held constant as diversity L increases, then the implementation of diversity effectively increases the overall average energy per symbol by a factor of L. For space diversity, there is no effect on signal bandwidth. For frequency diversity, as diversity L increases, signal bandwidth increases by a factor of L for a fixed information bit rate. For sequential diversity systems, if signal bandwidth is held constant as diversity L increases, then the implementation of diversity also effectively increases the average energy per diversity transmission by a factor of L but decreases the information bit rate by L.

It is not possible to obtain generalized expressions for the probability of bit error for systems that use diversity since there are a large number of ways in which the diversity receptions can be combined to form a decision statistic. In this report, the matched filter outputs for each diversity

reception are assumed to be linearly combined to form an overall decision statistic for each symbol based on all diversity receptions for that particular symbol.

5.1 Performance of BPSK and GMSK with Diversity over Frequency-Nonselective, Slowly Fading Ricean Channels

For BPSK and GMSK with diversity, optimum performance over fading channels is obtained by using a *maximal ratio combiner* receiver [1]. For a maximal ratio combiner, the receiver estimates the amplitude of the received signal for each diversity reception in addition to the received signal phase estimate required for coherent detection. The consequence of this is to weight each diversity reception with a factor proportional to signal strength. Hence, strongly received diversity receptions will have greater weight in the overall decision than will weakly received diversity receptions. Note that for noncoherent MFSK, this weighting occurs naturally as a consequence of the squaring circuits in each branch of the MFSK receiver.

For parallel diversity, $T_b = T_c$, while for sequential diversity $T_b = LT_c$ where T_c is the duration of each diversity reception, and $\sigma_{0_c}^2 = N_0/T_c$. By analogy with (91) and (92), we get

$$\overline{\gamma_c} = \frac{2\sigma^2}{\sigma_{0_c}^2} \left(1 + \zeta\right) \tag{125}$$

and

$$\overline{\gamma_c} = \frac{\alpha^2}{\sigma_{0_c}^2} \left(\frac{1 + \zeta}{\zeta}\right) \tag{126}$$

where $\overline{\gamma_c}$ is the average signal-to-noise ratio for each diversity reception.

For the maximal ratio combiner, the matched filter output can be modeled as a Gaussian random variable with mean [1]

$$\overline{X_{k\pm}} = \pm\overline{X_k} = \pm b\sqrt{2}a_{c_k}^2 \tag{127}$$

and variance

$$\sigma_k^2 = \frac{a_{c_k}^2 N_0}{T_c} \tag{128}$$

where $\sqrt{2}a_{c_k}$ is the amplitude of the kth diversity reception of a bit. Since we assume that each diversity reception of a bit is received independently, then the random variables X_k, $k = 1, 2, \ldots, L$ modeling the matched filter output for the kth diversity reception of a bit are independent random variables.

Without loss of generality, we assume that a bit 1 is transmitted. Since the sum of independent Gaussian random variables is also a Gaussian random variable, the mean and variance of the random variable X that models the detector output *after* diversity combining are, respectively,

$$\overline{X} = \sum_{k=1}^{L} \overline{X_k} = b\sqrt{2} \sum_{k=1}^{L} a_{c_k}^2 \tag{129}$$

60

and

$$\sigma_X^2 = \sum_{k=1}^{L} \sigma_k^2 = \frac{N_0}{T_c} \sum_{k=1}^{L} a_{c_k}^2 \tag{130}$$

Now we have

$$\frac{\overline{X}^2}{\sigma_X^2} = \frac{2b \left(\sum_{k=1}^{L} a_{c_k}^2 \right)^2}{\frac{N_0}{T_c} \sum_{k=1}^{L} a_{c_k}^2} \tag{131}$$

which can be simplified to

$$\frac{\overline{X}^2}{\sigma_X^2} = \frac{2b}{\sigma_{0_c}^2} \sum_{k=1}^{L} a_{c_k}^2 \tag{132}$$

Defining

$$\gamma_b = \frac{1}{\sigma_{0_c}^2} \sum_{k=1}^{L} a_{c_k}^2 \tag{133}$$

and substituting (133) into (132), we get

$$\frac{\overline{X}^2}{\sigma_X^2} = 2b\gamma_b \tag{134}$$

The conditional probability of bit error is given by

$$P_b\left(\gamma_b\right) = Q\left(\sqrt{\frac{\overline{X}^2}{\sigma_X^2}}\right) \tag{135}$$

Substituting (134) into (135), we get

$$P_b\left(\gamma_b\right) = Q\left(\sqrt{2b\gamma_b}\right) \tag{136}$$

Comparing (67) with (133) and (80) with (136), we see that the probability of bit error for a system with diversity L and the probability of selecting a path a Hamming distance L from the correct path with soft decision Viterbi decoding is mathematically the same; hence, substituting $\overline{\gamma_b}$ with $\overline{\gamma_c}$ and setting $r = 1$ in (93), we get

$$P_b = \frac{1}{2\sqrt{\pi c}} \left[\frac{2\left(1 + \zeta\right)}{2\left(1 + \zeta\right) + b\overline{\gamma_c}} \right]^L \exp\left[\frac{-bL\zeta\overline{\gamma_c}}{2\left(1 + \zeta\right) + b\overline{\gamma_c}} \right] \tag{137}$$

where $c = 1.0 + 0.1\zeta$ and is obtained empirically. Similarly, substituting $\overline{\gamma_b}$ with $\overline{\gamma_c}$ and setting $r = 1$ in (82) and (83), we obtain for the special case of Rayleigh fading

$$P_b = \left(\frac{1 - \mu}{2} \right)^L \sum_{m=0}^{L-1} \binom{L - 1 + m}{m} \left(\frac{1 + \mu}{2} \right)^m \tag{138}$$

61

where

$$\mu = \sqrt{\frac{b\overline{\gamma_c}}{2 + b\overline{\gamma_c}}} \tag{139}$$

The probability of bit error of BPSK in AWGN with diversity and no channel fading is plotted in Figure 26 as a function of the average energy per diversity reception-to-noise power spectral density ratio $\overline{\gamma_c}$, while the probability of bit error of BPSK in AWGN with diversity and Rayleigh fading is plotted in Figure 27 as a function of $\overline{\gamma_c}$. In both cases, an increase in diversity significantly improves performance. It is interesting to note that diversity is more effective in improving performance for Rayleigh fading channels than for channels with no fading. For channels with no fading, each time the order of diversity is doubled, the average energy per diversity reception-to-noise power spectral density ratio required to achieve a specified P_b is reduced by 3 dB; while for channels with Rayleigh fading, each time the order of diversity is doubled, the $\overline{\gamma_c}$ required to achieve a specified P_b is reduced by anywhere from 5 dB to more than 10 dB for $P_b \leq 10^{-2}$. This leads to the superficially surprising result that BPSK actually performs better when transmitted over Rayleigh fading channels than when transmitted over channels with no fading when the order of diversity is high enough. This apparently counterintuitive result can be explained by noting that for channels with no fading, diversity is equivalent to simply increasing the average energy per bit. An increase in the order of diversity by a factor of two is equivalent to increasing E_b by 3 dB. For Rayleigh fading channels, on the other hand, in addition to increasing E_b, since maximal ratio combining is assumed, the receiver is also using channel state information which enhances the diversity receptions that are received with larger signal energy. If maximal ratio combining is not used when channel fading is present, then the receiver will not perform nearly as well. It should also be noted that, whether channel fading is present or not, if the diversity is sequential, then the improvement in performance comes at the expense of data bit rate. Each time the order of diversity in increased by a factor of two, the data bit rate is reduced by a factor of two.

5.2 Performance of Noncoherent MFSK with Diversity over Frequency-Nonselective, Slowly Fading Ricean Channels

The probability of symbol error for orthogonal, noncoherent MFSK is given by

$$P_s = 1 - P_c \tag{140}$$

$$P_s = 1 - \int_0^\infty f_{V_1}(v_1|1) \left[\int_0^{v_1} f_{V_2}(v_2|1)\, dv_2 \right]^{M-1} dv_1 \tag{141}$$
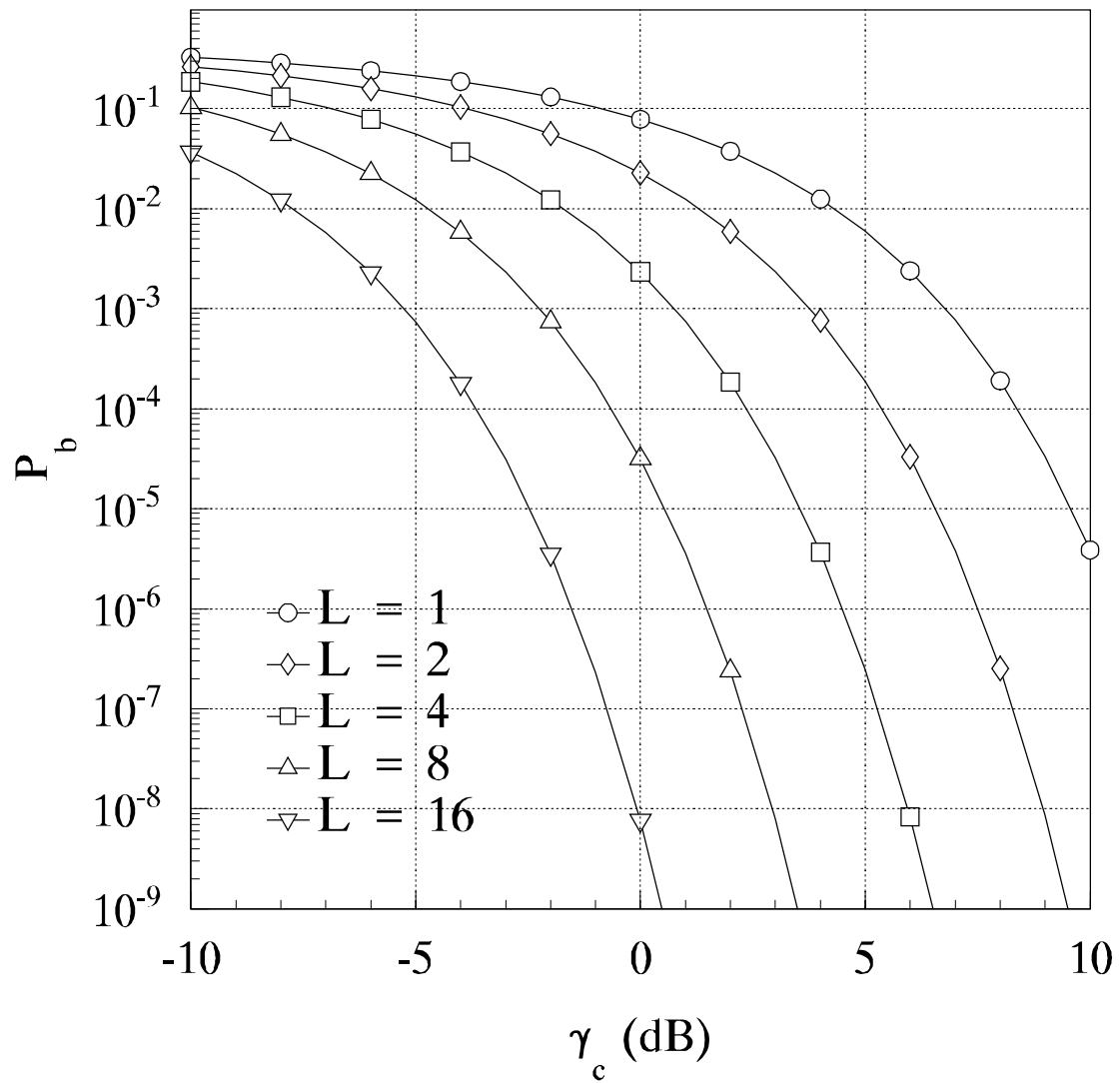
Figure 26: Performance of BPSK with no channel fading and diversity.
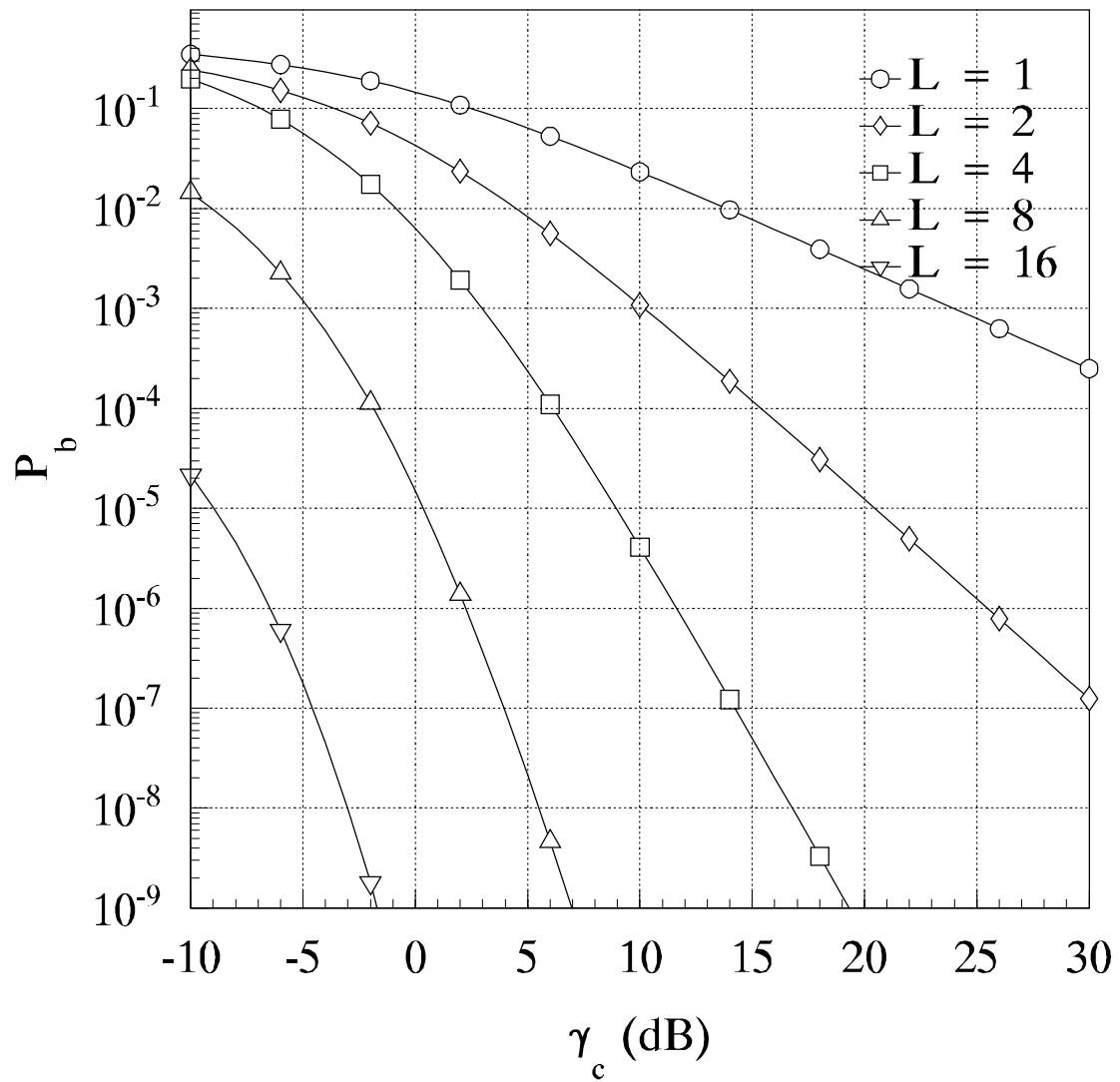
Figure 27: Performance of BPSK with Rayleigh fading and diversity.

where P_c is the probability of *not* making a symbol error and, without loss of generality, we assume that the signal corresponds to branch one of the detector. This is a general result that is valid for both fading and non-fading channels as well as for both diversity and non-diversity systems as long as the noise is AWGN or otherwise does not violate the symmetry considerations required in the derivation.

In order to continue, we must obtain the appropriate $f_{V_1}(v_1|1)$ and $f_{V_2}(v_2|1)$. In this report, we will assume that the noncoherent detector is a square-law detector. When there is no diversity, a square-law detector and an envelope detector have identical performance. With diversity, there is a slight difference, but the difference is small, and the square-law detector is significantly easier to analyze [1]. Hence, in this report, a square-law detector will be assumed.

For square-law detection, the probability density function of a random variable that represents the output of a non-signal branch when there is no channel fading is given by

$$f_{V_2}(v_2|1) = \frac{v_2^{L-1}}{(2\sigma_{0_c}^2)^L(L-1)!} \exp\left(\frac{-v_2}{2\sigma_{0_c}^2}\right) u(v_2) \tag{142}$$

Clearly, channel fading has no effect on the output of branches that do not correspond to the signal. Substituting (142) into (141), we get

$$P_s = 1 - \int_0^\infty f_{V_1}(v_1|1) \left[\int_0^{v_1} \frac{v_2^{L-1}}{(2\sigma_{0_c}^2)^L(L-1)!} \exp\left(\frac{-v_2}{2\sigma_{0_c}^2}\right) dv_2\right]^{M-1} dv_1 \tag{143}$$

which can be evaluated to obtain

$$P_s = 1 - \int_0^\infty f_{V_1}(v_1|1) \left[1 - \exp\left(\frac{-v_1}{2\sigma_{0_c}^2}\right) \sum_{n=0}^{L-1} \frac{v_1^n}{(2\sigma_{0_c}^2)^n \, n!}\right]^{M-1} dv_1 \tag{144}$$

The next step is to obtain $f_{V_1}(v_1|1)$. Without channel fading, the probability density function for the random variable modeling the output of the signal branch of a square-law detector *prior* to diversity combining is [1]

$$f_{V_{1_k}}(v_{1_k}|1) = \frac{1}{2\sigma_{0_c}^2} \exp\left[\frac{-(v_{1_k} + 2A_c^2)}{2\sigma_{0_c}^2}\right] I_0\left(\frac{A_c\sqrt{2v_{1_k}}}{\sigma_{0_c}^2}\right) u(v_{1_k}) \tag{145}$$

where $I_0(\bullet)$ is the modified Bessel function of the first kind and order zero. Following the derivation used to obtain (78), we get the probability density function for the random variable modeling the output of the signal branch *after* diversity combining as

$$f_{V_1}(v_1|1) = \frac{v_1^{(L-1)/2}}{2\sigma_{0_c}^2 \, (2LA_c^2)^{(L-1)/2}} \exp\left[\frac{-(v_1 + 2LA_c^2)}{2\sigma_{0_c}^2}\right] I_{L-1}\left(\frac{A_c\sqrt{2Lv_1}}{\sigma_{0_c}}\right) u(v_1) \tag{146}$$

where $I_{L-1}(\bullet)$ is the modified Bessel function of the first kind and order $L-1$. With channel fading, the probability density function for V_{1_k} is now conditional on a_{c_k}, and the conditioning must be removed by evaluating

$$f_{V_{1_k}}(v_{1_k}|1) = \int_0^\infty f_{V_{1_k}}(v_{1_k}|a_{c_k},1) f_{A_{c_k}}(a_{c_k})\, da_{c_k} \tag{147}$$

Substituting (145) into (147), we get

$$\begin{aligned}
f_{V_{1_k}}(v_{1_k}|1) &= \int_0^\infty \frac{1}{2\sigma_{0_c}^2} \exp\left[\frac{-(v_{1_k}+2a_{c_k}^2)}{2\sigma_{0_c}^2}\right] I_0\left(\frac{a_{c_k}\sqrt{2v_{1_k}}}{\sigma_{0_c}^2}\right) \\
&\qquad \times \frac{a_{c_k}}{\sigma^2} \exp\left[\frac{-\left(a_{c_k}^2+\alpha^2\right)}{2\sigma^2}\right] I_0\left(\frac{\alpha a_{c_k}}{\sigma^2}\right) da_{c_k} \tag{148} \\[2mm]
&= \frac{1}{2\sigma_{0_c}^2\sigma^2} \exp\left[-\left(\frac{v_{1_k}}{2\sigma_{0_c}^2}+\frac{\alpha^2}{2\sigma^2}\right)\right] \\
&\qquad \times \int_0^\infty a_{c_k} \exp\left[-a_{c_k}^2\left(\frac{1}{\sigma_{0_c}^2}+\frac{1}{2\sigma^2}\right)\right] I_0\left(\frac{a_{c_k}\sqrt{2v_{1_k}}}{\sigma_{0_c}^2}\right) I_0\left(\frac{\alpha a_{c_k}}{\sigma^2}\right) da_{c_k} \tag{149}
\end{aligned}$$

which can be evaluated using (84) to obtain

$$f_{V_{1_k}}(v_{1_k}|1) = \frac{1}{2\left(\sigma_{0_c}^2+2\sigma^2\right)} \exp\left[-\frac{1}{2}\left(\frac{v_{1_k}+2\alpha^2}{\sigma_{0_c}^2+2\sigma^2}\right)\right] I_0\left(\frac{\alpha\sqrt{2v_{1_k}}}{\sigma_{0_c}^2+2\sigma^2}\right) u(v_{1_k}) \tag{150}$$

If we now compare the probability density function for V_{1_k} without fading, given by (145), to that with Ricean fading, given by (150), we see that the two probability density functions have the same functional form. To be precise, in (145), if we substitute α for A_c and $\left(\sigma_{0_c}^2+2\sigma^2\right)$ for $\sigma_{0_c}^2$, respectively, then we obtain (150). It follows that the probability density function for the random variable modeling the output of the signal branch *after* diversity combining and *with* Ricean fading is obtained from the probability density function for V_1 *without* fading, given by (146), simply by substituting α for A_c and $\left(\sigma_{0_c}^2+2\sigma^2\right)$ for $\sigma_{0_c}^2$, respectively, to obtain

$$f_{V_1}(v_1|1) = \frac{v_1^{(L-1)/2}}{2\left(\sigma_0^2+2\sigma^2\right)(2L\alpha^2)^{(L-1)/2}} \exp\left[\frac{-(v_1+2L\alpha^2)}{2\left(\sigma_0^2+2\sigma^2\right)}\right] I_{L-1}\left(\frac{\alpha\sqrt{2Lv_1}}{\sigma_0^2+2\sigma^2}\right) u(v_1) \tag{151}$$

where we assume that $\alpha^2/2\sigma^2$ is constant for each diversity reception.

We can now evaluate P_s for noncoherent MFSK over frequency-nonselective, slowly fading Ricean channels by substituting (151) into (144). The resulting analytic expression is extremely complicated, and a numerical evaluation of the integral expression for P_s is actually easier to compute than is the analytic expression except for $M=2$. Substituting (151) into (144) with

$M = 2$ and interchanging the order of summation and integration, we obtain the probability of bit error for noncoherent BFSK with diversity and Ricean fading as

$$
P_b = \sum_{n=0}^{L-1} \frac{\exp\left(\dfrac{-L\alpha^2}{\sigma_{0_c}^2 + 2\sigma^2}\right)}{2\left(\sigma_{0_c}^2 + 2\sigma^2\right)(2L\alpha^2)^{(L-1)/2}(2\sigma_{0_c}^2)^n\, n!}
$$

$$
\times \int_0^\infty v_1^{n+(L-1)/2} \exp\left[-v_1\left(\frac{1}{2\left(\sigma_{0_c}^2 + 2\sigma^2\right)} + \frac{1}{2\sigma_{0_c}^2}\right)\right] I_{L-1}\left(\frac{\alpha\sqrt{2Lv_1}}{\sigma_{0_c}^2 + 2\sigma^2}\right) dv_1 \quad (152)
$$

This can be evaluated with the aid of (84) to obtain

$$
P_b = \left(\frac{\sigma_{0_c}^2}{2\sigma_{0_c}^2 + 2\sigma^2}\right)^L \exp\left(\frac{-L\alpha^2}{2\sigma_{0_c}^2 + 2\sigma^2}\right) \sum_{n=0}^{L-1}\left(\frac{\sigma_{0_c}^2 + 2\sigma^2}{2\sigma_{0_c}^2 + 2\sigma^2}\right)^n
$$

$$
\times \sum_{p=0}^{n}\frac{1}{p!}\left(\begin{array}{c} L-1+n \\ n-p \end{array}\right)\left[\frac{\sigma_0^2 L\alpha^2}{\left(\sigma_{0_c}^2 + 2\sigma^2\right)\left(2\sigma_{0_c}^2 + 2\sigma^2\right)}\right]^p \quad (153)
$$

Substituting (125) and (126) into (153), we get

$$
P_b = \left[\frac{1+\zeta}{2(1+\zeta)+\overline{\gamma}_c}\right]^L \exp\left(\frac{-\zeta L\overline{\gamma}_c}{2(1+\zeta)+\overline{\gamma}_c}\right) \sum_{n=0}^{L-1}\left[\frac{1+\zeta+\overline{\gamma}_c}{2(1+\zeta)+\overline{\gamma}_c}\right]^n
$$

$$
\times \sum_{p=0}^{n}\frac{1}{p!}\left(\begin{array}{c} L-1+n \\ n-p \end{array}\right)\left[\frac{\zeta(1+\zeta)L\overline{\gamma}_c}{2(1+\zeta)^2+(2+\zeta)\overline{\gamma}_c}\right]^p \quad (154)
$$

For the special case of Rayleigh fading ($\zeta = 0$), (154) simplifies considerably to

$$
P_b = \left(\frac{1}{2+\overline{\gamma}_c}\right)^L \sum_{n=0}^{L-1}\left(\begin{array}{c} L-1+n \\ n \end{array}\right)\left(\frac{1+\overline{\gamma}_c}{2+\overline{\gamma}_c}\right)^n \quad (155)
$$

As usual, the probability of bit error of DPSK is obtained by replacing $\overline{\gamma}_c$ in (154) and (155) with $2\overline{\gamma}_c$.

The probability of bit error of DPSK in AWGN with diversity and no channel fading is plotted in Figure 28 as a function of the average energy per diversity reception-to-noise power spectral density ratio $\overline{\gamma}_c$, while the probability of bit error of DPSK in AWGN with diversity and Rayleigh fading is plotted in Figure 29 as a function of $\overline{\gamma}_c$. As with BPSK, in both cases, an increase in diversity significantly improves performance. Also as with BPSK, diversity is more effective in improving performance for Rayleigh fading channels than for channels with no fading. For channels with no fading, each time the order of diversity is doubled, the average energy per diversity reception-to-noise power spectral density ratio required to achieve a specified P_b is reduced, although not by

as much as for BPSK and not consistently. That is, the improvement is less than 3 dB, and the amount of improvement depends on both P_b and the order of diversity. For channels with Rayleigh fading, each time the order of diversity is doubled, the $\overline{\gamma_c}$ required to achieve a specified P_b is reduced by anywhere from 5 dB to more than 10 dB for $P_b \leq 10^{-2}$. As with BPSK, this leads to the result that DPSK actually performs better when transmitted over Rayleigh fading channels than when transmitted over channels with no fading when the order of diversity is high enough.

Finally, we note that Figures 28 and 29 can also be used to obtain the performance of noncoherent BFSK with diversity for no channel fading and for Rayleigh fading, respectively, by adding 3 dB to the ordinate of each figure.
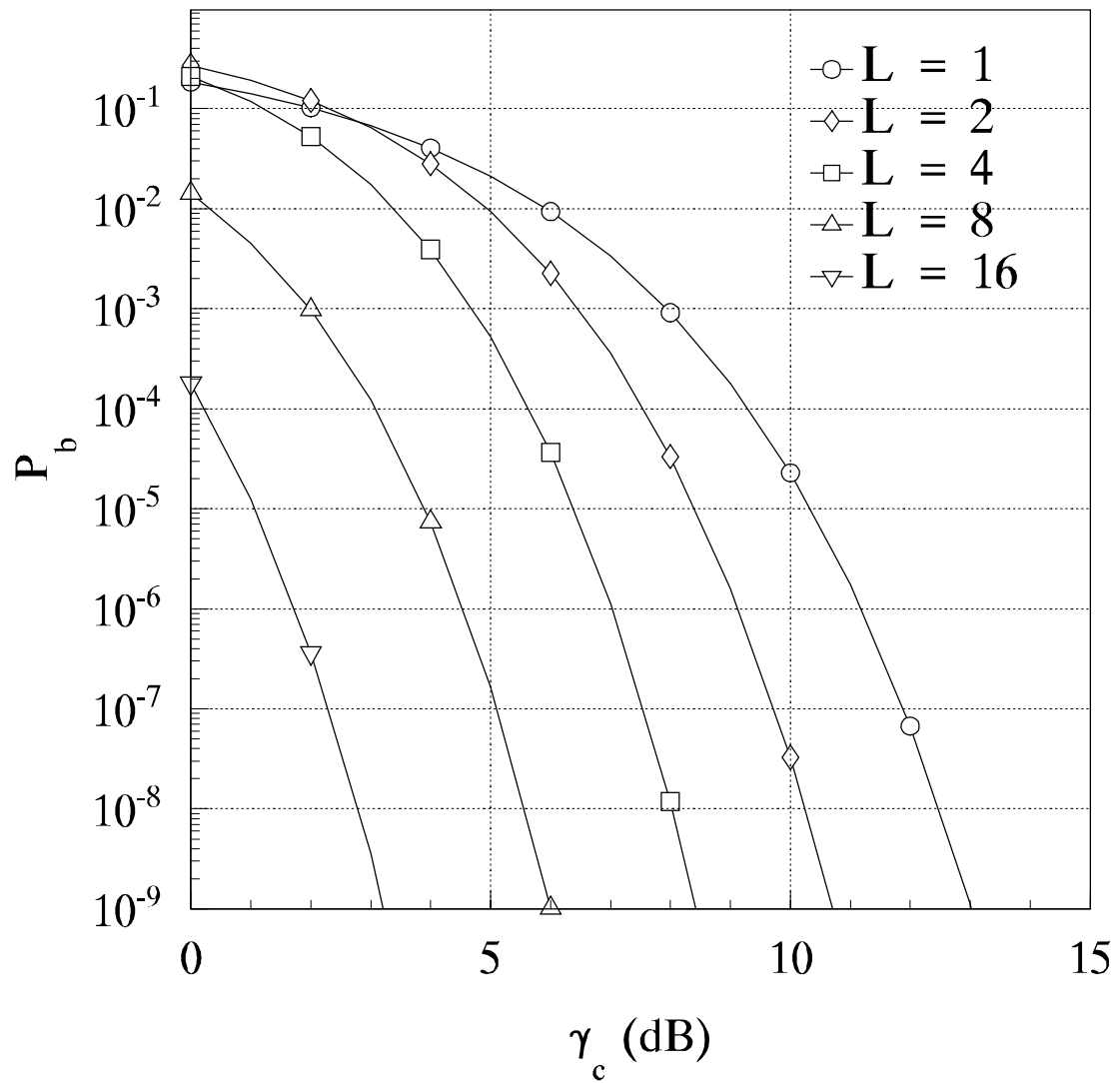
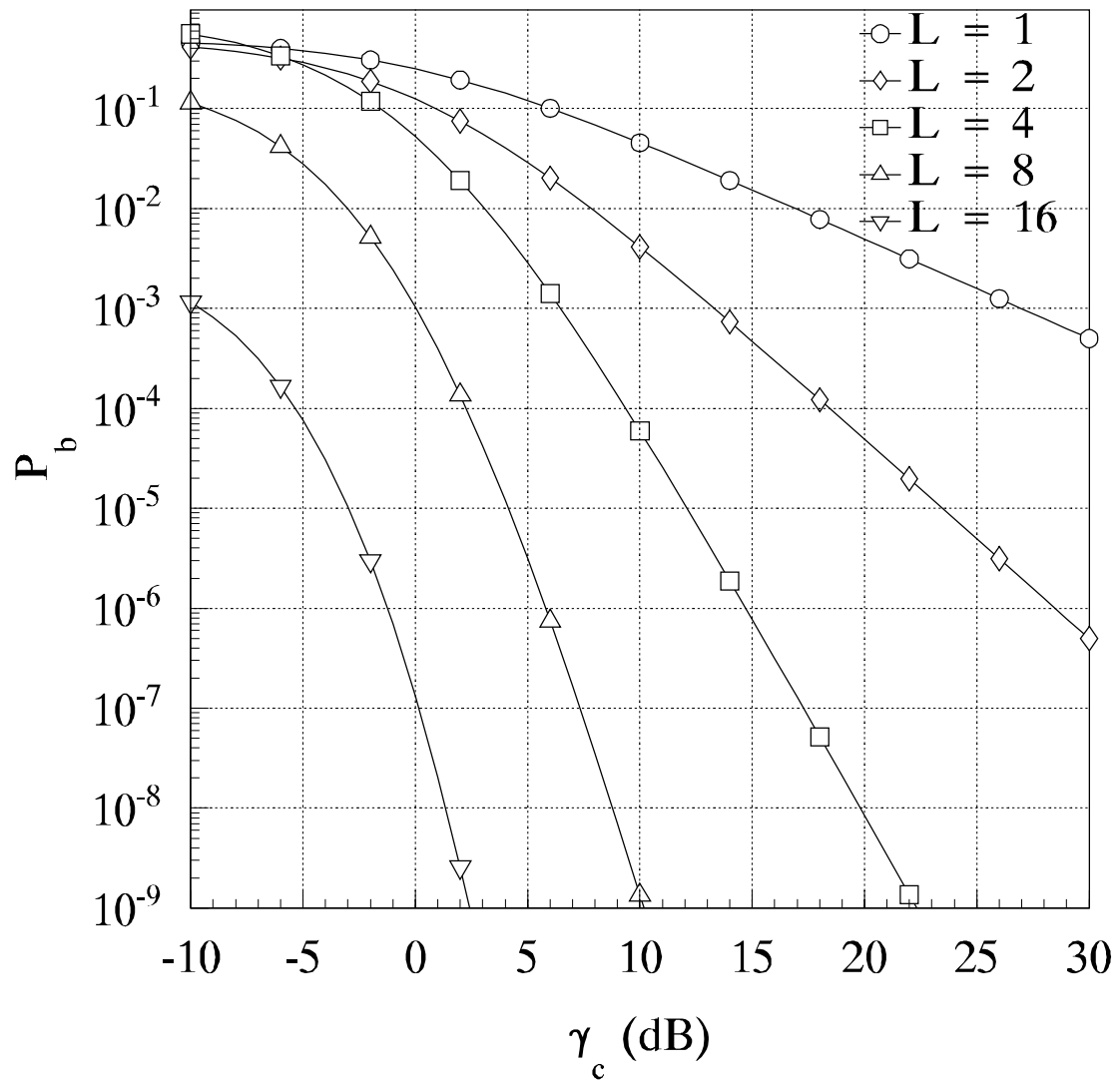Figure 28: Performance of DPSK with no channel fading and diversity.

Figure 29: Performance of DPSK with Rayleigh fading and diversity.

6   Forward Error Correction and Diversity

For hard decision decoding, the analysis of the probability of bit error is straightforward since the channel transition probability required in (64), (94), and (97) is obtained directly from the equations presented in Section 5 where $\overline{\gamma_c}$ is replaced by $r\overline{\gamma_c}$. For example, consider BPSK and GMSK with diversity and convolutional coding transmitted over frequency-nonselective, slowly fading Ricean channels, discussed in Section 5.1. For soft decision detection and hard decision decoding, we get the probability of channel bit error from (137) as

$$p = \frac{1}{2\sqrt{\pi c}} \left[\frac{2\left(1+\zeta\right)}{2\left(1+\zeta\right)+rb\overline{\gamma_c}} \right]^{L} \exp\left[\frac{-rbL\zeta\overline{\gamma_c}}{2\left(1+\zeta\right)+rb\overline{\gamma_c}} \right] \tag{156}$$

which is then used in (64).

When forward error correction with soft decision decoding and diversity are combined, the analysis can become extremely complicated, and generally, the receiver type must be specified in order to proceed with the analysis. For soft decision detectors of the type discussed in Section 3, P_d is replaced by P_{dL}. For example, consider BPSK and GMSK with diversity and convolutional coding transmitted over frequency-nonselective, slowly fading Ricean channels, discussed in Section 5.1. For soft decision detection and soft decision decoding, we get from (137)

$$P_{dL} = \frac{1}{2\sqrt{\pi c}} \left[\frac{2\left(1+\zeta\right)}{2\left(1+\zeta\right)+rb\overline{\gamma_c}} \right]^{dL} \exp\left[\frac{-rbdL\zeta\overline{\gamma_c}}{2\left(1+\zeta\right)+rb\overline{\gamma_c}} \right] \tag{157}$$

where

$$P_b < \frac{1}{k} \sum_{d=d_{free}}^{\infty} B_d P_{dL} \tag{158}$$

71

THIS PAGE INTENTIONALLY LEFT BLANK

7 Spread Spectrum Communications

The ideal conventional communication system, whether digital or analog, maximizes performance (minimizes P_b for digital systems) with minimum transmission power, minimum transmission bandwidth, and minimum transmitter/receiver complexity. In some applications, military applications in particular, there may be other considerations that supersede the more conventional ones. Some typical concerns for military applications are to enhance the ability of the communication system to reject hostile interference (anti-jam (AJ) protection), to decrease the ability of a hostile observer to even know communications are taking place, here referred to as a *low probability of detection* (LPD) communication system, and to decrease the ability of a hostile observer to "listen in" when communications are taking place, here referred to as a *low probability of intercept* (LPI) communication system. Frequently both transmitter/receiver complexity and transmission bandwidth are sacrificed in order to attain one or more of the preceding goals.

The general class of communication systems that require significantly more complicated transmitter/receiver circuitry and significantly more transmission bandwidth than the minimum that is required to transmit a particular signal are called *spread spectrum* communication systems. The two primary types of spread spectrum systems currently in use are *direct sequence* (DS) spread spectrum, which typically uses coherent modulation, and *frequency-hopped* (FH) spread spectrum, which typically uses noncoherent modulation. In addition, a *hybrid spread spectrum* system consisting of some combination of DS and FH is not uncommon.

Spread spectrum communication systems have rapidly moved from exclusively military applications to widespread commercial applications. Both FH and DS spread spectrum systems can be used for multiple access applications. These systems are referred to as *frequency-hopped multiple access* (FHMA) and *code division multiple access* (CDMA). Both FH and DS spread spectrum systems can be used for ranging applications. DS spread spectrum is the basis for the Global Positioning System (GPS).

In direct sequence spread spectrum, symbols are exclusive-ored with a *pseudo-noise* (PN) sequence, also referred to as the *chipping sequence*, prior to transmission. The result is that the peak PSD of the channel waveform is reduced by the *processing gain*, the ratio of chips-to-symbols, and the channel bandwidth is increased by the processing gain. For a processing gain much greater than one, even a strong signal will have a PSD with a very small magnitude, and it is more difficult for a hostile observer to detect the presence of a signal without special equipment. For this reason, DS spread spectrum is considered to be a LPD system. In order to correctly receive a DS signal,

the receiver must know the chipping sequence. For this reason, DS spread spectrum is also LPI.

In frequency-hopped spread spectrum, rather than transmit all symbols with the same carrier frequency f_c, the carrier frequency is changed (hopped) periodically according to some pre-designated (but apparently random to a third party observer) code (a PN sequence). A FH system can be either *fast frequency-hopped* (FFH) or *slow frequency-hopped* (SFH). Whether a FH system is fast or slow has nothing to do with the actual rate of frequency hopping. If more than one symbol is transmitted prior to each hop of the carrier frequency, the system is described as slow frequency-hopped. If one symbol per hop is transmitted or if the same symbol is transmitted on several different hops, the system is described as fast frequency-hopped. The duration of each hop (sometimes called *chip* so that the language of DS and FH is consistent) is T_c seconds. FFH is a form of *frequency/time diversity*. Diversity is a form of repetition coding that is used to introduce data redundancy in an effort to improve performance under some conditions. Since the *instantaneous* PSD of FH spread spectrum signals is the same as for the underlying modulation, FH spread spectrum signals are not considered LPD. Since the PN code used to generate the frequency-hopping sequence is required in order to recover the FH signal, FH systems are considered LPI systems.

A key question is how the addition of either DS or FH spread spectrum affects performance parameters other than bandwidth, such as probability of bit error. It can be shown that when there are no synchronization problems, regardless of channel fading, the effect of AWGN on the probability of bit error for either DS or FH spread spectrum communications is the same as if spread spectrum were not being used. In other words, there is no effect on system performance as a result of implementing spread spectrum when AWGN is the only noise source, and all of the results for the various types of modulation, both with and without error correction coding, discussed in this report for AWGN can be applied directly to spread spectrum systems that use a particular modulation type and a particular type of error correction code. When other noise sources, such as narrowband noise interference, are considered, performance can be very different. In fact, this difference is the basis for the AJ capability of spread spectrum systems. A detailed analysis of the effect of narrowband noise on DS and FH spread spectrum systems is beyond the scope of this report. The interested reader is referred to [10].

8 Received Signal-to-Noise Ratio and Link Budget Analysis

The signal-to-noise *power* ratio at the receiver input is given by [11]

$$\frac{S}{N} = \frac{P_T G_T G_R}{L_C k T_S B_{eq}} \tag{159}$$

where S is the average received signal power, N is the average noise power at the receiver, P_T is the average transmitted signal power, G_T is the gain of the transmitting antenna, G_R is the gain of the receiving antenna, L_C is the channel loss, k is Boltzmann's constant, T_S is the system equivalent noise temperature, and B_{eq} is the receiver noise equivalent bandwidth. For digital communications we are interested in the received average energy per bit-to-noise PSD ratio E_b/N_0. Since $S = E_b R_b$ and $N = N_0 B_{eq}$, we get

$$\frac{E_b}{N_0} = \frac{S B_{eq}}{N R_b} \tag{160}$$

Combining (159) and (160), we get

$$\frac{E_b}{N_0} = \frac{P_T G_T G_R}{L_C k T_S R_b} \tag{161}$$

Frequently, E_b/N_0 is expressed in terms of either the *effective isotropic radiated power* (EIRP)

$$\text{EIRP} = P_T G_T \tag{162}$$

and/or the *receiver sensitivity*

$$\mathcal{R} = \frac{G_R}{T_S} \tag{163}$$

Substituting (162) and (163) into (161), we get

$$\frac{E_b}{N_0} = \frac{\text{EIRP}\,\mathcal{R}}{L_C k R_b} \tag{164}$$

8.1 Link Budget

The *link margin* is the safety margin that is designed into communication systems to insure reliability and is defined as the increase in signal-to-noise ratio over the minimum required if conditions were ideal. Hence,

$$\frac{E_b}{N_0} = M \left(\frac{E_b}{N_0}\right)_{min} \tag{165}$$

where M is the link margin and $M \geq 1$ is desired. Substituting (164) into (165) and solving for M, we get

$$M = \frac{\text{EIRP}\,\mathcal{R}}{L_C k R_b \left(\frac{E_b}{N_0}\right)_{min}} \tag{166}$$

The link margin is frequently expressed in decibels. From (166), we obtain

$$M_{\text{dB}} = \text{EIRP}_{\text{dBW}} + \mathcal{R}_{\text{dBi/K}} - L_{C_{\text{dB}}} + 228.6 \text{ dB} - R_{b_{\text{dB-Hz}}} - \left(\frac{E_b}{N_0}\right)_{min_{\text{dB}}} \tag{167}$$

Positive link margin (expressed in dB) is good (the link is *closed*), while negative link margin is bad (the link is *open*). The equation for link margin in dB provides a convenient tool for allocating system resources since a dB of antenna gain is just as useful as a dB of EIRP, etc.

Equation (167) can be expressed in at least three other completely equivalent forms depending of whether $P_T G_T$ is used in place of EIRP and/or G_R/T_S is used in place of $\mathcal{R}$. Substituting (163) into (167), we get

$$M_{\text{dB}} = \text{EIRP}_{\text{dBW}} + G_{R_{\text{dBi}}} - T_{S_{\text{dBK}}} - L_{C_{\text{dB}}} + 228.6 \text{ dB} - R_{b_{\text{dB-Hz}}} - \left(\frac{E_b}{N_0}\right)_{min_{\text{dB}}} \tag{168}$$

Substituting (162) into (167), we get

$$M_{\text{dB}} = P_{T_{\text{dBW}}} + G_{T_{\text{dBi}}} + \mathcal{R}_{\text{dBi/K}} - L_{C_{\text{dB}}} + 228.6 \text{ dB} - R_{b_{\text{dB-Hz}}} - \left(\frac{E_b}{N_0}\right)_{min_{\text{dB}}} \tag{169}$$

Substituting (163) into (169), we get

$$M_{\text{dB}} = P_{T_{\text{dBW}}} + G_{T_{\text{dBi}}} + G_{R_{\text{dBi}}} - T_{S_{\text{dBK}}} - L_{C_{\text{dB}}} + 228.6 \text{ dB} - R_{b_{\text{dB-Hz}}} - \left(\frac{E_b}{N_0}\right)_{min_{\text{dB}}} \tag{170}$$

As previously mentioned, (167), (168), (169), and (170) are all equivalent to one another.

8.2 Channel Loss

All of the parameters in (167), (168), (169), and (170) are determined by the specific communication system under consideration except the channel loss L_C. The channel loss is determined by the type of channel the signal is transmitted over and, for the same communication system, can vary widely depending on location. For example, for a wireless communication system such as GSM the channel loss in a rural area with a line-of-sight to a basestation is significantly different than the channel loss for the same GSM system used in an urban area with no line-of-sight to the basestation.

All wireless communication systems experience channel loss, just as all communication systems are affected by AWGN. In general, the most benign channel loss encountered is when there is a line-of-sight between transmitter and receiver and there is no multipath. In this case, the channel loss is the free space channel loss and is given by [11]

$$L_C = \left(\frac{4\pi r f}{c}\right)^2 \tag{171}$$

76

where r is the distance from the transmitter to the receiver in meters, $c = 3 \times 10^8$ m/s is the speed of light in a vacuum, and f is the signal frequency in Hz.

In many wireless applications, such as cellular communications, the channel loss can vary significantly as the location of either the transmitter or the receiver changes. In this case, the channel loss must be modeled as a random variable. Typically, the channel loss expressed in dB is modeled as a Gaussian random variable characterized by the average channel loss $\overline{L_C}$ and the standard deviation σ_{L_C}.

THIS PAGE INTENTIONALLY LEFT BLANK

9   GSM 900

Global System for Mobile (GSM) is a second generation cellular system standard that was developed to solve the fragmentation problems of the first cellular system in Europe. GSM is the world's first cellular system to specify digital modulation and network level architectures and services. This section will concentrate on the physical layer of the GSM standard. [4, 12]

9.1   GSM 900 Radio Subsystem

GSM 900 utilizes two bands of 25 MHz which have been set aside for system use in all member countries. The spectrum allocation at 900 MHz is categorized into the primary GSM band and the extended GSM band. Both bands support full duplex transmission using two sub-bands spaced 45 MHz apart. The primary GSM frequencies are from 930 to 960 MHz for the downlink and from 890 to 915 MHz for the uplink. The extended GSM frequencies are from 925 to 960 MHz for the downlink and from 880 to 915 MHz for the uplink.

GSM uses frequency-division duplex (FDD) and a combination of time-division multiple access (TDMA) and frequency-hopped multiple access (FHMA) schemes to provide base stations with simultaneous access to multiple users. The available forward and reverse frequency bands are divided into 200 kHz wide channels and are marked by their center frequency, called the *absolute radio frequency channel number* (ARFCN). For the primary GSM band, the radio frequency channels (ARFCN) are numbered from 1 to 124; the corresponding frequency can be found from $f_{up}(n) = 890.2 + 0.2(n-1)$ MHz for the uplink (mobile transmits) and $f_{down}(n) = f_{up}(n) + 45$ MHz for the downlink (base transmits).

With a guard band of 100 kHz at each end of the sub-bands and the radio frequency channel spacing of 200 kHz, a maximum of 174 carriers is allowed in the extended GSM band. Each channel is time shared between as many as eight subscribers using TDMA. Each of the eight subscribers uses the same ARFCN and occupies a unique timeslot (TS) per frame. Radio transmissions on both the forward and reverse link are made at a channel data rate of 270.833 kbps (1625.0/6.0 kbps) using binary $BT = 0.3$ GMSK modulation. Thus, the signaling bit duration is 3.692 s, and the effective channel transmission rate per user is 33.854 kbps (270.833 kbps/8 users). With GSM overhead (described subsequently), user data is actually sent at a maximum rate of 24.7 kbps. Each TS has an equivalent time allocation of 156.25 channel bits, but of this, 8.25 bits of guard time and six total start and stop bits are provided to prevent overlap with adjacent timeslots. Each TS has a time duration of 576.92 s as shown in Figure 30, and a single GSM TDMA frame spans 4.615 ms. The total number of available channels within a 25 MHz bandwidth is 125 (assuming no guard band).

Since each radio channel consists of eight timeslots, there are thus a total of 1000 traffic channels within GSM. In practical implementations, a guard band of 100 kHz is provided at the upper and lower end of the GSM spectrum, and only 124 channels are implemented. The combination of a TS number and an ARFCN constitutes a physical channel for both the forward and reverse link. Each physical channel in a GSM system can be mapped into different logical channels at different times. That is, each specific timeslot of frame may be dedicated to either handling traffic data (user data such as speech, facsimile, or teletext data), signaling data (required by the internal workings of the GSM system), or control channel data (from the MSC, base station, or mobile user). The GSM specification defines a wide variety of logical channels which can be used to link physical layer with the data link layer of the GSM network. These logical channels efficiently transmit user data while simultaneously providing control of the network on each ARFCN. GSM provides explicit assignments of timeslots and frames for specific logical channels.

9.2 GSM 900 Frame and Timing Structure

The data structure within a normal burst is illustrated in Figure 30. It consists of 148 bits which are transmitted at a rate of 270.833 kbps (an unused guard time of 8.25 bits is provided at the end of each burst). Out of the total 148 bits per timeslot, 114 are information-bearing bits, which are transmitted as two, 57 bit sequences close to the beginning and the end of the burst. The midamble consists of a 26 bit training sequence which allows the adaptive equalizer in the mobile or base station receiver to analyze the radio channel characteristics before decoding the user data. On either side of the midamble are control bits called stealing flags. These two flags are used to distinguish whether the timeslot contains voice or control data. During a frame, a GSM subscriber unit uses one timeslot to transmit, one timeslot to receive, and may use the six spare timeslots to measure signal strength of five adjacent base stations as well as its own base station.

As shown in Figure 30, there are eight timeslots per TDMA frame, and the frame period is 4.615 ms. A frame contains 8 x 156.25 = 1250 bits, although some bit periods are not used. The frame rate is 270.833 kbps/1250 bits/frame, or 216.66 frames per second. The 13th and 26th frame are not used for traffic but for control purposes. Each of the normal speech frames are grouped into larger structures called multiframes, which in turn are grouped into superframes and hyperframes (hyperframes are not shown in Figure 30). One multiframe contains 26 TDMA frames, and one superframe contains 51 multiframes, or 1326 TDMA frames. A hyperframe contains 2048 superframes, or 2,715,648 TDMA frames. A complete hyperframe is sent every 3 hours 28 minutes and 53.760 seconds and is important to GSM since the encryption algorithms rely on the particular

frame number. Sufficient security can only be obtained by using a large number of frames as provided by the hyperframe.
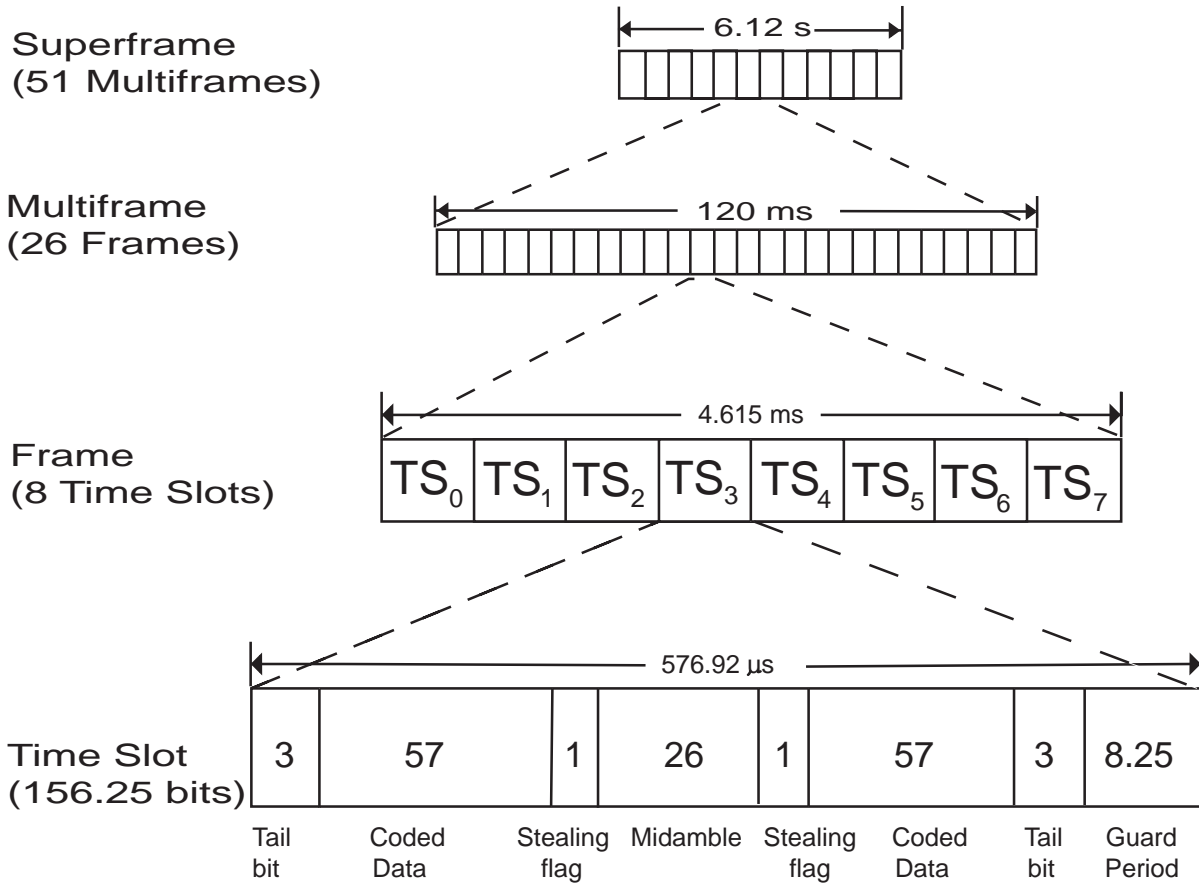

Figure 30: GSM 900 frame structure (after [4]).

9.3   GSM 900 Transmitter/Receiver

GSM 900 operations from transmitter to receiver are illustrated in Figure 31.

9.3.1   Speech Source Coding

The coding principal used for speech source coding is known as *regular pulse excitation-long term prediction* (RPE-LTP), and the analog voice signal is sampled at 8000 times per second using a 13-bit code (word) and uniform (linear) quantizing. The speech encoder provides 260 bits for each 20 ms block of speech. This yields a bit rate of 13 kbps.

9.3.2 Speech Channel Coding

The output bits of the speech encoder are ordered into groups for error protection based upon their significance in contributing to speech quality. Out of the total 260 bit frame, the most important 50 bits, called type *Ia* bits, have three parity check (CRC) bits added to them. This facilitates the detection of non-correctable errors at the receiver. The next 132 bits along with the first 53 (50 type *Ia* bits + 3 parity bits) are reordered and appended by four trailing zero bits, thus providing a data block of 189 bits. This block is then encoded for error protection using a rate 1/2 convolutional encoder with constraint length $\nu = 5$, providing a sequence of 378 bits. The least important 78 bits do not have any error protection and are concatenated to the existing sequence to form a block of 456 bits in a 20 ms frame. The error protection coding scheme increases the channel data rate of the GSM speech signal with channel coding to 22.8 kbps.
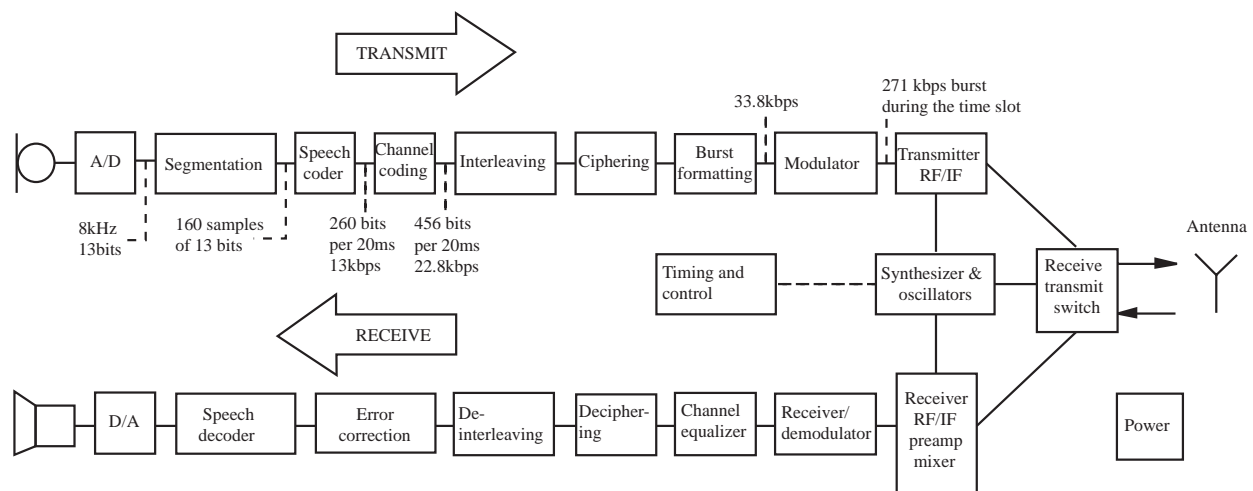

Figure 31: Functional block diagram of GSM 900 from speech input to speech output (after [12]).

9.3.3 Interleaving

In order to minimize the effects of sudden fades on the received data, the total of 456 encoded bits within each 20 ms speech frame or control message frame are broken into eight 57 bit sub-blocks. These eight sub-blocks which make up a single speech frame are spread over eight consecutive traffic channel time slots; i.e., eight consecutive frames for a specific timeslot. If a burst is lost due to interference or fading, channel coding ensures that enough bits will still be received correctly to allow the error correction to work. Each traffic channel timeslot carries two 57 bit blocks of data from two different 20 ms (456 bit) speech (or control) segments. Figure 33 illustrates exactly how
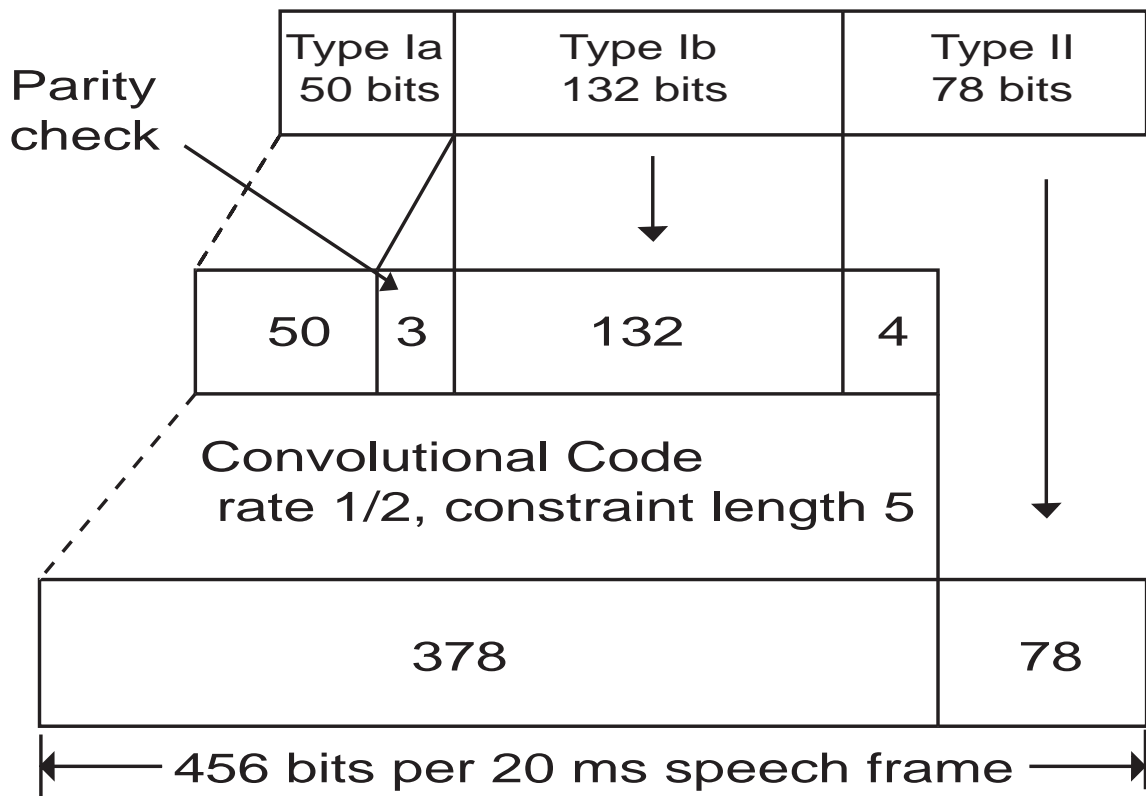
Figure 32: GSM 900 error detection and correction (after [4]).

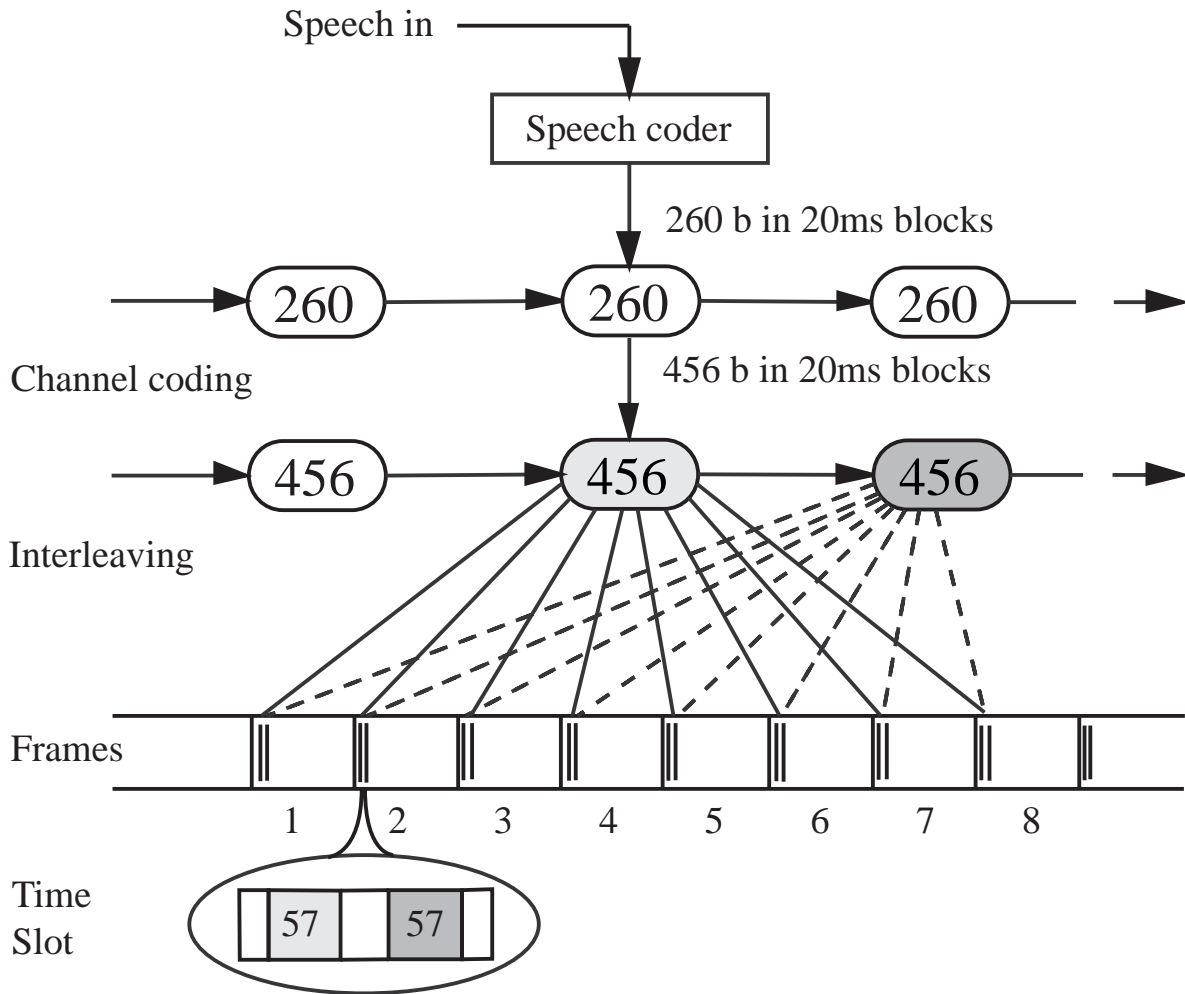the speech frames are diagonally interleaved within the timeslots.

Figure 33: Interleaving 57 bit bursts of coded voice data over eight frames to make up the 20 ms speech burst (after [12]).

9.3.4   Ciphering

Ciphering modifies the contents of the eight interleaved blocks through the use of encryption techniques known only to the particular mobile station and base transceiver station. Security is further enhanced by the fact that the encryption algorithm is changed from call to call. Two types of ciphering algorithms, called A3 and A5, are used in GSM to prevent unauthorized network access and privacy for the radio transmission respectively. The A3 algorithm is used to authenticate each mobile by verifying the users passcode within the Subscriber Identity Module with the crypto-

graphic key at the Mobile Switching Center. The A5 algorithm provides the scrambling for the 114 coded data bits sent in each timeslot.

9.3.5 Burst formatting

Burst formatting adds binary data to the ciphered blocks, in order to help synchronization and equalization of the received signal.

9.3.6 Modulation

The modulation scheme used by GSM is 0.3 Gaussian minimum-shift keying where 0.3 describes the 3 dB bandwidth of the Gaussian pulse shaped filter with relation to the bit rate (e.g., $BT = 0.3$). Binary ones and zeros are represented in GSM by shifting the RF carrier by ± 67.708 kHz. The channel data rate of GSM is 270.833 kbps, which is exactly four times the RF frequency shift. This minimizes the bandwidth occupied by the modulation spectrum and hence improves channel capacity. The minimum-shift keying modulated signal is passed through a Gaussian filter to smooth the rapid frequency transitions which would otherwise spread energy into adjacent channels. The modulation efficiency of 270.833 kbps operating within a 200 kHz carrier spacing is 1.35 bps/Hz. With a bit interval of 3.7 s, which can exceed typical delay spreads, the GSM signal will encounter significant intersymbol interference in the mobile radio multipath propagation environment. As a consequence, an important component of a GSM receiver is the adaptive equalizer necessary to provide reliable binary signal detection, apart from the channel coding strategies.

9.3.7 Equalization

Equalization is performed at the receiver with the help of the training sequences transmitted in the midamble of every time slot. The type of equalization for GSM is not specified and is left up to the manufacturer.

9.3.8 Demodulation

The portion of the transmitted forward channel signal which is of interest to a particular user is determined by the assigned timeslot and Absolute Radio Frequency Channel Number. The appropriate timeslot is demodulated with the aid of synchronization data provided by the burst formatting. After demodulation, the binary information is deciphered, de-interleaved, channel decoded, and speech decoded.

9.4 Link Budget Analysis

As mentioned earlier, GSM 900 uses Gaussian minimum-shift keying with $BT = 0.3$ and rate $1/2$, constraint length $\nu = 5$ convolutional coding. We will assume soft decision decoding as the most likely choice for the GSM 900 receivers manufacturers to make.

From (63), (80), and Table 4, we get for non-fading channels

$$P_b < \sum_{d=7}^{14} B_d\, Q\left(\sqrt{0.7\gamma_d}\right) \tag{172}$$

where $b/2 = \delta = 0.7$ is used. Only the first eight terms in the infinite series are used where $B_7 = 4$, $B_8 = 12$, $B_9 = 20$, $B_{10} = 72$, $B_{11} = 225$, $B_{12} = 500$, $B_{13} = 1324$, and $B_{14} = 3680$.

Similarly, from (63), (93), and Table 4, we get for Ricean fading channels

$$P_b < \sum_{d=7}^{14} B_d\, \frac{1}{\sqrt{2\pi c}} \left[\frac{2\,(1+\zeta)}{2\,(1+\zeta)+0.7\overline{\gamma_b}}\right]^d \exp\left[\frac{-0.7d\zeta\overline{\gamma_b}}{2\,(1+\zeta)+0.7\overline{\gamma_b}}\right] \tag{173}$$

where $b/2 = \delta = 0.7$ is used.

Similarly, from (63), (82), (83), and Table 4, we get for Rayleigh fading channels

$$P_b < \sum_{d=7}^{14} B_d \left(\frac{1-\mu}{2}\right)^d \sum_{m=0}^{d-1} \binom{d-1+m}{m} \left(\frac{1+\mu}{2}\right)^m \tag{174}$$

where

$$\mu = \sqrt{\frac{0.7\overline{\gamma_b}}{2+0.7\overline{\gamma_b}}} \tag{175}$$

where $b/2 = \delta = 0.7$ is used.

Equations (172), (173), and (174) can be used to determine the $(E_b/N_0)_{min}{}_{\text{dB}}$ required by the link budget equation (167) to achieve a particular P_b for a specified fading channel. For example, if we assume a Rayleigh fading channel, then from (174) we determine that for $P_b \leq 10^{-5}$ we require $E_b/N_0 > 11$ dB.

10 Summary

In this report, the probabilities of bit error for the most commonly used digital modulation techniques were analyzed. Analytic solutions were developed for the probability of bit error when the signal is affected by the most commonly encountered impairment to system performance for a wireless channel, the transmission of the signal over a fading channel. In this report, the effect of a slow, flat Ricean fading channel on communications systems performance was examined. Since channel fading significantly degrades the performance of a communication system, the performance of digital communication systems that also use forward error correction channel coding was analyzed for hard decision decoding and, where appropriate, for soft decision decoding. Diversity, another technique to mitigate the effect of fading channels on digital communication systems performance, was also discussed. Also included was a discussion of the effect of narrowband noise interference, both continuous and pulsed, on digital communication systems. We then discussed the analysis of the probability of bit error for the combination of error correction coding and diversity. Following this, we briefly discussed spread spectrum systems. Next, we examined the link budget analysis and various models for channel loss. Finally, we examined in detail the second generation digital wireless standard *Global System for Mobile* (GSM).

THIS PAGE INTENTIONALLY LEFT BLANK

List of References

[1] J. G. Proakis, *Digital Communications, 4th ed.*, McGraw-Hill, New York, NY, 2001.

[2] M. Abramowitz and I. A. Stegun, Editors, *Handbook of Mathematical Functions with Formulas, Graphs, and Mathematical Tables*, National Bureau of Standards, U.S. Government Printing Office, Washington, DC, 1972.

[3] I. S. Gradshteyn and I. M. Ryzhik, *Table of Integrals, Series and Products*, translated and edited by Alan Jeffrey, Academic Press, New York, NY, 1980.

[4] T. S. Rappaport, *Wireless Communications, principles and practice, 2nd ed.*, Prentice Hall PTR, Upper Saddle River, NJ, 2002.

[5] S. Lin and D. J. Costello, Jr., *Error control coding: fundamentals and applications*, Prentice Hall, Englewood Cliffs, NJ, 1983.

[6] J. P. Odenwalder, *Optimum decoding of convolutional codes*, Ph.D. dissertation, University of California, Los Angeles, 1970.

[7] G. C. Clark, Jr. and J. B. Cain, *Error-Correction Coding for Digital Communications*, Plenum Press, New York, NY, 1981.

[8] S. B. Wicker, *Error Control Systems for Digital Communication and Storage*, Prentice-Hall, Inc., Englewood Cliffs, NJ, 1995.

[9] A. Erdelyi, Editor, *Table of Integral Transforms, Volume I*, McGraw-Hill, New York, NY, 1954.

[10] R. L. Peterson, R. E. Ziemer, and D. E. Borth, *Introduction to Spread-Spectrum Communications*, Prentice-Hall, Inc., Upper Saddle River, NJ, 1995.

[11] B. Sklar, *Digital Communications, Fundamentals and Applications, 2nd ed.*, Prentice Hall PTR, Upper Saddle River, NJ, 2001.

[12] R. C. V. Macario, *Cellular Radio, 2nd ed.*, MacMillan, London, 1997.

THIS PAGE INTENTIONALLY LEFT BLANK

Initial Distribution List

1. Defense Technical Information Center
   Ft. Belvoir, Virginia

2. Dudley Knox Library
   Naval Postgraduate School
   Monterey, California

3. Research Office (Code 09)
   Naval Postgraduate School
   Monterey, California

4. Chairman, Code EC/Po
   Department of Electrical and Computer Engineering
   Naval Postgraduate School
   Monterey, California

5. Professor R. Clark Robertson, Code EC/Rc
   Department of Electrical and Computer Engineering
   Naval Postgraduate School
   Monterey, California

6. Nathan Beltz
   Department of Electrical and Computer Engineering
   Naval Postgraduate School
   Monterey, California

7. John T. Pearson
   453 EWS
   102 Hall Blvd., Ste. 333
   Mailstop 453 EWS/EWA
   San Antonio, Texas 78243-7020

8. Ray Grant
   Air Force Information Warfare Center
   102 Hall Blvd., Ste. 331
   San Antonio, Texas 78243-7020

9. Kurt D. Welker
   Idaho National Engineering and Environmental Laboratory
   Bechtel BWXT Idaho, LLC - MS 3818
   2525 N. Freemont Ave.
   Idaho Falls, Idaho 83415-3818

THIS PAGE INTENTIONALLY LEFT BLANK